Off-Target Activities of Lipoxygenase Inhibitors Confound the Role of Enzyme-Catalyzed (Phospho)Lipid Peroxidation in Ferroptosis

By

Katherine Shirley

A thesis submitted to the Department of Chemistry and Biomolecular Sciences
in conformity with the requirements for the degree of Master of Science in Chemistry

University of Ottawa

Ottawa, Ontario, Canada

December 2021

Abstract

Ferroptosis is a recently characterized iron-dependent form of regulated cell death associated with the accumulation of (phospho)lipid hydroperoxides. Since its characterization, there has been a spirited debate in the literature over the origin of the lipid hydroperoxides in ferroptotic cells. Many investigators have implicated lipoxygenases (LOXs), enzymes known to catalyze the oxidation of polyunsaturated fatty acids (especially linoleate and arachidonate) to yield lipid hydroperoxides. Previous work by our group, investigated the induction and suppression of ferroptosis in human embryonic kidney (HEK-293) cells transfected to overexpress the three most widespread isoforms of LOX (5-LOX, 15-LOX-1 and p12-LOX). The results suggested that LOX catalysis is not required for ferroptosis.

Our previous work did not include investigations into cells transfected to overexpress 15-LOX-2. However, a series of recent publications has since implicated the 15-LOX-2/PEPB1 complex as a key player in ferroptotic cell death. Therefore, in this work, HEK-293 cells were transfected to overexpress the 15-LOX-2 isoform, as confirmed by immunodetection, and were subject to induction and suppression of ferroptosis pharmacologically. A library of small molecules was assembled consisting of LOX inhibitors, radical-traping antioxidants (RTAs) and LOX inhibitors that display off-target RTA activity. Consistent with our previous investigations, only LOX inhibitors with radical trapping activity or iron chelators were effective at suppressing ferroptosis. Furthermore, the poor performance of 15-LOX-2 inhibitors at rescuing cells transfected to overexpress 15-LOX-2 from ferroptosis does not support the role of the 15-LOX-2/PEBP1 complex as a central mediator of ferroptotic lipid peroxidation.

We also report the details of corresponding investigations in cell lines that are reported to express high levels of LOXs and that have been used to establish characteristics of ferroptosis, including HT-22 mouse hippocampal cells (15-LOX-1 and/or 15-LOX-2) and HT-1080 human fibrosarcoma cells (all LOXs). The two cellular models were also subject to cell-rescue studies with our small molecule library. Again, only LOX inhibitors that possess radical-trapping antioxidant activity or which are good iron chelators

could rescue cells from ferroptosis. These results underscore our previous conclusion that although lipoxygenase activity may contribute to the pool of cellular lipid hydroperoxides, autoxidation drives ferroptotic cell death.

Acknowledgements

Over the course of my graduate degree, I have received a tremendous amount of support. I would like to start by expressing my deep appreciation to Dr. Derek Pratt, for providing me with guidance, expertise, and constructive critiques of my research. His passion for excellence and extensive knowledge in the field served as a constant source of motivation.

I am extremely grateful to both, Jai-Fei Poon and Zosia Zielinski who acted as mentors to me during my time in the laboratory. I would also like to extend my thanks to Ron Shah, whose extensive research served as a foundation for my thesis project and who provided me with valuable technical advice. I also wish to thank Spencer Short, for his contribution and dedication towards this project.

To the Pratt lab members, both past and present, I could not have asked for a better group of scientists and friends to share the laboratory space. I wish you all success and happiness, wherever your future takes you; Anas Abou-Zaid, Demar Pitter, Dmitry Saraev, Emily Schaeffer, Evan Haidasz, J-P Chauvin, Kareem Harrison, Luke Farmer, Mark Raycroft, Markus Griesser, Melodie Mallais, Matt Dods, Neill Penner, Omkar Zilka, Zijun Wu and the undergraduate students.

Lastly, this work could not have been completed without my family's unwavering patience and encouragement. I would like to thank my parents, my brother Eric, my partner Jake, and Buddy for remaining my greatest supporters throughout this entire process.

Statement of Originality

I hereby certify that all of the work described in this thesis is the original work of the author, with exceptions for work performed by collaborators noted in the preface to each chapter. The work in this thesis draws upon a great deal of previously published research. Any published (or unpublished) work by others is cited and fully acknowledged within the references.

Katherine A. Shirley

Table of contents

List of Figures

List of Schemes

List of Tables

List of Abbreviations

AA	Arachidonic acid
ACSL4	Acyl-CoA synthetase 4
AIBN	Azobisisobutyronitrile
AO	Antioxidant
α-TOH	Alpha-tocopherol
BDE	Bond dissociation enthalpy
BH4	tetrahydrobiopterin
BHT	Butylated hydroxy toluene
BSO	Buthionine sulfoximine
CGL	Cystathionine gamma-lyase
COX	Cyclooxygenase
$cPLA_2\alpha$	Cytosolic phospholipase $A_2\alpha$
DFOM	Desferrioxamine Mesylate
DMEM	Dulbecco's Modified Eagle Medium
DPBS	Dulbecco's phosphate buffered saline
DTUN	Di-tert-undecyl hyponitrite
DMSO	Dimethylsulfoxide
Egg-PC	Egg Phosphatidylcholine
EPR	Electron paramagnetic resonance
ESI	Electrospray
ETC	Electron transport chain
FBS	Fetal bovine serum
FENIX	Fluorescence enabled inhibited autoxidation
FSP1	Ferroptosis suppressor protein 1
GPX4	Glutathione peroxidase 4
GSH	Glutathione
HEK	Human embryonic kidney cells
HETE	Hydroxyeicosatetraenoic acid
HPETE	hydroperoxyeicosatetraenoic acid
HRMS	High resolution mass spectrometry

HRP	Horseradish peroxidase
IgG	Immunoglobulin G
KSE	Kinetic solvent effect
LA	linoleic acid
LC	Liquid chromatography
LOX	Lipoxygenase
LPCAT	Lysophatidylcholine acyltransferase
LTA_4	Leukotriene A_4
MEF	Mouse embryonic fibroblast
MEM	Minimum Essential Media
MeO-AMVN	2,2'-Azobis (4-Methoxy-2,4-Dimethylvaleronitrile)
MS	Mass spectrometry
MS/MS	Tandem mass spectrometry
m/z	mass-to-charge ratio
NDGA	Nordihydroguaiaretic acid
NMR	Nuclear magnetic resonance
PEBP1	Phosphatidylethanolamine Binding Protein 1
PCET	Proton coupled electron transfer
PUFA	Polyunsaturated fatty acids
PVDF	polyvinylidene fluoride
PL	Phospholipid
ROS	Reactive oxygen species
RTA	Radical trapping antioxidant
SDS-PAGE	Sodium dodecyl sulfate polyacrylamide gel electrophoresis
shRNA	Short hairpin RNA
siRNA	Small interfering RNA
SOD	Superoxide dismutase
TAM	Tamoxifen
UPLC	Ultra performance liquid chromatography
UV-vis	Ultraviolet-visible
WT	Wild type

Molecular Structure Reference sheet

Small Molecule Library:

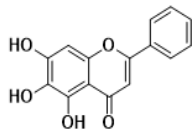
Baicalein

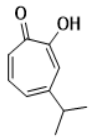
β-Thujaplicin

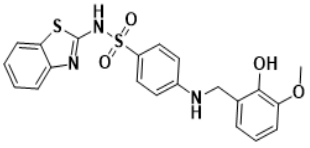
ML355

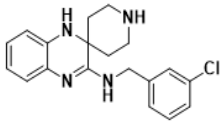
Lip-1

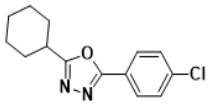
MLS000545091

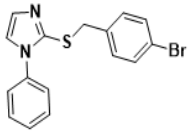
MLS000327186

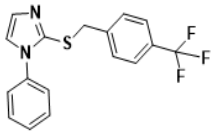
MLS000327069

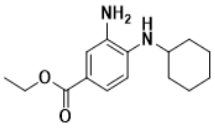
Fer-1

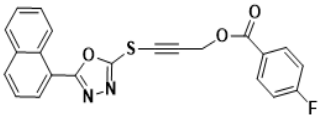
ML094

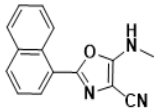
ML351

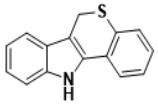
PD146176

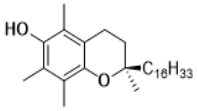
α-TOH

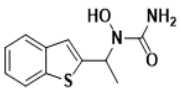
Zileuton

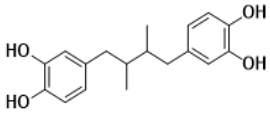
NDGA

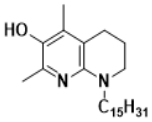
C_{15}THN

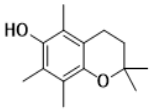
PMC

Arachidonic Acid Oxidation Products of Interest:

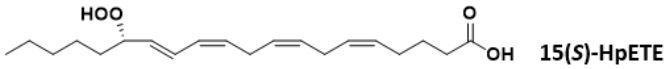
15(*S*)-HpETE

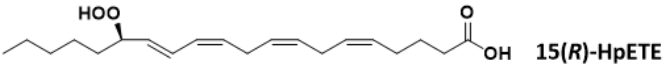
15(*R*)-HpETE

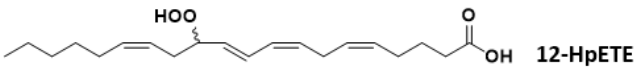
12-HpETE

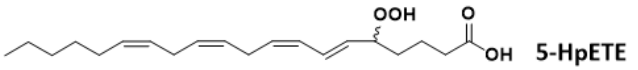
5-HpETE

1 Introduction

1.1 Reactive Oxygen species and Oxidative Stress

Under aerobic conditions, the availability of molecular oxygen (triplet), and the ease at which it accepts electrons (E°(V) + 1.3 vs SHE),[1] renders it a likely source of reactive oxygen species (ROS). Superoxide (O_2^{-}•) is the primary radical product of molecular oxygen reduction and is released as a by-product of enzyme oxidations, cellular metabolism and from organelles like the mitochondria.[2] From superoxide, are derived a number of secondary ROS, such as H_2O_2, HOO• and the notoriously reactive HO•. From a pathological standpoint, free radicals are often implicated with oxidative stress and disease (**Figure 1.1**).

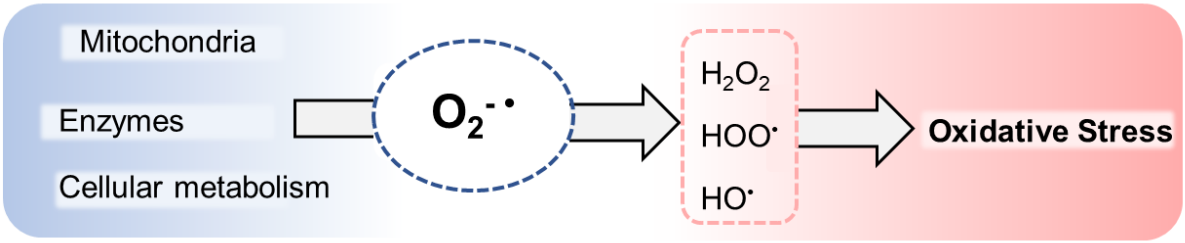

Figure 1.1 Free radicals, like superoxide and secondary ROS are often implicated with oxidative stress.

Superoxide (O_2^{-}•) and its conjugate acid (pKa 4.8), hydroperoxyl (HOO•) readily undergo dismutation to form hydrogen peroxide (H_2O_2). Although this is a fast reaction ($k \approx 2 \times 10^5$ $M^{-1}s^{-1}$), it is highly pH dependent, and at physiological pH the pre-equilibrium is unfavourable. Superoxide dismutase (SOD) accelerates this reaction to near diffusion control ($k \approx \sim 2 \times 10^9$ $M^{-1}s^{-1}$).[3,4] Hydrogen peroxide (H_2O_2) can undergo one-electron reduction by, for example, low-valent transition metals like iron(II) and copper(I), to form hydroxyl radicals (HO•).[5] Superoxide (O_2^{-}•) and hydrogen peroxide (H_2O_2) pose some danger to biological molecules and tissue, but downstream products such as the hydroxyl radical (HO•) are highly damaging as they react with almost everything at near diffusion controlled rates (**Figure 1.2**).[6,7]

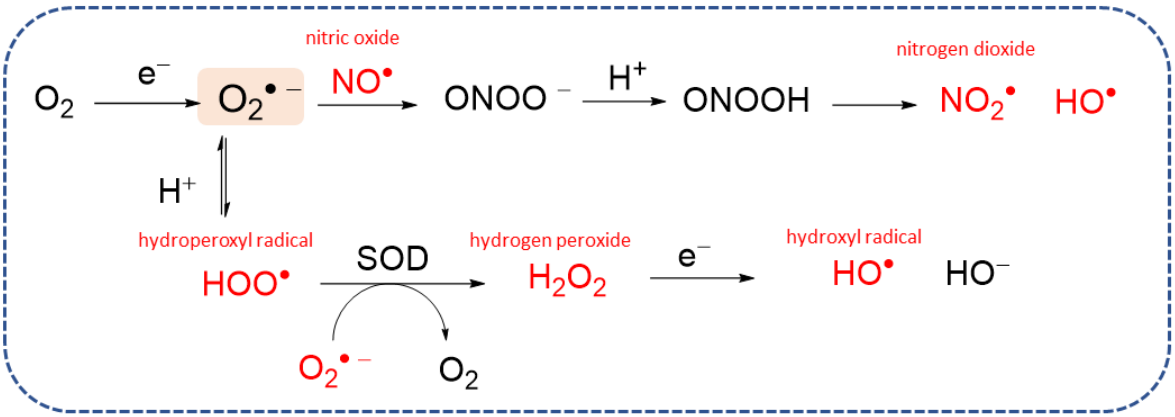

Figure 1.2 Superoxide fuels pathways that produce secondary cytotoxic ROS products.

Other sources of ROS within the cell include nitric oxide (NO•), an endothelial-derived relaxing factor.[8] Nitric oxide (NO•) and superoxide (O_2^-•) can combine at near diffusion controlled rates (6.7 ± 0.9 x 10^9 $M^{-1}s^{-1}$) to form peroxynitrite ($ONOO^-$), that once protonated becomes unstable and decomposes into NO_2• and HO•. [9,10] This pathway has been suggested as a lucrative source of hydroxyl radical given the speed at which nitric oxide (NO•) and superoxide (O_2^-•) combine.

There exists a number of endogenous ROS sources.[11] Enzymes, such as NADPH oxidase,[12,13] nitric oxide synthase,[14,15] and xanthine oxidase[3,16] generate ROS, such as superoxide, nitric oxide and hydrogen peroxide (**Figure 1.3**). In addition, lipoxygenase (non-heme iron) and cytochrome P450 (heme iron) directly catalyzes the oxidation of polyunsaturated fatty acids (PUFAs).[17,18]

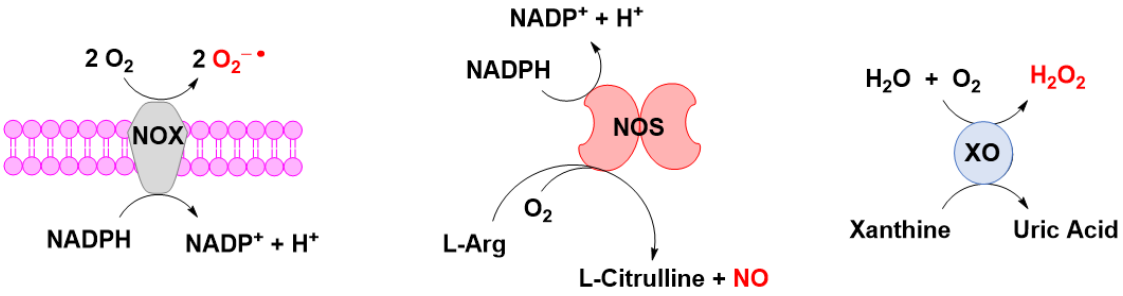

Figure 1.3 Simplified depictions featuring net transformations of NADPH oxidase synthase[19] nitric oxidase [20] and xanthine oxidase.[21]

Sub-cellular systems like the endoplasmic reticulum and the mitochondrial electron transport chain are reported sources of ROS.[22,23] In particular, complex I (NADH dehydrogenase) and complex III (ubiquinone-cytochrome c reductase) of the ETC are reported sites of increased ROS production.[24] During oxidative phosphorylation, reducing cofactor NADH donates electrons at complex I, and FADH at complex II, of the electron transport chain. Donated electrons are carried by ubiquinone (Q), in its reduced form, ubiquinol (QH), to complex III, where electrons are further transferred to cytochrome c. Electron transfer is necessary for proton translocation from the matrix to the inner mitochondrial space, thus generating a transmembrane potential required for ATP synthesis. However, the incomplete reduction/oxidation of Q/QH_2 can lead to the transfer of electrons to molecular oxygen instead, generating superoxide and the rapid transformation to H_2O_2 by superoxide dismutase.

Oxidative stress arises when the cell is unable to manage the production of free radicals, and the balance between oxidant and prooxidant unravels.[25] To date, redox imbalance has been implicated in a number of human pathologies[26] including, acute lung inflammation, [27,28] atherosclerosis,[29–31] ischemia-reperfusion, [32,33] cancer,[34] diabetes,[35] and neurodegenerative disorders like Parkinson's [36] and Alzheimer's diseases.[37]

1.2 Lipid Peroxidation

Although the foregoing oxidants can react with a variety of biomolecules, their reactions with lipids are particularly problematic as these can initiate chain reactions. Lipids are a diverse class of biologically active molecules that are essential for life. In water, they spontaneously aggregate to form micelles, and bilayers, driven by favourable geometry, thermodynamics, and interactive forces.[38] As a result, lipids serve an integral role in subcellular structuring and membrane architecture. Lipids also contribute to signal transduction, energy storage and protein sorting and membrane anchoring[39,40]. The

study of lipids and the subsequent reaction with molecular oxygen has garnered extensive investigations and is formally known as lipid peroxidation.[25]

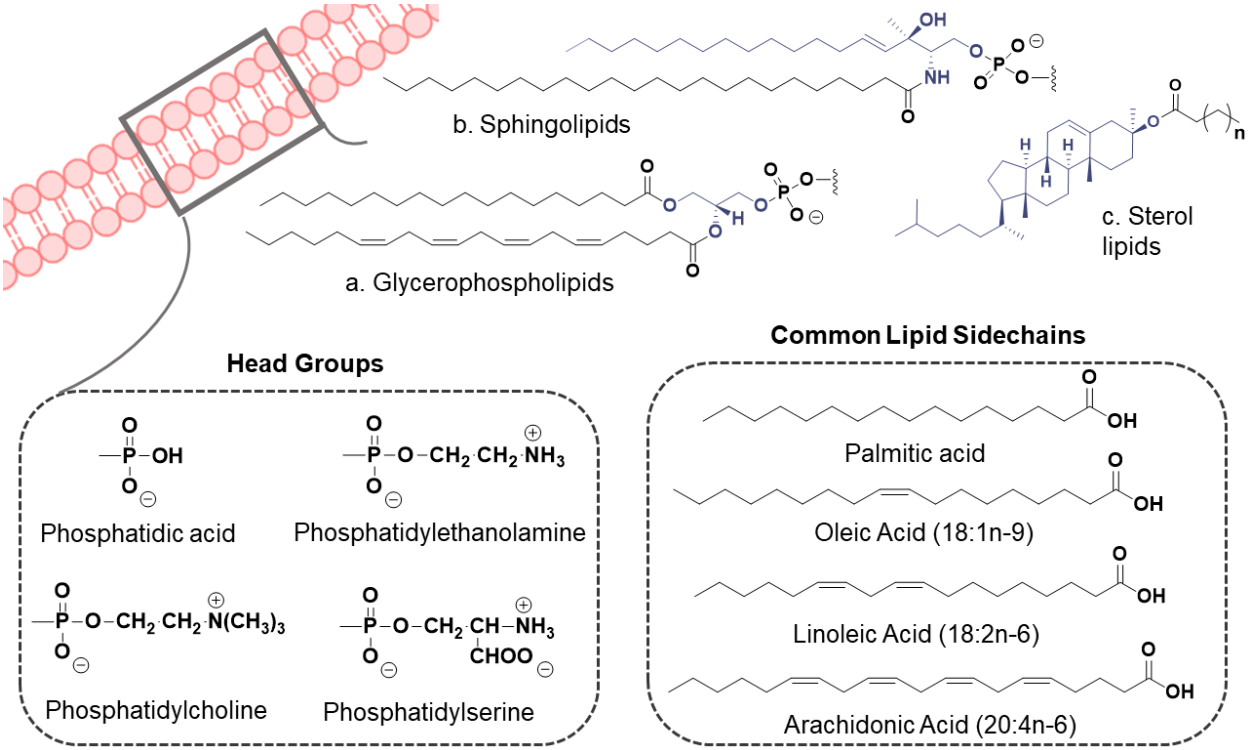

Figure 1.4 Shown are three classes of lipids commonly found in human and animal lipid membranes, glycerophospholipids, sphingolipids and sterol lipids.

The free and esterified lipids that comprise mono-bilayers are ideal substrates for free radical oxidation. Structurally, most esterified lipids are constructed from combinations of biological precursor fatty acyls and polar head groups affixed to a glycerol backbone[40] (**Figure 1.4**). Increased points of unsaturation along the hydrocarbon backbone render polyunsaturated fatty acids (PUFA) more prone to oxidation than saturated fatty acids.[41] The incorporation of oxygen onto the lipid backbone alters lipid organization,[42] membrane rigidity,[43] permeability[44] and other biophysical properties.[45] Moreover, highly reactive electrophilic products can be formed as byproducts of lipid peroxidation such as, 4-hydroxynonenal (4-HNE) and malondialdehyde (MDA).[46] Maintaining the biological assembly of lipids is crucial for cellular, tissue and organism integrity.

1.2.1 Mechanism of Lipid Peroxidation: Initiation

Lipid peroxidation is an example of an autoxidation chain reaction, with initiating, propagating, and terminating steps. Initiation describes the inception of reactive radical species (In•) from both endogenous and exogenous sources. Initiating radicals go on to abstract H atoms from weak C-H bonds along lipid hydrocarbon backbones, resulting in lipid derived radicals (L•) (**Figure 1.5**).[11]

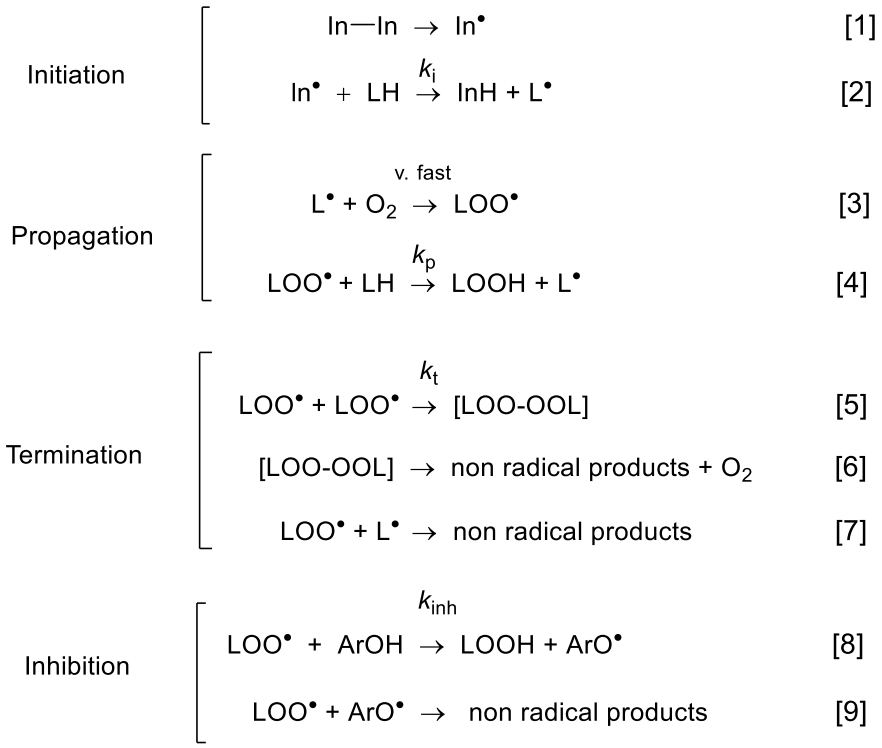

Figure 1.5 Simplified mechanism of autoxidation.

Initiating radicals can arise from exogenous sources such as air pollution, pesticides, UV light and ionizing radiation (X,γ- rays, β,α-particles, etc.). Initiators are compounds that readily accept or donate electrons to yield a radical and an ion, or, contain weak bonds that either thermally or photochemically homolyze to yield a pair of radicals. Aldehydes, for example, exposed to UV light, readily decompose to generate a carbonyl radical and a hydrogen atom [10].[47]

$$RCHO \rightarrow RCO^{\bullet} + H^{\bullet} \qquad [10]$$

$$ROOH \rightarrow RO^{\bullet} + HO^{\bullet} \qquad [11]$$

In the context of free radical lipid peroxidation, thermal decomposition of hydroperoxides remains the predominant mode of initiation at high temperatures. Hydroperoxides (LOOH) decompose following first order kinetics to form alkoxyl species (LO•) and the notoriously reactive hydroxyl radicals (HO•) [11].[48] However, at physiological temperature (37 ˚C), low valent transition metals like iron and copper, as well as other one electron reductants, such as ascorbate, are more likely to promote the Fenton-type decomposition of hydroperoxyls to reactive alkoxyl (LO•) or hydroxyl (HO•) radical species [12-13].[5] Low concentrations of hydroperoxide are sufficient to serve as the predominant chain initiating species as one hydroperoxide decomposes into two radical chain initiating species.[49]

$$Fe(III) + O_2^{-\bullet} \rightarrow Fe(II) + O_2 \qquad [12]$$

$$Fe(II) + LOOH \rightarrow Fe(III) + HO^{-} + LO^{\bullet} \qquad [13]$$

For the study of free radical chain reactions, azo compounds are often used as initiators due to the facile homolysis of the C-N bond to form nitrogen gas and two equivalents of a carbon centred radical. The decomposition of azo compounds, like AIBN and MeO-AMVN[50] are characterized by the decomposition constant, k_d , at a given temperature for a respective medium (**Figure 1.6**).

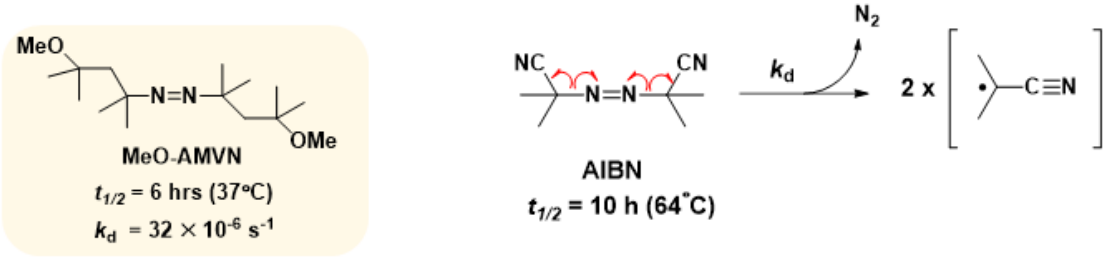

Figure 1.6 Common aza-initiators, AIBN and MeO-AMVN, decompose following first order kinetics to form molecular nitrogen and two equivalents of radical fragment. k_d and $t_{1/2}$ MeO-AMVN[51] and $t_{1/2}$ AIBN were measured in MeOH.[25]

1.2.2 Mechanism of Lipid Peroxidation: Propagation

Propagation follows a two-step process. First, the newly formed lipid radical (L•) undergoes rapid addition of molecular oxygen at near diffusion controlled rates 10^9 $M^{-1}s^{-1}$, forming peroxyl radical LOO•.[52] The addition of molecular oxygen is very rapid so peroxyl radicals (LOO•) are the dominant radical species present in the chain reaction. The rate limiting propagation step is instead characterized by the second step, hydrogen atom transfer from substrate (LH) to peroxyl radical (LOO•). Ultimately, for each lipid derived radical consumed, there is one lipid derived radical formed until substrate is consumed or termination pathways become more favourable.

The rate constant for propagation, k_p characterizes the bimolecular H atom transfer from labile C-H bonds to peroxyl radicals. The rate is largely governed by the bond dissociation enthalpy (BDE) of the C-H bond, which is dictated by the resonance stabilization of the newly formed radical and additional electronic effects.[25,53,54] Typical molecular targets are organic material containing weak C-H bonds, such as allylic C-H bonds and labile H atoms adjacent to heteroatoms as these sites are capable of stabilizing unpaired electrons by resonance and stereo-electronic effects (**Figure 1.7**). Therefore, unsaturated lipids become more oxidizable given increased points of unsaturation.

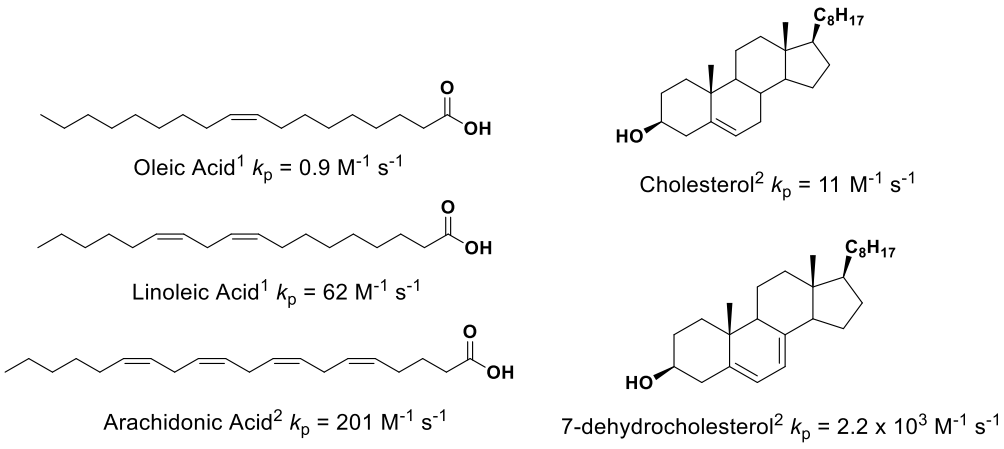

Figure 1.7 Propagation rate constants k_p, for oxidizable substrates 1. Measured at 30 ˚C[55] 2. Measured at 37C.[56]

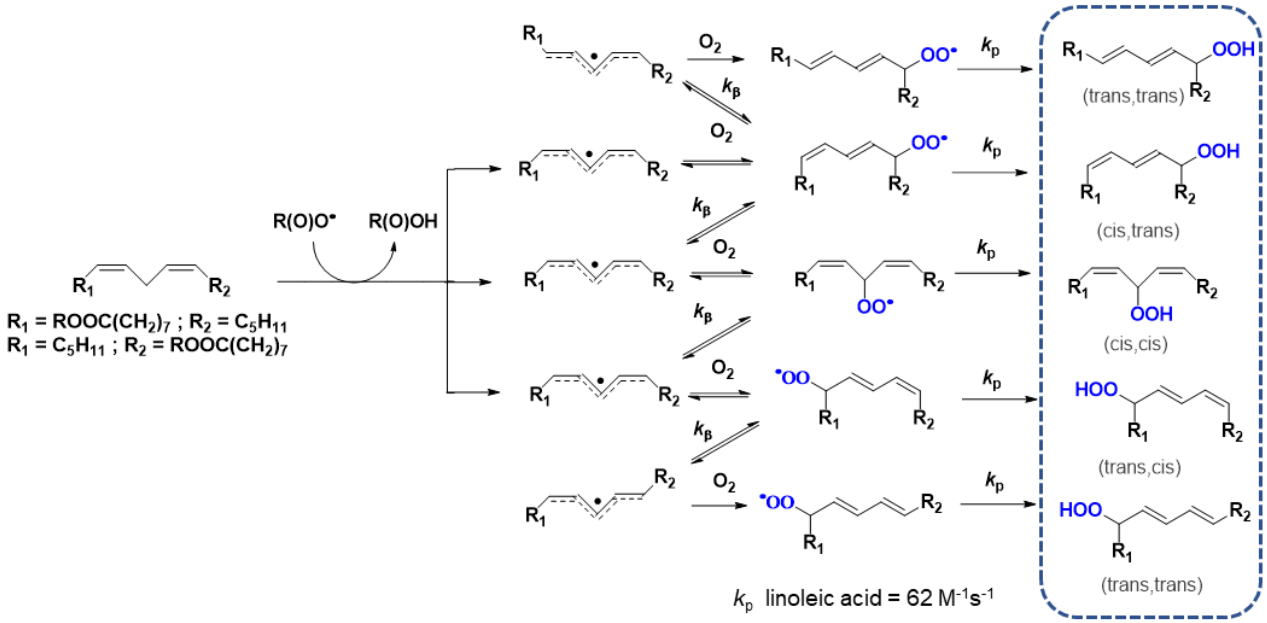

Figure 1.8 Lipid peroxidation products of linoleate. k_p measured at 30 ˚C. [25,55]

The product distribution of oxidized unsaturated lipids has been extensively studied and documented in the literature.[25,26,57] For instance, linoleate, which contains two points of unsaturation, undergoes H atom abstraction from the C11 position (BDE: 73 -74 kcal/mol)[58] to form a highly delocalized pentadienyl radical (**Figure 1.8**). Subsequent addition of molecular oxygen to C9 and C13 positions form the kinetic products (cis,trans)(trans,cis). Following addition of O_2 at position C11, the resulting peroxyl radical is only trapped into the (cis,cis) form in the presence of a good H atom donor (i.e.: α-TOH). The addition of molecular oxygen is a reversible process, as described by k_β, the rate constant for beta fragmentation. Beta fragmentation of the peroxyl radical can promote thermal isomerization to form trans-alkene products (trans,trans).[59] Ultimately, product distribution is dependent on factors such as the rate of H atom transfer and the reversibility of molecular oxygen addition.

The composition of autoxidation products grows more complex given increased points of unsaturation. This is demonstrated, for example, by the difference in product distribution between

linoleate and arachidonate, as the initial H atom abstraction can occur at any of the three bisallylic positions. (**Figure 1.9**).

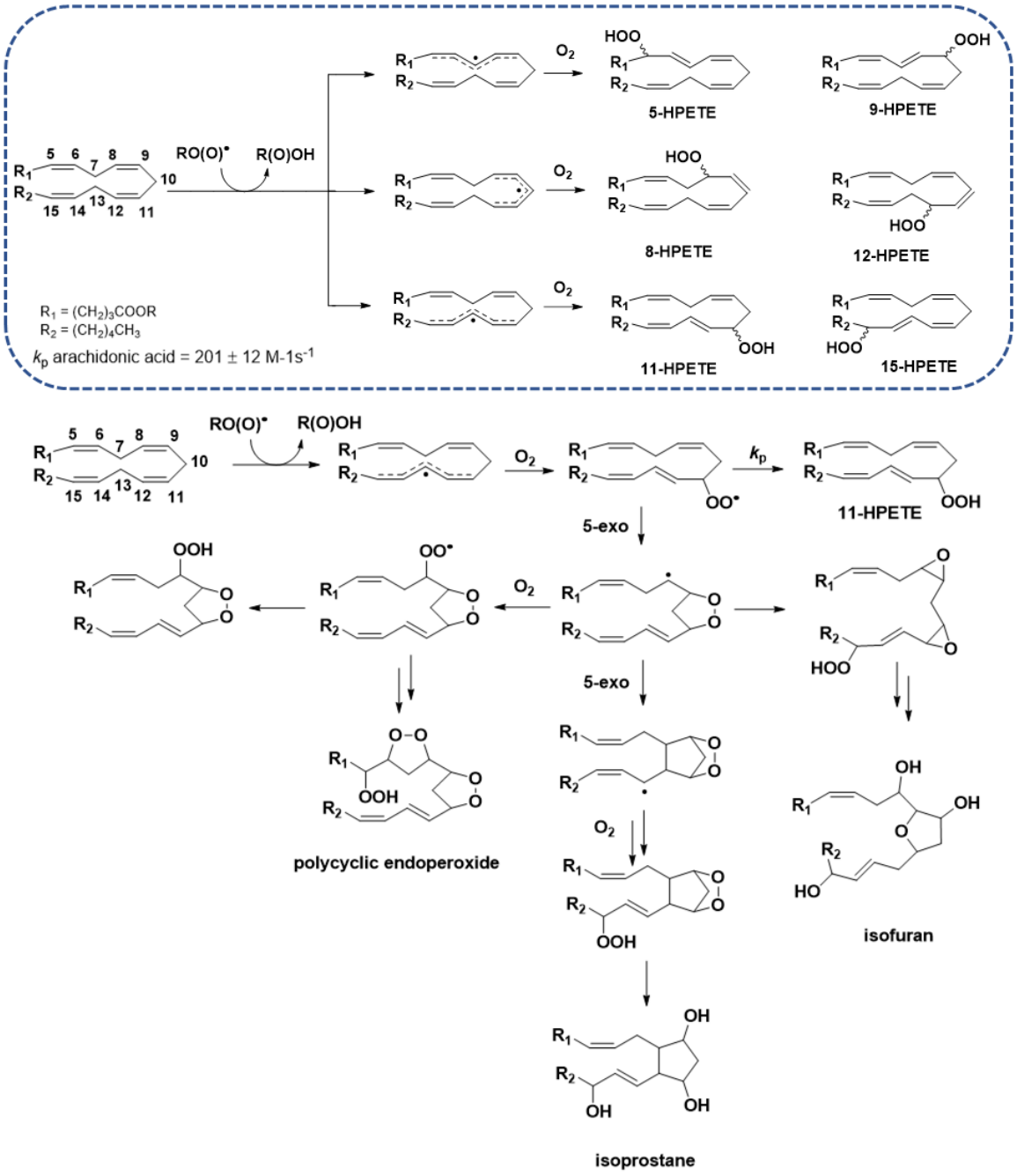

Figure 1.9 (**A**)Evolution of arachidonate oxidation products. Arachidonate H atom abstraction can occur at C7, C10 and C13 bisallylic positions and following addition of molecular oxygen, results in six regioisomeric hydroperoxyeicosatetraenoic acid (HPETE) products. (**B)** Illustrated are known downstream isoprostane, isofuran and cyclic endoperoxide products of arachidonate oxidation. Scheme adapted from Adapted from.[25,57,60] k_p of arachidonic acid measured at 37˚C .[56]

Arachidonate contains four double bonds that can participate in subsequent oxidations and radical cyclizations, leading to downstream products such as isofurans, isoprostanes and cyclic endoperoxides. Arachidonate derived isoprostanes are structural isomers of biologically active prostaglandins,[61] normally accessed enzymatically by cyclooxygenases (COX).[62,63] Efforts to isolate and characterize isoprostanes and other arachidonate oxidation products are necessary to identify ulterior bioactivity or off-target pathways.[64,65]

1.2.3 Mechanism of Lipid Peroxidation: Termination

As the concentrations of radicals increase, termination can outcompete propagation, resulting in the reaction of two radical species to form non radical products, marking the end of chain carrying species. Radical consumption can also be promoted following inhibition by chain breaking molecules, such as radical trapping antioxidants (RTAs).[48,66] Given the swift addition of molecular oxygen to lipid derived radicals (L•), peroxyls LOO• are the dominant radical species present, hence, they are most likely to react.[67] The termination rate constant, k_t, characterizes these peroxyl-peroxyl radical reactions and varies considerably with the structure of the substrate. The reaction of either two primary or secondary peroxyl radicals forms an initial tetroxide intermediate (**Figure 1.10**) that shortly decomposes to molecular oxygen, a carbonyl and an alcohol species (k_t = 10^6 to 10^8 $M^{-1}s^{-1}$ [55]).[68–70]

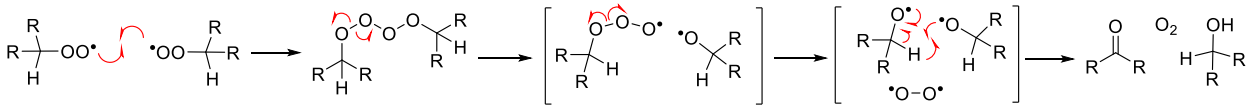

Figure 1.10 Russell termination is the accepted mechanism for termination of primary and secondary peroxyl radicals.

Tertiary radicals cannot access this mechanism of termination as they lack an alpha C-H bond. Instead tertiary peroxyl radicals (T > 158 K), combine and undergo an alternative mechanism (k_t = 10^3 to 10^5 M^{-1} s^{-1})[55] to form non-radical products (**Figure 1.11**).[71]

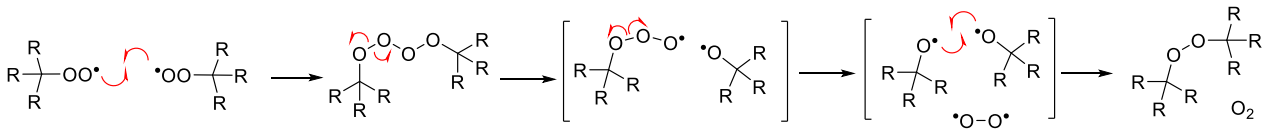

Figure 1.11 Proposed mechanism of termination for tertiary peroxyl radicals.

1.2.4 Lipoxygenase mediated lipid peroxidation

Lipid peroxidation products also arise from enzyme-catalyzed reactions. Lipoxygenases (LOX) are a family of enzymes that catalyze the regio- and stereoselective peroxidation of PUFAs to hydroperoxide products.[18] In total there are six distinct isoforms of human LOX (eLOX-3,5-LOX, 12-LOX-1. 12-LOX-2, 15-LOX-1, 15-LOX-2), which are named in accordance to their respective hydroperoxide products; hydroperoxyeicosatetraenoic acid (HPETE). [72] LOX products are important signalling molecules (HPETE, HETE) and mediators of inflammation (leukotrienes, lipoxins).[73–75] However, certain isoforms have been implicated in mediating ferroptotic cell death[76–78] and contributing to disease states such as ischemia[79] and atherosclerosis (**Table 1.1**).[80,81]

Table 1.1 Primary localization of LOX isoforms in mammals.

h5-LOX [82]	**h12S-LOX**	**h15-LOX-1** [83]	**h15-LOX-2**
Leukocytes	Blood platelets [84]	Prostasomes	Eosinophils[86]
Macrophages	Epidermal cells [85]	Epidermal cells	Bronchoalveolar epithelial
Mast cells		Hair roots	
Dendritic cells		Cornea	
β-lymphocytes			

Typical LOX substrates are homoconjugated PUFAs – particularly free arachidonic and linoleic acid. Given low concentrations of free fatty acids, cytosolic phospholipid lipase A2 ($cPLA_2$) cleaves esterified arachidonate and linoleate to their corresponding acids for uptake by LOXs.[87] Although, there is precedence that certain LOX isoforms will also dioxygenate membrane bound phospholipids, and cholesterol esters in lipoproteins (**Figure 1.12**).[88,89]

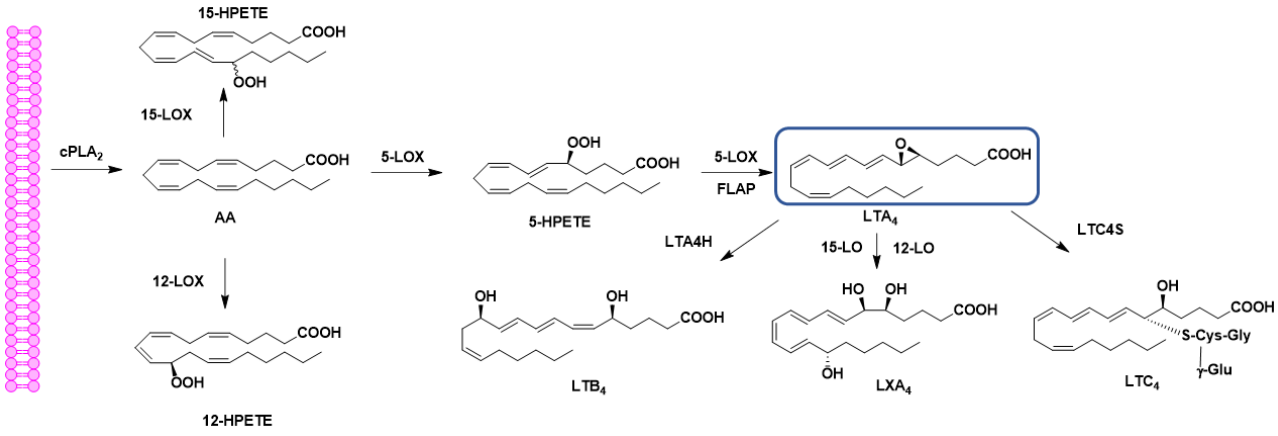

Figure 1.12 Synthesis of Lipoxins and Leukotrienes. Phospholipase $cPLA_2$ cleaves esterified AA to free fatty acid, where subsequent enzymatic transformation by 5-LOX generates Leukatriene A_4. LTC4S catalyzes the first step in the biosynthesis of cysteinyl leukotrienes such as LTC_4. LTA_4 hydrolase (LTA4H) converts LTA_4 to LXA_4. 5-LOX or 12-LOX catalyze the formation of LTB_4. Scheme adapted from [90]

Crystal structures of soybean L-1, L-3 , mammalian 15 LOX and human 5 LOX have been published in an effort to characterize enzyme structure and mechanistic pathways of LOX.[91–94] The general structure for LOX includes two domains. The first, an N-terminal β-barrel domain, that plays a role in localizing LOX proximally to substrate within membranes and lipoproteins.[93] And, the second, a C-terminal catalytic domain, that contains the active site non-heme iron core, coordinated to five ligands. Typically, the active site iron is coordinated to five amino acid residues and a hydroxide/water ligand[95,96] Rabbit reticulocyte 15 LOX contains amino acid residue histidine (His-361, His-366, His-541, His-545) and isoleucine (Ile-663) as ligands, although the identity of the residues varies between isoforms.[93]

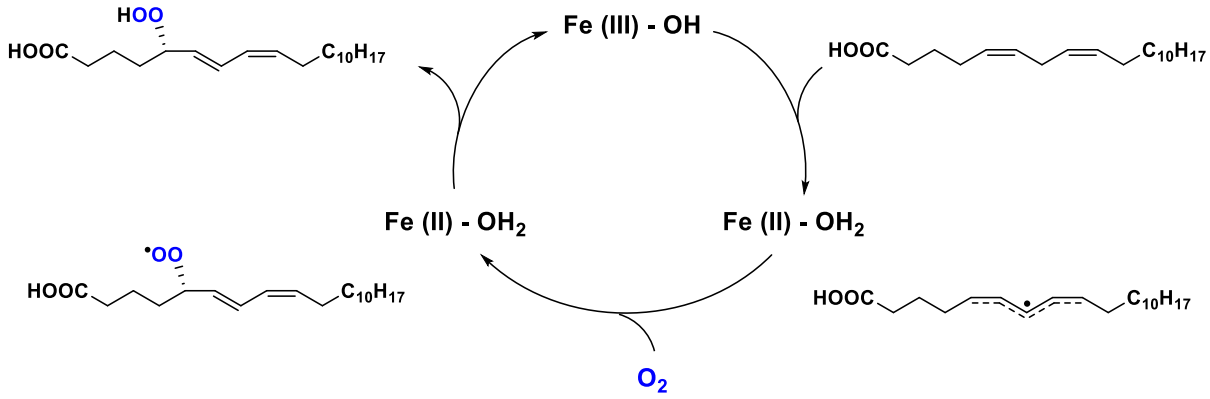

Figure 1.13 Proposed catalytic cycle for 5-lipoxygenase wherein arachidonic acid undergoes H atom abstraction from the bisallylic site at C7 to form a pentadienyl radical spanning C5 to C10, followed by the addition of molecular oxygen to C5 and subsequent reduction to form 5-hydroperoxyeicosatetraenoic acid.

Mechanistically (**Figure 1.13**), PUFAs enter the substrate binding pocket, a hydrophobic cavity accessible from the enzyme surface. Herein, the lipid is positioned to promote the correct stereo- and regioselectivity of oxygenation. The iron(III)-OH active site[97] abstracts a H atom from an allylic or bisallylic position to generate a delocalized pentadienyl lipid radical.[98,99] This is the irreversible rate determining state and is proposed to follow a proton coupled electron transfer (PCET) reaction that occurs by proton tunnelling.[98,100] A separate channel promotes the partition of molecular oxygen from solvent where it diffuses into the enzyme active site.[101] Molecular oxygen approaches and adds to the lipid radical antarafacially, relative to proton abstraction, forming a peroxyl radical.[93] The peroxyl radical is subsequently reduced to its conjugated hydroperoxyl fatty acid.[98] There has been much debate whether LOX mechanism proceeds via organo-iron[102] or free radical intermediates[103] though EPR experiments have favoured the latter.

1.3 Inhibition of Radical Mediated Lipid Peroxidation: Antioxidants

Autoxidation promotes oxidative degradation of organic materials such as petroleum-derived rubbers, and lubricants, polymers, cosmetics, food products and has even been implicated as a key player in oxidative stress. It is of both medical and economic benefit to employ the use of antioxidants (AO);

molecules that slow or inhibit the process of autoxidation. Antioxidants can serve as radical trapping antioxidants (RTAs), which react with chain-carrying species, or, preventative antioxidants, that reduce the rate at which new radical chains are being formed.[66] Superoxide dismutase (SOD) is an essential preventative antioxidant that scavenges superoxide, precluding the formation of initiating radicals.[104] Whereas, H atom donors like phenols and diarylamines are common RTA scaffolds (**Figure 1.14**). Synthetic antioxidants such as butylated hydroxytoluene (BHT)[105] and alkylated diphenylamines are the industrial choice for additives in oils and lubricants. In vivo, nature's best antioxidant is the most biologically-active form of vitamin E, alpha tocopherol.[106,107]

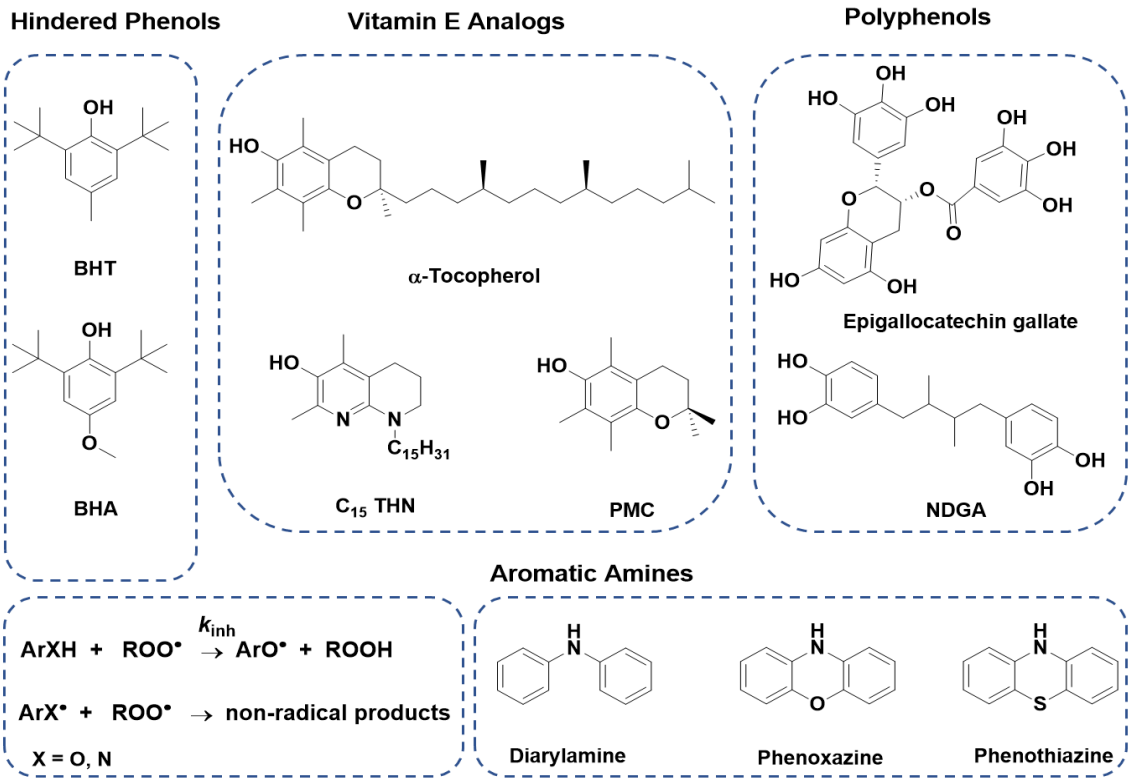

Figure 1.14 The structures of common classes of radical-trapping antioxidants, and representative examples, are shown. A simplified scheme is included, depicting the inhibition of autoxidation to form non-radical products.

An effective chain breaking antioxidant outcompetes propagation pathways (k_{inh} >>> k_p) by donating a labile H atom to peroxyl radicals.[105] This reaction generally follows a proton coupled electron transfer (PCET) mechanism when possible.[108,109] The resulting radical (ArX•) does not react with molecular oxygen or substrate, and instead, consumes another equivalent of chain carrying radical to form non-radical products. In the case of hindered phenols, bulky substituents flanking the phenoxyl radical, and delocalization of the unpaired electron into the aromatic ring, render the radical persistent enough to combine with a peroxyl radical at ortho or para positions (**Figure 1.15**).[104] Phenolic antioxidants capture two equivalents of chain carrying radicals and are therefore characterized by a stoichiometry of n = 2 . The stoichiometry, n, describes the number of radical chains that have been broken (**Figure 16D**).

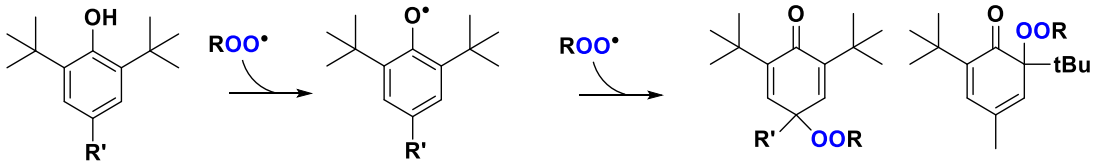

Figure 1.15 Hindered phenols capture two equivalents of peroxyl radical. First, the phenol donates a labile H atom to ROO•, followed by combination of the resultant radical (ArO•) with a second equivalent of ROO• to the para (less hindered) or ortho positions.

The H atom transfer to peroxyl radical is the rate limiting step of autoxidation inhibition and is characterized by inhibition rate constant, k_{inh}.[110] The absolute value of k_{inh} serves as a reliable measure of an RTA's potency. A strong correlation can be made between RTA potency and low bond dissociation enthalpies (BDE) of the ArX-H bond (X = O, NHAr').[111] However, factors such as solvent, steric and substituent effects must also be taken into account.

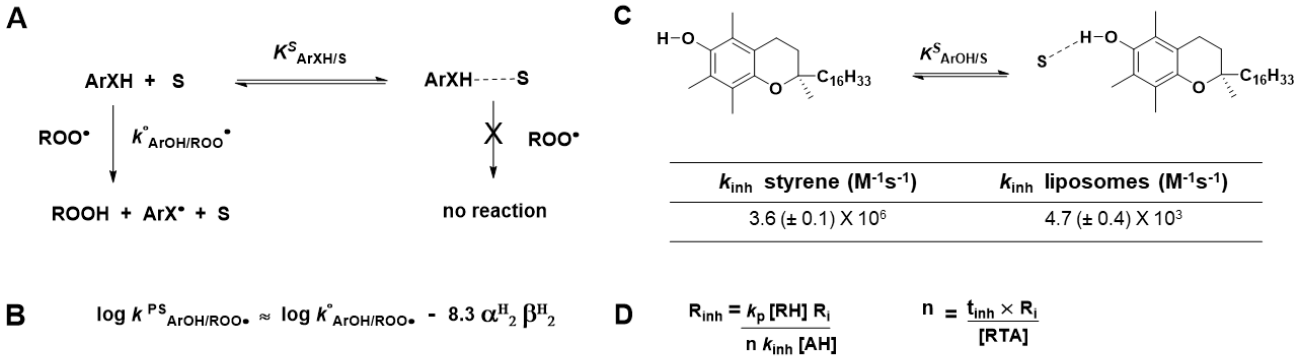

Figure 1.16 (**A**) Kinetic solvent effect of H donor ArXH. In the presence of solvent, S, with H-bonding capacity, ArXH is unable to react with peroxyl radicals. (**B**) The kinetic solvent effect for H atom abstraction from phenols depends on the above relationship with Abraham's parameters; α^H_2 : solute H-bonding acidity and β^H_2: solvent H bonding basicity. (**C**) k_{inh} rate constant measured for α-tocopherol from co-autoxidations in styrene versus Egg PC liposomes suspended in Tris buffer (pH 7.4)[112] (**D**) Expression that describes the kinetics of autoxidation in the presence of an RTA, where n refers to the number of peroxyl radicals an RTA (AH) traps, and k_{inh} is the rate of H atom transfer from the RTA to the peroxyl radical.

Early investigations revealed the phenolic O-H BDE is greatly influenced by electron donating groups (EDG) and electron withdrawing groups (EWG) .[105,113] EDGs stabilize phenoxyl radicals, and therefore, lower the BDE of the O-H bond, resulting in more exothermic reactions with peroxyl radicals.[111] Furthermore, the H bonding capacity of solvent can also impact the kinetics of inhibition, as described by the kinetic solvent effect (KSE) (**Figure 1.16.A**).[114,115] The majority of classic and modern RTAs generally include a polar H-donor group (ArXH, X = N,O) which forms a complex with peroxyl radicals (H bond acceptor) in a pre-reaction complex. However, solvents with a capacity for H-bonding can also form an H-bond complex with the RTAs labile H atom, resulting in a complex that is unreactive to peroxyl radicals.[109] The magnitude of the kinetic solvent effect will ultimately depend on the H bonding capacity of the solvent (β^H_2)[116] and the H donor capacity of the donor (α^H_2) (**Figure 1.16.B**).[117]As a result, rate constants measured in nonpolar organic solution are not truly representative of the RTA potency in water or lipid membranes (**Figure 1.16.C-D**).

Antioxidants such as α- tocopherol and designer RTAs, Lip-1 and Fer-1 have proven to be extremely potent alternatives. The role of antioxidants as anti-ferroptotic agents is further discussed in ***Chapter 1.5.***

1.4 Inhibition of Enzymatic Lipid Peroxidation

In recent years there has been great interest in small molecules that inhibit lipoxygenases, given their putative role in atherosclerosis[118], cancer[119] and stroke.[79] Broadly speaking, the mechanism of LOX inhibitors can be classified into five distinct categories; redox Inhibitors, iron chelators, active site inhibitors, allosteric inhibitors and suicide probes (**Table 1.2**).[96]

Table 1.2 Categories of LOX inhibitors.

	Mechanism of Action
Redox Inhibitor	Affect oxidation state of catalytic non-heme iron
Iron chelator	Coordinate to non-heme iron, displacing activating ligands
Active site inhibitor	Competes with and obstructs PUFA substrate from entering active site
Allosteric inhibitor	Bind to secondary site and promotes conformational change
Suicide probes	Form covalent, irreversible bond in enzyme active site

Traditionally, LOX inhibition activity is determined by spectrometric kinetic assays that monitor the formation of hydroperoxide (HPETE) product by absorbance of the conjugated diene moiety at 234 nm, or colourmetrically using agents like xylenol orange.[87,120] Modern strategies have modified these techniques for use in high throughput screens of small molecule libraries and in rational drug design.[121–123]

To date, the h5-LOX inhibitor, and anti-asthmatic drug, Zileuton is the only FDA approved LOX inhibitor on the market.[124] Zileuton contains a hydroxamic acid moiety that binds to h5-LOX iron as a ligand, inhibiting enzymatic activity. The h5-LOX isoform is involved in the synthesis of leukotrienes, a known bronchoconstriction agent.[90] However, Zileuton is not oxidatively stable and suffers a low half-life in vivo.[125]

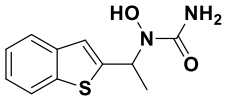

Zileuton

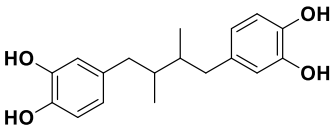

NDGA

A common molecular standard in the study of LOX inhibition is NDGA, a natural product antioxidant isolated from the creosole bush. NDGA is a pan-LOX inhibitor[126–128] that is proposed to reduce lipoxygenase non-heme Fe^{2+} to its inactive Fe^{3+} and corresponding semiquinone derivative.[129] However, given the unique functions of LOX isoforms in vivo, there has been a desire to construct LOX specific isoform inhibitors.

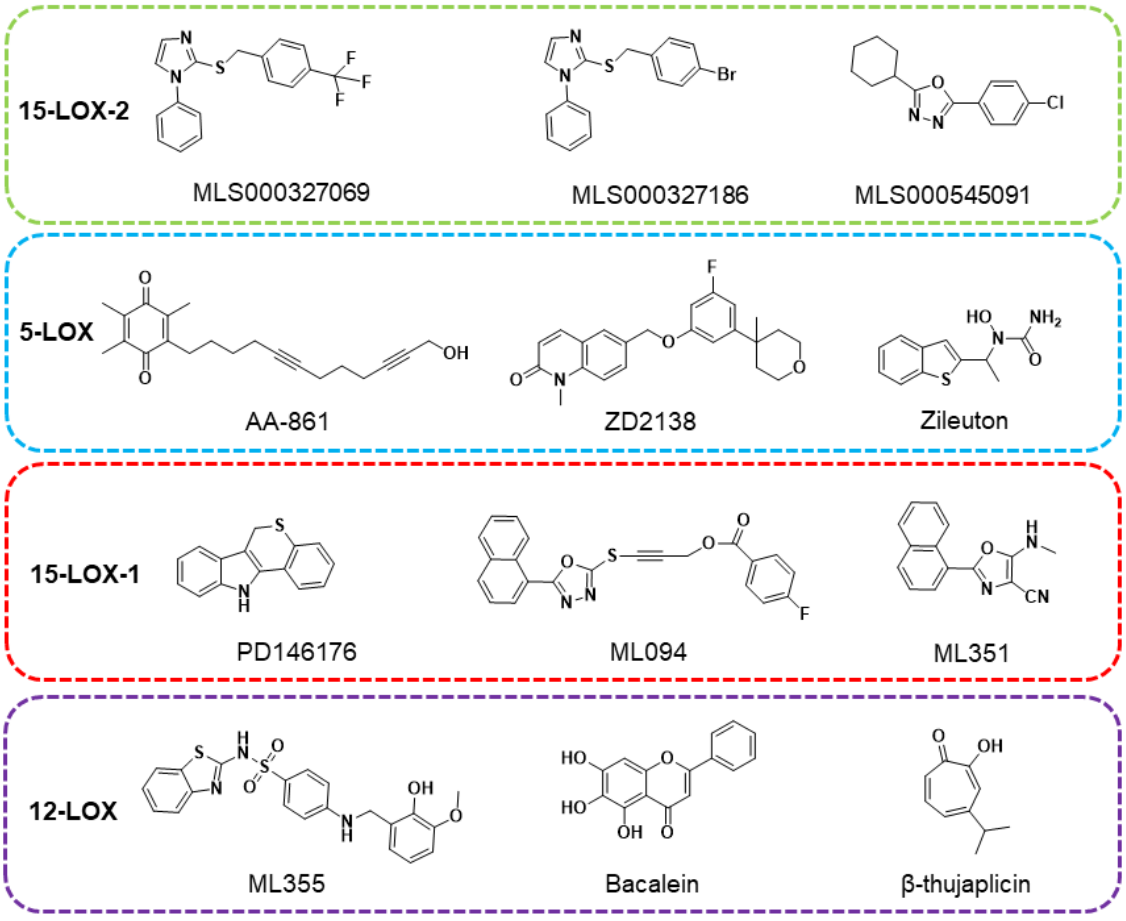

Figure 1.17 Molecular structures of common LOX inhibitors, highlighted according to reported isoform selectivity.

There remain a series of challenges associated with discovering novel LOX inhibitors. To date, there is a limited inventory of published lipoxygenase crystal structures and isoform characterization data. Furthermore, it is often a challenge to find suitable animal models given the variance in LOX homologs between species. In humans, the hALOX15 codes for 15-LOX-1 but murine alox15 encodes for a 12-LOX.[81] Given the recent implication of LOX in ferroptosis, there has been renewed interest and demand for both pan and isoform specific LOX inhibitors.

1.5 "Oxidative Cell Death": Oxytosis & Ferroptosis

Lipid peroxidation is often implicated in cell death and disease. The insertion of polar oxygen groups along the carbon lipid backbone alters membrane bilayer properties and promotes fragmentation and formation of downstream electrophilic byproducts that can undergo further reactions. A classic link between oxidized lipids and cell death was explored in the late 50's, wherein the neurotoxic effect of glutamate was investigated by Lucas and Newhouse[130] who exposed retinal neurons to continuous glutamate exposure and observed their death. Since then, it has been postulated that excitatory neurotransmitter induced cell death is linked to neurological disease states like Alzheimer's and Parkinson's diseases.[131] Efforts to deconvolute the mode of glutamate induced cell death in neurons has sparked much debate.

Neurons, in the presence of elevated concentrations of glutamate can trigger two observed forms of cell death.[132] The first pathway is mediated by excitotoxic glutamate stimulation of ionotropic receptors.[133] The second "oxidative" pathway termed, "oxytosis", is mediated by inhibition of system x_c^- and the disruption of cysteine homeostasis.[134,135] Investigations using primary neurons and neuronal cell lines describe an initial swelling of the neuron, followed by a slow degeneration in parallel with decreased glutathione, formation of ROS and calcium fluctuations.[132,134,136,137]

Over 20 years since "oxytosis" was first documented, parallel observations emerged in 2012 regarding a novel form of regulated, nonapoptotic cell death in cancer cell lines.[138] Ferroptosis was also marked by an accumulation ROS, in the form of lipid hydroperoxides. Cells experienced loss in lipid membrane integrity and interruption of cysteine homeostasis.[138,139] Traditional hallmarks of apoptosis, such as chromatin fragmentation and membrane blebbing were not observed.[138] Both ferroptosis and oxytosis have also been highlighted as a key-players in "oxidative stress" and are implicated in numerous degenerative disorders pertaining to neurological and cardiovascular systems and cancer.[140]

1.5.1 Mechanism of Ferroptosis

The recent emergence of the novel, non-apoptotic, regulated cell death modality termed 'ferroptosis' has been associated with extensive investigations into the respective biochemical pathways associated with the accumulation of oxidized lipids past a manageable threshold. Within the cell, lipid hydroperoxides are the product of two separate pathways; 1. radical mediated lipid peroxidation and 2. the lipoxygenase catalyzed substitution of molecular oxygen onto polyunsaturated lipids at regiospecific positions. Polyunsaturated phospholipids can be sourced into both cycles following the catalyzed addition of coenzyme A by acyl-CoA synthetase 4 (ACSL4)[141], and subsequent esterification by lysophatidylcholine acyltransferase (LPCAT-3)[142], resulting in PUFA-esterified phospholipids. This places lipid monolayers and bilayers at direct risk of oxidative damage, resulting in lipid re-organization, damage to membrane proteins and loss of membrane integrity.

The identification of ferroptosis as a regulated form of cell death was controversial. Apoptosis and its definitive characteristics have long been synonymous with regulated cell death (ie: cytoplasmic shrinking, chromatin condensation, nuclear fragmentation, plasma membrane blebbing and phagocytization of apoptotic bodies).[143,144] Instead, ferroptosis is morphologically more similar to necrotic

cell death, which is associated with early plasma membrane permeabilization and subsequent rupture and swelling of cytoplasmic organelles.[145]

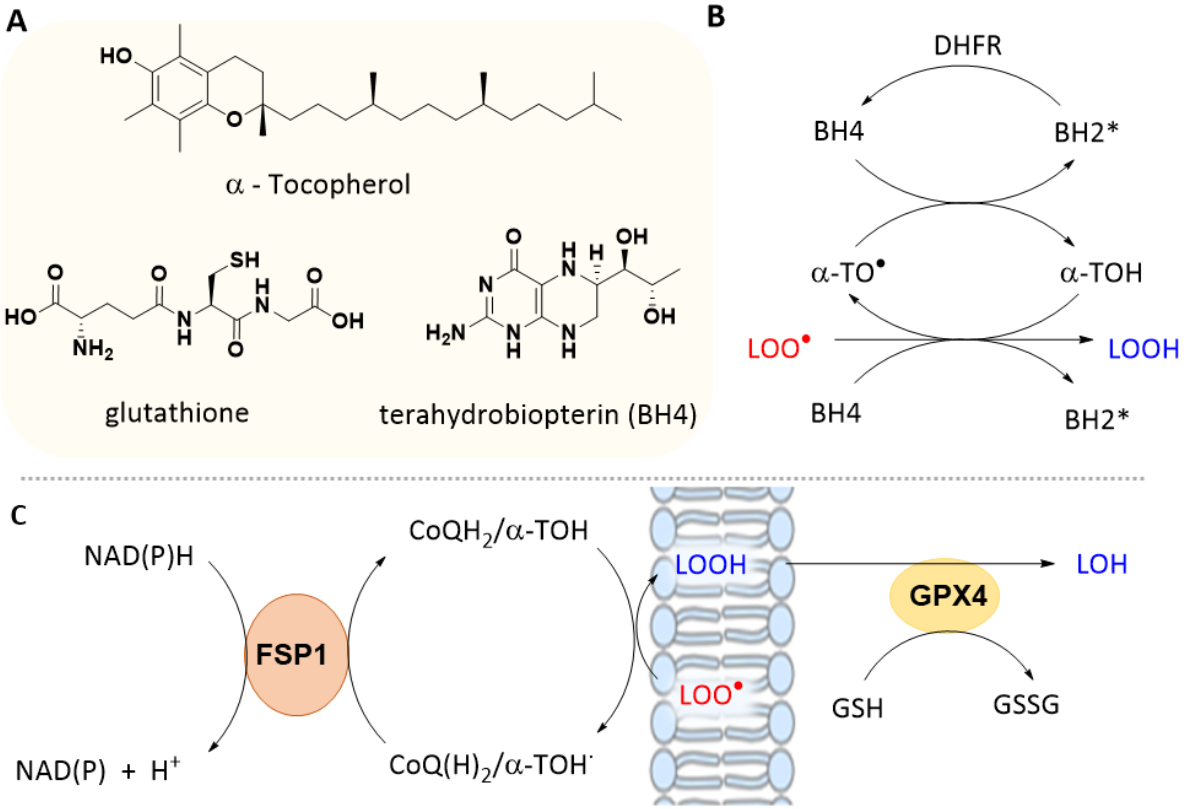

Figure 1.18 (**A**) Examples of Endogenous RTAs (**B**) Glutathione peroxidase 4 detoxifies lipid hydroperoxides to the corresponding lipid alcohols. (**C**) FSP1 pathway works in parallel with GPX4 to eliminate sources of ROS.

Typically, a cell is equipped with the necessary machinery to maintain the cellular redox balance. The cell can employ endogenous radical trapping antioxidants (RTAs), such as α-tocopherol that inhibit (phospho)lipid peroxidation (**Figure 1.18.A**). However, it is the GPX4/glutathione pathway that is responsible for eliminating lipid hydroperoxides and is required for cellular survival. The glutathione - dependent system oversees the production of antioxidant molecule glutathione (GSH) from precursor molecule cysteine.[146] Cysteine cannot be synthesized intracellularly and undergoes rapid oxidation to the corresponding disulfide (cystine) in medium. However, the cell circumvents this issue by reducing cystine to cysteine within the cell.[147] Glutathione cellular homeostasis also plays an essential role as a reducing

agent for glutathione peroxidase 4, one of eight peroxidases necessary for life.[78,148] GPX4 (PHGPx) is the only peroxidase known to serve alongside endogenous antioxidants by detoxifying oxidized phospholipids in membranes to their reduced form (**Figure 1.18.B**).[149–151] Evidence has suggested GPX4 plays a specific role in regulating arachidonic acid metabolism.[78] Recently, the rather exciting characterization of flavoprotein FSP1 (formerly AIFM2) was shown to prevent lipid oxidation in a parallel pathway to GPX4. FSP1 suppresses ferroptosis by catalyzing the regeneration of CoQ10, a lipid-soluble RTA, using NADPH (**Figure 1.18.C**).[152]

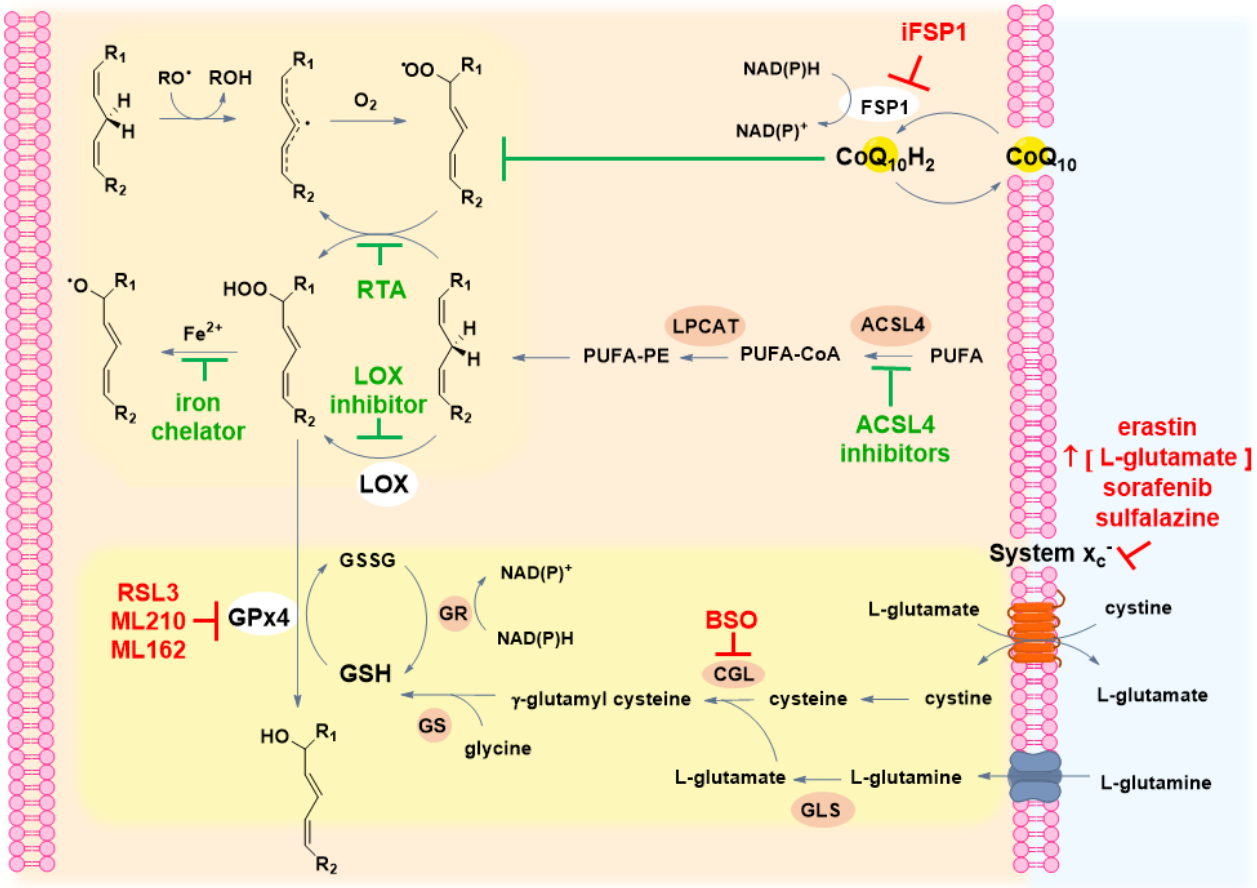

Figure 1.19 Cystine and glutamate are located in abundance in the intra- and extra- cellular space. In the presence of these amino acids, system x_c^-, a disulfide linked heterodimer, mediates the entry of cystine and exodus of L-glutamate. This exchange occurs in a 1:1 ratio.[146] Once inside, cystine is reduced to cysteine and undergoes a series of catalyzed reactions to form glutathione (GSH), the reducing cofactor of GPX4.[153] Lipid hydroperoxides are the product of radical mediated lipid peroxidation or lipoxygenase catalyzed deoxygenation. Lipid hydroperoxides can undergo Fenton chemistry in the presence of Iron $^{2+}$

species. Red text indicates pro-ferroptotic targets and the respective ferroptotic inducers. Green text indicates anti-ferroptotic targets. GLS: glutaminase, GR: Glutathione reductase, GS: Glutamine synthetase

There is precedent in the literature that loss of any part of this key cellular machinery poses a lethal threat to the cell. For instance, human fibroblasts exposed to cystine-free medium rapidly die, as cysteine is also a synthetic precursor to several thiol-containing proteins.[154] Likewise, neuron-specific GPX4 knockout mice and tam-inducible GPX4 knockout MEFs were reported to undergo an increase in lipid peroxidation, followed by cell death.[78] Glutathione is a necessity for cell survival, mice lacking the GSH-synthesizing enzyme, γ-glutamylcysteine synthetase (γ-GCS) died at the same developmental stage as GPX4 knockout mice.[78,155] And finally, loss of FSP1 also sensitized cancer cells to ferroptosis.[152]

1.5.2. Induction of Ferroptosis

The discovery that pharmacological intervention by a small molecule could be achieved provided crucial evidence that ferroptosis execution was not programmable. The first breakthrough, (*1S*,3*R*)-RSL3, was discovered in a screening assay for oncogene HRAS lethal molecules.[156] (*1S*,3*R*)-RSL3 was determined, using affinity based chemoproteomics, to covalently bind and inhibit selenoprotein GPX4, the cell's main defense for detoxifying lipid hydroperoxides.[140] Similar screening processes also identified two more GPX4inhibitors , ML210 and ML162.[157] More recent efforts lead to the discovery of FIN56, which promotes the degradation of GPX4 (**Figure 1.20**).[158]

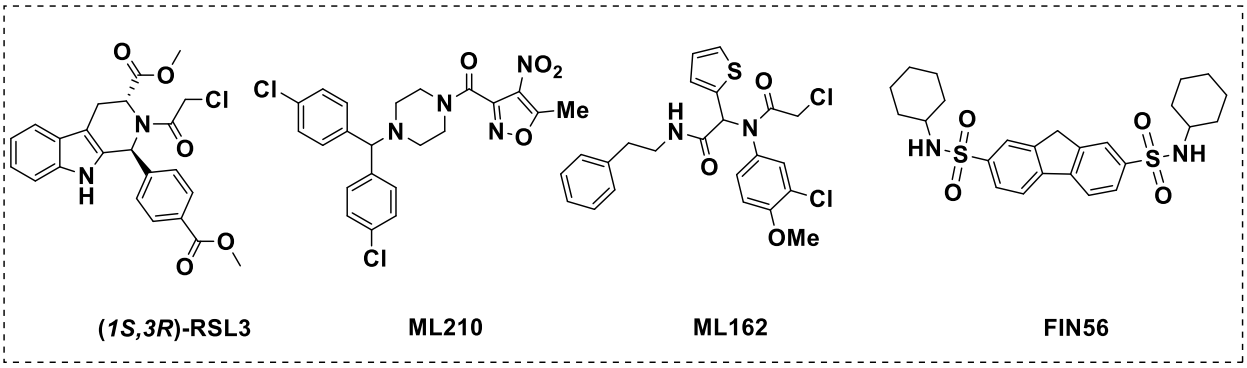

Figure 1.20 Small molecules that induce ferroptosis pharmacologically by inhibition of GPX4.

Another strategy targets the cystine glutamate antiporter, system x_c^- (**Figure 1.21**). Erastin was discovered from a 23,000-compound library in screening for cancer therapeutics; it modulates VDAC2/VDAC3 and disrupts the influx of cystine by inhibiting system x_c^-.[159] Erastin's toxic effects can be circumvented by supplementing the cell with GSH. Several other pharmacological inhibitors of system x_c^- have been discovered: sulfasalazine,[138] sorafenib,[160,161] and notably, increased concentrations of glutamate.[135]

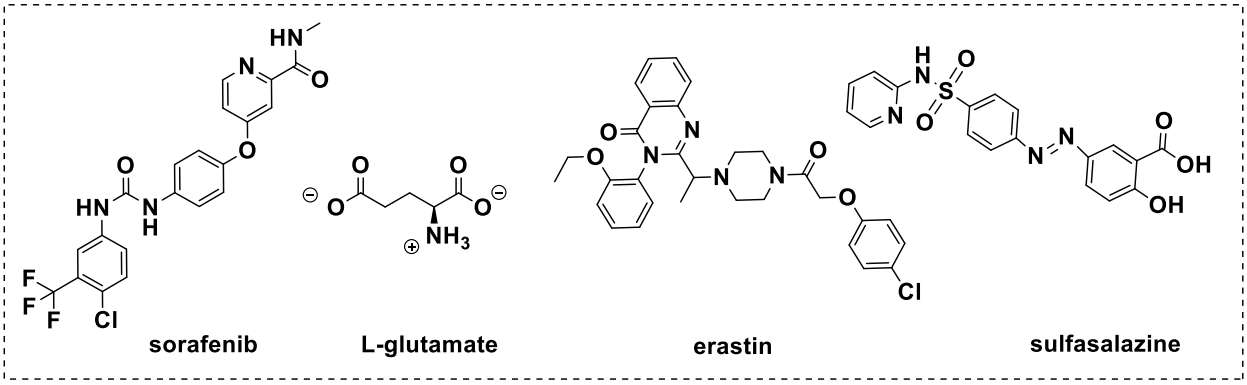

Figure 1.21 Small molecules that induce ferroptosis pharmacologically by inhibition of system x_c^-.

Ferroptosis can also be induced at alternative sites (**Figure 1.22**). Buthionine sulfoximine (BSO) inhibits the enzyme glutamate-cysteine ligase, thereby, disrupting synthesis of glutathione.[140] Inhibitor iFSP1 inhibits flavoprotein FSP1, an essential reducing agent for enzyme CoQ_{10}.[152] And, recently, the synthetic diterpene derivative, ferropticide, has been shown to be a potent ferroptosis inducer. Though

its mechanism has not yet been elucidated, the chloroacetyl group would suggest a mechanism of action to similar to RSL3 or ML162.[162] Ferroptosis can also be induced by genetic mediation targeting key genes involved in lipid metabolism, iron regulation and endogenous antioxidants. Previous reports targeted GPX4 using short hairpin RNA (shRNA) and short interference RNA (siRNA) to knockout the selenoenzyme in HT-1080 cells. Cell rescue could only be achieved following culture in medium supplemented with α-TOH and iron chelator, DFOM.[140]

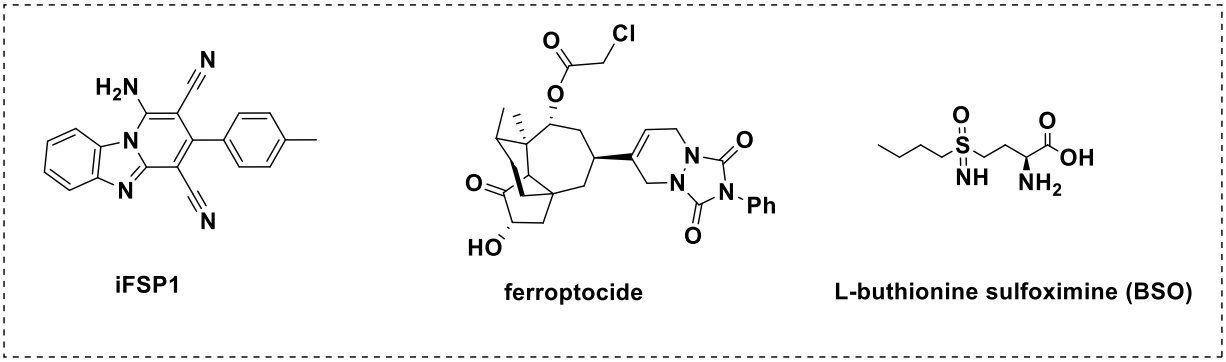

Figure 1.22 Small molecules that induce ferroptosis pharmacologically by alternative methods.

1.4.4. Inhibition of Ferroptosis

Given the recent characterization of ferroptotic cell death, extensive efforts are underway to discover potential ferroptosis inhibitors. Breakthrough screening of small molecule libraries have identified ferrostatin-1 (Fer-1) and liprostatin-1 (Lip-1), potent inhibitors of erastin induced cell death.[138,163] Research from our group has shown that both Lip-1 and Fer-1 are potent RTAs whose anti-ferroptotic activity steams from inhibiting lipid peroxidation.[112] Earlier investigations have established the potential of natural antioxidants as potential ferroptotic inhibitors (**Figure 1.23**). Polyphenols,[164] flavonoids and vitamin E analogs[165] are reported as effective agents against glutamate challenge. In particular, alpha tocopherol, the most active form of vitamin E, has been proven especially effective in vivo.[112,138,163] The vitamin E

scaffold has served an inspiration for synthetic derivatives such as the tetrahydronaphthyridinol motif (THNs). To date, THN derivatives are the most potent phenol-like antioxidants recorded[166] and make exceptionally efficient anti-ferroptotic agents.[112]

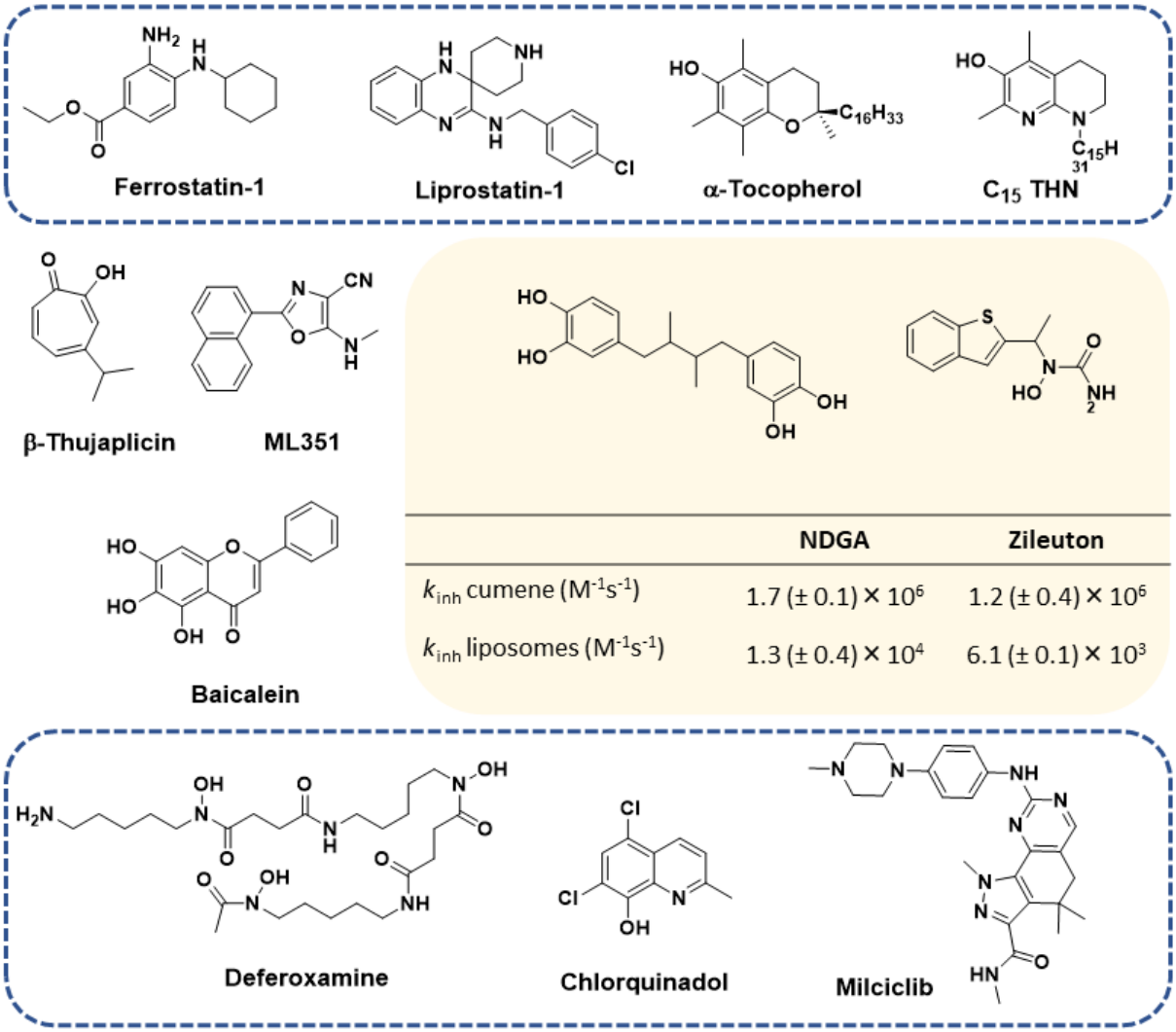

	NDGA	Zileuton
k_{inh} cumene ($M^{-1}s^{-1}$)	1.7 (± 0.1) × 10^6	1.2 (± 0.4) × 10^6
k_{inh} liposomes ($M^{-1}s^{-1}$)	1.3 (± 0.4) × 10^4	6.1 (± 0.1) × 10^3

Figure 1.23 Common anti-ferroptotic agents, antioxidants, lipoxygenase inhibitors and iron chelators. Redox activity for NDGA and Zileuton was accessed in inhibited co-autoxidations in cumene and liposomes, and corresponding rate constants were derived.[167]

There exists precedence in the literature that supports lipoxygenase inhibitors as cytoprotective agents against oxidative cell death (**Figure 1.23**). For example, 15-LOX-1 inhibitor ML351[121] was shown to

be protective against glutamate challenge in HT-22 cells. Furthermore, our group recently investigated a series of lipoxygenase inhibitors in HEK 293 cells transfected to overexpress either 5-LOX, p12-LOX or 15-LOX-1.[167] Therein, it was determined that pan-LOX inhibitor, NDGA, and 5h-LOX inhibitor Zileuton were effective at rescuing over-expressing HEK cells from ferroptosis due to their radical trapping activity (**Figure 1.23**).

Although the role of iron in ferroptosis is important, it is still poorly understood. Iron chelators such as deferoxamine have been reported as potent anti-ferroptotic agents against erastin challenge in HT-1080 cells[138,156] yet the molecule's mechanism of action still remains unknown. A recent compound library screen by Dixon et al, reported iron chelators chlorquinadol and milciclib as potentially effective ferroptosis inhibitors.[168]

Additionally, the replacement of reactive site, bis-allylic, positions on PUFAs with deuterium atoms (*d*-PUFA) was proposed by Shcheponov et al.[77] According to kinetic isotope theory, hydrogen atom abstraction occurs more rapidly than abstraction of heavy deuterium atoms, ultimately slowing the propagation of lipid oxidation.[169] Deuterated linoleic acid (11,11-d_2-LA) halts lipid peroxidation, and the kinetic isotope effect for propagation rate constant (k_p) of LA over deuterated substrate was reported as 12.8.[170] Remarkably, it has been observed that substituting with as little as 20% deuterated lipids provides protection against oxidative cell death.[167,170–172]

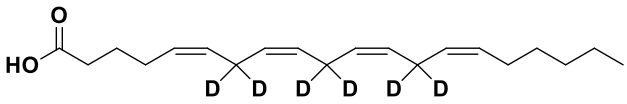

7,7,10,10,13,13-d_6-Arachidonic Acid

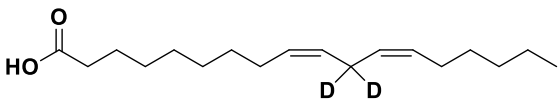

11,11-d_2-Linoleic Acid

1.6 Research Objectives

Ferroptosis, an apoptosis distinct, form of regulated cell death is marked by a lethal accumulation of lipid hydroperoxides.[138] Since its characterization, there has been lively debate regarding the origin of lipid hydroperoxides within the cell. A number of investigators have implicated lipoxygenases (LOX), enzymes that catalyze deoxygenation of PUFAs to corresponding lipid hydroperoxides.[78] The recent work by our group using 5-LOX, 12-LOX and 15-LOX-1-overexpressing HEK 293 cells suggest that LOX does not occupy a central role in regulated cell death, instead radical mediated lipid peroxidation, or, autoxidation is the central pathway responsible for driving ferroptosis,[167] but several questions remain unaddressed.

In this work, our group's previous investigations will be extended beyond transfected HEK 293 cells to include non-transfected cell lines that have been reported to express lipoxygenases. HT-22 and HT-1080 cells were selected as suitable models, as both are established cell lines in the field of ferroptosis and have been previously characterized to express LOX. Furthermore, 15-LOX-2 expression is linked to both model cell lines. A recent publication has implicated 15-LOX-2 and PEBP1, a RAF1 kinase inhibitory protein, as key mediators in ferropotitic cell death.[173] To probe the role of LOX in ferropotsis, in particular 15-LOX-2, in our selected model cell lines, the following research objectives were proposed;

1) Engineer HEK 293 cells to stably express 15-LOX-2, in order to evaluate its proposed role as a key mediator of ferroptotic cell death.
2) Expand the molecular library from 2018 work to include a more diverse range of LOX inhibitors, such as inhibitors of isoforms, p-12LOX, 15-LOX-1 and 15-LOX-2, as well as LOX inhibitors that display off-target RTA activity (ie: NDGA, Zileuton, PD146176 and baicalein).
3) Assess the anti-ferropotic potency of both RTAs and LOX inhibitors in selected model cell lines using multiple ferroptotic inducing agents.
4) Re-characterize established cell models HT-22 and HT-1080 for LOX expression.

1.7 References

1. Atkins, P. *Physical Chemistry*. (W. H. Freeman. & Co, 1997).
2. Chance, B., Sies, H. & Boveris, A. Hydroperoxide metabolism in mammalian organs. *Physiol. Rev.* **59**, 527–605 (1979).
3. McCord, J. M. & Fridovich, I. Superoxide Dismutase an Enzymic Function for Erythrocuprein (Hemocuprein). *J. Biol. Chem.* **244**, 6049–6055 (1969).
4. Fridovich, I. Superoxide Radical: An Endogenous Toxicant. *Annu. Rev. Pharmacol. Toxicol.* **23**, 239–257 (1983).
5. Haber, V. F. & WEiss, J. Ober die Katalyse des Hydroperoxydes. 3.
6. Halliwell, B. Oxidants and human disease: some new concepts. *FASEB J.* **1**, 358–364 (1987).
7. Kuwabara, M., Zhi-Yi, Z. & Yoshii, G. E.S.R. of Spin-trapped Radicals in Aqueous Solutions of Pyrimidine Nucleosides and Nucleotides. Reactions of the Hydroxyl Radical. *Int. J. Radiat. Biol. Relat. Stud. Phys. Chem. Med.* **41**, 241–259 (1982).
8. Moncada, S., Palmer, R. M. J. & Higgs, E. A. The discovery of nitric oxide as the endogenous nitrovasodilator. *Hypertension* **12**, 8 (1988).
9. Huie, R. E. & Padmaja, S. The Reaction of no With Superoxide. *Free Radic. Res. Commun.* **18**, 195–199 (1993).
10. Beckman, J. S., Beckman, T. W., Chen, J., Marshall, P. A. & Freeman, B. A. Apparent hydroxyl radical production by peroxynitrite: implications for endothelial injury from nitric oxide and superoxide. *Proc. Natl. Acad. Sci.* **87**, 1620–1624 (1990).
11. Freeman, B. & Crapo, J. Free Radicals and Tissue Injury. *Lab. Investig. J. Tech. Methods Pathol.* **47**, 412–26 (1982).
12. Meier, B. Radeke, H.; Selle, S.; Younes, M.; Sies, H.; Resch, K.; Habermehl, G.. Human fibroblasts release reactive oxygen species in response to interleukin-1 or tumour necrosis factor-α. *Biochem. J.* **263**, 539–545 (1989).
13. Vallet, P.;Charnay, Y.; Steger,K.; Ogier-Denis, E.; Kovari, E.; Herrmann, F.;Michel, J.P.; Szanto, I.; Neuronal expression of the NADPH oxidase NOX4, and its regulation in mouse experimental brain ischemia. *Neuroscience* **132**, 233–238 (2005).
14. Noble, M. A.; Munro, A.; Rivers, S.; Robledo, L.; Daff, S.; Yellowlees, L.; Shimizu, T.; Sagami, I.; Guillemette, J.; Chapman, S.; Potentiometric Analysis of the Flavin Cofactors of Neuronal Nitric Oxide Synthase. *Biochemistry* **38**, 16413–16418 (1999).
15. Stuehr, D., Pou, S. & Rosen, G. M. Oxygen Reduction by Nitric-oxide Synthases. *J. Biol. Chem.* **276**, 14533–14536 (2001).
16. Fridovich, I. Superoxide radical and superoxide dismutase. *Acc. Chem. Res.* 6 14533 - 14536 (1971).
17. Capdevila, J. *et al.* The oxidative metabolism of arachidonic acid by purified cytochromes P-450. *Biochem. Biophys. Res. Commun.* **101**, 1357–1363 (1981).
18. Brash, A. R. Lipoxygenases: Occurrence, Functions, Catalysis, and Acquisition of Substrate. *J. Biol. Chem.* **274**, 23679–23682 (1999).

19. Babior, B. M. NADPH oxidase: an update. *Blood* **93** 1464 – 1476 (1999)

20. Förstermann, U. & Sessa, W. C. Nitric oxide synthases: regulation and function. *Eur. Heart J.* **33**, 829–837 (2012).

21. Okamoto, K., Kusano, T. & Nishino, T. Chemical Nature and Reaction Mechanisms of the Molybdenum Cofactor of Xanthine Oxidoreductase. *Curr. Pharm. Des.* **19**, 2606–2614 (2013).

22. Boveris, A. & Cadenas, E. Mitochondrial production of superoxide anions and its relationship to the antimycin insensitive respiration. *FEBS Lett.* **54**, 311–314 (1975).

23. Dionisi, O., Galeotti, T., Terranova, T. & Azzi, A. Superoxide radicals and hydrogen peroxide formation in mitochondria from normal and neoplastic tissues. *Biochim. Biophys. Acta BBA - Enzymol.* **403**, 292–300 (1975).

24. Chen, Q., Vazquez, E. J., Moghaddas, S., Hoppel, C. L. & Lesnefsky, E. J. Production of Reactive Oxygen Species by Mitochondria: CENTRAL ROLE OF COMPLEX III*. *J. Biol. Chem.* **278**, 36027–36031 (2003).

25. Yin, H., Xu, L. & Porter, N. A. Free Radical Lipid Peroxidation: Mechanisms and Analysis. *Chem. Rev.* **111**, 5944–5972 (2011).

26. Bochkov, V. N. *et al.* Generation and Biological Activities of Oxidized Phospholipids. *Antioxid. Redox Signal.* **12**, 1009–1059 (2009).

27. Imai, Y. *et al.* Identification of Oxidative Stress and Toll-like Receptor 4 Signaling as a Key Pathway of Acute Lung Injury. *Cell* **133**, 235–249 (2008).

28. Nonas, S. *et al.* Oxidized Phospholipids Reduce Vascular Leak and Inflammation in Rat Model of Acute Lung Injury. *Am. J. Respir. Crit. Care Med.* **173**, 1130–1138 (2006).

29. Berliner, J. A. & Heinecke, J. W. The role of oxidized lipoproteins in atherogenesis. *Free Radic. Biol. Med.* **20**, 707–727 (1996).

30. Beckmann, J. S. *et al.* Extensive Nitration of Protein Tyrosines in Human Atherosclerosis Detected by Immunohistochemistry. *Biol. Chem.* **375**, 81–88 (1994).

31. Leeuwenburgh, C. *et al.* Reactive Nitrogen Intermediates Promote Low Density Lipoprotein Oxidation in Human Atherosclerotic Intima. *J. Biol. Chem.* **272**, 1433–1436 (1997).

32. Lee, C.-Y. J., Seet, R. C. S., Huang, S. H., Long, L. H. & Halliwell, B. Different Patterns of Oxidized Lipid Products in Plasma and Urine of Dengue Fever, Stroke, and Parkinson's Disease Patients: Cautions in the Use of Biomarkers of Oxidative Stress. *Antioxid. Redox Signal.* **11**, 407–420 (2008).

33. Fukai, M. *et al.* Lipid peroxidation during ischemia depends on ischemia time in warm ischemia and reperfusion of rat liver. *Free Radic. Biol. Med.* **38**, 1372–1381 (2005).

34. Wu, R. P. *et al.* Nrf2 responses and the therapeutic selectivity of electrophilic compounds in chronic lymphocytic leukemia. *Proc. Natl. Acad. Sci.* **107**, 7479–7484 (2010).

35. Silverstein, R. L. & Febbraio, M. CD36, a Scavenger Receptor Involved in Immunity, Metabolism, Angiogenesis, and Behavior. *Sci. Signal.* **2**, re3–re3 (2009).

36. Porter, F. D. *et al.* Cholesterol Oxidation Products Are Sensitive and Specific Blood-Based Biomarkers for Niemann-Pick C1 Disease. *Sci. Transl. Med.* **2**, 56ra81-56ra81 (2010).

37. Montine, T. J. *et al.* F2-Isoprostanes in Alzheimer and Other Neurodegenerative Diseases. *Antioxid. Redox Signal.* **7**, 269–275 (2004).

38. Israelachvili, J. N., Mitchell, D. J. & Ninham, B. W. Theory of self-assembly of lipid bilayers and vesicles. *Biochim. Biophys. Acta BBA - Biomembr.* **470**, 185–201 (1977).

39. Watson, A. D. *Thematic review series: Systems Biology Approaches to Metabolic and Cardiovascular Disorders.* Lipidomics: a global approach to lipid analysis in biological systems. *J. Lipid Res.* **47**, 2101–2111 (2006).

40. Wenk, M. R. The emerging field of lipidomics. *Nat. Rev. Drug Discov.* **4**, 594–610 (2005).

41. Porter, N. A., Mills, K. A. & Carter, R. L. A Mechanistic Study of Oleate Autoxidation: Competing Peroxyl H-Atom Abstraction and Rearrangement. *J. Am. Chem. Soc.* **116**, 6690–6696 (1994).

42. Sabatini, K., Mattila, J.-P., Megli, F. M. & Kinnunen, P. K. J. Characterization of Two Oxidatively Modified Phospholipids in Mixed Monolayers with DPPC. *Biophys. J.* **90**, 4488–4499 (2006).

43. Boulanger Chantal M., Amabile Nicolas, & Tedgui Alain. Circulating Microparticles. *Hypertension* **48**, 180–186 (2006).

44. Dobretsov, G. E., Borschevskaya, T. A., Petrov, V. A. & Vladimirov, Yu. A. The increase of phospholipid bilayer rigidity after lipid peroxidation. *FEBS Lett.* **84**, 125–128 (1977).

45. Megli, F. M. & Sabatini, K. Respiration state IV-generated ROS destroy the mitochondrial bilayer packing order in vitro. An EPR study. *FEBS Lett.* **550**, 185–189 (2003).

46. Porter, N. A., Caldwell, S. E. & Mills, K. A. Mechanisms of free radical oxidation of unsaturated lipids. *Lipids* **30**, 277–290 (1995).

47. Cooper, H. R. & Melville, H. W. 444. The kinetics of the autoxidation of n-decanal. Part I. The mechanism of reaction. *J Chem Soc* 1984–1993 (1951).

48. Bateman, L. Olefin oxidation. *Q. Rev. Chem. Soc.* **8**, 147–167 (1954).

49. Jensen, R. K., Korcek, S., Zinbo, M. & Johnson, M. D. Initiation in hydrocarbon autoxidation at elevated temperatures. *Int. J. Chem. Kinet.* **22**, 1095–1107 (1990).

50. Noguchi, N. *et al.* 2,2′-Azobis (4-Methoxy-2,4-Dimethylvaleronitrile), a New Lipid-Soluble Azo Initiator: Application to Oxidations of Lipids and Low-Density Lipoprotein in Solution and in Aqueous Dispersions. *Free Radic. Biol. Med.* **24**, 259–268 (1998).

51. Culbertson, S. M., Vinqvist, M. R., Barclay, L. R. C. & Porter, N. A. Minimizing Tocopherol-Mediated Radical Phase Transfer in Low-Density Lipoprotein Oxidation with an Amphiphilic Unsymmetrical Azo Initiator. *J. Am. Chem. Soc.* **123**, 8951–8960 (2001).

52. Maillard, B., Ingold, K. U. & Scaiano, J. C. Rate constants for the reactions of free radicals with oxygen in solution. *J. Am. Chem. Soc.* **105**, 5095–5099 (1983).

53. Russell, G. A. The Rates of Oxidation of Aralkyl Hydrocarbons. Polar Effects in Free Radical Reactions [1,2]. *J. Am. Chem. Soc.* **78**, 1047–1054 (1956).

54. Huang, R. L. & Singh, S. 172. The relative stabilising influences of substituents on free alkyl radicals. Part IV. Selective hydrogen-abstraction by free tert.-butoxy-radicals. *J. Chem. Soc. Resumed* 891–895 (1958).

55. Howard, J. A. & Ingold, K. U. Absolute rate constants for hydrocarbon autoxidation. VI. Alkyl aromatic and olefinic hydrocarbons. *Can. J. Chem.* **45**, 793–802 (1967).

56. Xu, L., Davis, T. A. & Porter, N. A. Rate Constants for Peroxidation of Polyunsaturated Fatty Acids and Sterols in Solution and in Liposomes. *J. Am. Chem. Soc.* **131**, 13037–13044 (2009).

57. Zielinski, Z. A. M. & Pratt, D. A. Lipid Peroxidation: Kinetics, Mechanisms, and Products. *J. Org. Chem.* **82**, 2817–2825 (2017).

58. Pratt, D. A., Mills, J. H. & Porter, N. A. Theoretical Calculations of Carbon−Oxygen Bond Dissociation Enthalpies of Peroxyl Radicals Formed in the Autoxidation of Lipids. *J. Am. Chem. Soc.* **125**, 5801–5810 (2003).

59. Porter, N. A., Weber, B. A., Weenen, H. & Khan, J. A. Autoxidation of polyunsaturated lipids. Factors controlling the stereochemistry of product hydroperoxides. *J. Am. Chem. Soc.* **102**, 5597–5601 (1980).

60. Yin, H., Brooks, J. D., Gao, L., Porter, N. A. & Morrow, J. D. Identification of Novel Autoxidation Products of the ω-3 Fatty Acid Eicosapentaenoic Acid *in Vitro* and *in Vivo*. *J. Biol. Chem.* **282**, 29890–29901 (2007).

61. Funk, M. O., Isaac, R. & Porter, N. A. Free radical cyclization of unsaturated hydroperoxides. *J. Am. Chem. Soc.* **97**, 1281–1282 (1975).

62. Needleman, P. *et al.* Identification of an enzyme in platelet microsomes which generates thromboxane A 2 from prostaglandin endoperoxides. *Nature* **261**, 558–560 (1976).

63. Funk, C. D. Prostaglandins and Leukotrienes: Advances in Eicosanoid Biology. *Science* **294**, 1871–1875 (2001).

64. Waugh, R. J., Morrow, J. D., Roberts, L. J. & Murphy, R. C. Identification and Relative Quantitation of F2-Isoprostane Regioisomers Formed in vivo in the Rat. *Free Radic. Biol. Med.* **23**, 943–954 (1997).

65. Yin, H., Porter, N. A. & Morrow, J. D. Separation and identification of F2-isoprostane regioisomers and diastereomers by novel liquid chromatographic/mass spectrometric methods. *J. Chromatogr. B* **827**, 157–164 (2005).

66. Ingold, K. U. Inhibition of the Autoxidation of Organic Substances in the Liquid Phase. *Chem. Rev.* **61**, 563–589 (1961).

67. Howard, J. A. & Ingold, K. U. Absolute Rate Constants for Hydrocarbon Autoxidation: I. Styrene. *Can. J. Chem.* **43**, 2729–2736 (1965).

68. Lee, R., Gryn'ova, G., Ingold, K. U. & Coote, M. L. Why are sec-alkylperoxyl bimolecular self-reactions orders of magnitude faster than the analogous reactions of tert-alkylperoxyls? The unanticipated role of CH hydrogen bond donation. *Phys. Chem. Chem. Phys.* **18**, 23673–23679 (2016).

69. Russell, G. A. Deuterium-isotope Effects in the Autoxidation of Aralkyl Hydrocarbons. Mechanism of the Interaction of PEroxy Radicals [1]. *J. Am. Chem. Soc.* **79**, 3871–3877 (1957).

70. Blanchard, H. S. A Study of the Mechanism of Cumene Autoxidation. Mechanism of the Interaction of t-Peroxy Radicals1. *J. Am. Chem. Soc.* **81**, 4548–4552 (1959).

71. Howard, J. A., Adamic, K. & Ingold, K. U. Absolute rate constants for hydrocarbon autoxidation. XIV. Termination rate constants for tertiary peroxy radicals. *Can. J. Chem.* **47**, 3793–3795 (1969).

72. Funk, C. D., Chen, X.-S., Johnson, E. N. & Zhao, L. Lipoxygenase genes and their targeted disruption. *Prostaglandins Other Lipid Mediat.* **68–69**, 303–312 (2002).

73. Samuelsson, B. Leukotrienes: mediators of immediate hypersensitivity reactions and inflammation. *Science* **220**, 568–575 (1983).

74. Samuelsson, B., Dahlen, S. E., Lindgren, J. A., Rouzer, C. A. & Serhan, C. N. Leukotrienes and lipoxins: structures, biosynthesis, and biological effects. *Science* **237**, 1171–1176 (1987).

75. Ford-Hutchinson, A. W. Inhibition of Leukotriene Biosynthesis. *Ann. N. Y. Acad. Sci.* **629**, 133–142 (1991).

76. Kagan, V. E. Mao, G.; Qu, F.; Friedmann Angeli, J.P.; Doll, S.; St Croix, C.; Dar, H.; Liu, B.; Tyurin, V.; Ritov, V.; Kapralov, A.; Amoscato, A.; Jiang, J.; Anthonymuthu, T.; Mohammadyani, D.; Yang, Q.; Proneth, B.; Seetharaman, J.K.; Watkins, S.; Bahar, I.; Greenberger, J.; Mallampalli, R.K.; Stockwell, B.; Tyurina, Y.Y.; Conrad, M.; Byair, H.. Oxidized arachidonic and adrenic PEs navigate cells to ferroptosis. *Nat. Chem. Biol.* **13**, 81–90 (2017).

77. Yang, W. S. Kim, K.; Gaschler, M.; Patel, M.; Shchepinov, M.; Stockwell, B.. Peroxidation of polyunsaturated fatty acids by lipoxygenases drives ferroptosis. *Proc. Natl. Acad. Sci.* **113**, E4966–E4975 (2016).

78. Seiler, A. Schneider, M.; Förster, H.; Roth, S.; Wirth, E.; Culmsee, C.; Plesnila, N.; Kremmer, E.; Rådmark, O.; Wurst, W.; Bornkamm, G.; Schweizer, U.; Conrad, M. Glutathione Peroxidase 4 Senses and Translates Oxidative Stress into 12/15-Lipoxygenase Dependent- and AIF-Mediated Cell Death. *Cell Metab.* **8**, 237–248 (2008).

79. van Leyen, K. Lipoxygenase: An Emerging Target for Stroke Therapy. *CNS Neurol. Disord. Drug Targets* **12**, 191–199 (2013).

80. Kühn, H., Belkner, J., Zaiss, S., Fährenklemper, T. & Wohlfeil, S. Involvement of 15-lipoxygenase in early stages of atherogenesis. *J. Exp. Med.* **179**, 1903–1911 (1994).

81. Kuhn, H., Banthiya, S. & van Leyen, K. Mammalian lipoxygenases and their biological relevance. *Biochim. Biophys. Acta BBA - Mol. Cell Biol. Lipids* **1851**, 308–330 (2015).

82. Rådmark, O. & Samuelsson, B. 5-Lipoxygenase: Regulation and possible involvement in atherosclerosis. *Prostaglandins Other Lipid Mediat.* **83**, 162–174 (2007).

83. Brash, A. R., Boeglin, W. E. & Chang, M. S. Discovery of a second 15S-lipoxygenase in humans. *Proc. Natl. Acad. Sci.* **94**, 6148–6152 (1997).

84. Funk, C. D., Furci, L. & FitzGerald, G. A. Molecular cloning, primary structure, and expression of the human platelet/erythroleukemia cell 12-lipoxygenase. *Proc. Natl. Acad. Sci.* **87**, 5638–5642 (1990).

85. Hammarström, S. Lindgren, J.; Marcelo, C.; Dueli, E.; Anderson, T.; Voorhees, J. Arachidonic Acid Transformations in Normal and Psoriatic Skin. *J. Invest. Dermatol.* **73**, 180–183 (1979).

86. Sigal, E.; Grunberger, D.; Cashman, J.R.; Craik, C.; Caughey, G.; Nadel, J.; Arachidonate 15-lipoxygenase from human eosinophil-enriched leukocytes: Partial purification and properties. *Biochem. Biophys. Res. Commun.* **150**, 376–383 (1988).

87. Ivanov, I., Kuhn, H. & Heydeck, D. Structural and functional biology of arachidonic acid 15-lipoxygenase-1 (ALOX15). *Gene* **573**, 1–32 (2015).

88. Wittwer, J. & Hersberger, M. The two faces of the 15-lipoxygenase in atherosclerosis. *Prostaglandins Leukot. Essent. Fatty Acids* **77**, 67–77 (2007).

89. Feussner, I., Kühn, H. & Wasternack, C. Do specific linoleate 13-lipoxygenases initiate β-oxidation? 1. *FEBS Lett.* **406**, 1–5 (1997).

90. Haeggström, J. Z. & Funk, C. D. Lipoxygenase and Leukotriene Pathways: Biochemistry, Biology, and Roles in Disease. *Chem. Rev.* **111**, 5866–5898 (2011).

91. Minor, W.; Steczko, J.; Stec, B.; Otwinowski, Z.; Bolin, J.; Walter, R.; Axelrod, B. Crystal Structure of Soybean Lipoxygenase L-1 at 1.4 Å Resolution. *Biochemistry* **35**, 10687–10701 (1996).

92. Skrzypczak-jankun, E., Amzel, L. M., Kroa, B. A. & Funk, M. O. Structure of soybean lipoxygenase L3 and a comparison with its L1 isozyme. Proteins. *Proteins Struct. Funct. Genet.* **29**, 15 (1997).

93. Gillmor, S. A., Villaseñor, A., Fletterick, R., Sigal, E. & Browner, M. F. The structure of mammalian 15-lipoxygenase reveals similarity to the lipases and the determinants of substrate specificity. *Nat. Struct. Biol.* **4**, 1003–1009 (1997).

94. Gilbert, N. C.; Bartlett, S.; Waight, M.; Neau, D.; Boeglin, W.; Brash, A.; Newcomer, M. The structure of human 5-lipoxygenase. *Science* **331**, 217–219 (2011).

95. Kuban, R. J.; Rathman, J.; Veldink, G.; Nolting, H.; Solé, V.A.; Kühn, H. The iron ligand sphere geometry of mammalian 15-lipoxygenases. *Biochem. J.* **332**, 237–242 (1998).

96. Ivanov, I.; Heydeck, D.; Hofheinz, K.; Roffeis, J.; O'Donnell, V.;Kuhn, H.; Walther, M. Molecular enzymology of lipoxygenases. *Arch. Biochem. Biophys.* **503**, 161–174 (2010).

97. Scarrow, R. C.; Trimitsis, M.; Buck, C.; Grove, G.; Cowling, R.; Nelson, M. X-ray Spectroscopy of the Iron Site in Soybean Lipoxygenase-1: Changes in Coordination upon Oxidation or Addition of Methanol. *Biochemistry* **33**, 15023–15035 (1994).

98. Glickman, M. H. & Klinman, J. P. Nature of rate-limiting steps in the soybean lipoxygenase-1 reaction. *Biochemistry* **34**, 14077–14092 (1995).

99. Glickman, M. H. & Klinman, J. P. Lipoxygenase Reaction Mechanism: Demonstration That Hydrogen Abstraction from Substrate Precedes Dioxygen Binding during Catalytic Turnover †. *Biochemistry* **35**, 12882–12892 (1996).

100. Lehnert, N. & Solomon, E. I. Density-functional investigation on the mechanism of H-atom abstraction by lipoxygenase. *JBIC J. Biol. Inorg. Chem.* **8**, 294–305 (2003).

101. Knapp, M. J. & Klinman, J. P. Kinetic Studies of Oxygen Reactivity in Soybean Lipoxygenase-1. *Biochemistry* **42**, 11466–11475 (2003).

102. Corey, E. J. & Nagata, R. Evidence in favor of an organoiron-mediated pathway for lipoxygenation of fatty acids by soybean lipoxygenase. *J. Am. Chem. Soc.* **109**, 8107–8108 (1987).

103. Nelson, M. J., Cowling, R. A. & Seitz, S. P. Structural Characterization of Alkyl and Peroxyl Radicals in Solutions of Purple Lipoxygenase. *Biochemistry* **33**, 4966–4973 (1994).

104. Foti, M. C. Antioxidant properties of phenols. *J. Pharm. Pharmacol.* **59**, 1673–1685 (2007).

105. Howard, J. A. & Ingold, K. U. The Inhibited Autoxidation of Styrene: Part I. The Deuterium Isotope Effect for Inhibition by 2,6-di-tert-butyl-4-methylphenol. *Can. J. Chem.* **40**, 1851–1864 (1962).

106. Burton, G. W. & Ingold, K. U. Vitamin E: application of the principles of physical organic chemistry to the exploration of its structure and function. *Acc. Chem. Res.* **19**, 194–201 (1986).

107. Burton, G. W.; Doba, T.; Gabe, E.J.; Hughes, L.; Lee, F.L.; Prasad, L.; Ingold, K. Autoxidation of biological molecules. 4. Maximizing the antioxidant activity of phenols. *J. Am. Chem. Soc.* **107**, 7053–7065 (1985).

108. Mayer, J. M., Hrovat, D. A., Thomas, J. L. & Borden, W. T. Proton-Coupled Electron Transfer versus Hydrogen Atom Transfer in Benzyl/Toluene, Methoxyl/Methanol, and Phenoxyl/Phenol Self-Exchange Reactions. *J. Am. Chem. Soc.* **124**, 11142–11147 (2002).

109. Litwinienko, G. & Ingold, K. U. Solvent Effects on the Rates and Mechanisms of Reaction of Phenols with Free Radicals. *Acc. Chem. Res.* **40**, 222–230 (2007).

110. Ingold, K. U. & Pratt, D. A. Advances in Radical-Trapping Antioxidant Chemistry in the 21st Century: A Kinetics and Mechanisms Perspective. *Chem. Rev.* **114**, 9022–9046 (2014).

111. Pratt, D. A., DiLabio, G. A., Mulder, P. & Ingold, K. U. Bond Strengths of Toluenes, Anilines, and Phenols: To Hammett or Not. *Acc. Chem. Res.* **37**, 334–340 (2004).

112. Zilka, O.; Shah, R.; Li, B.; Friedmann Angeli, J.P.; Griesser, M.; Conrad, M.; Pratt, D. On the Mechanism of Cytoprotection by Ferrostatin-1 and Liproxstatin-1 and the Role of Lipid Peroxidation in Ferroptotic Cell Death. *ACS Cent. Sci.* **3**, 232–243 (2017).

113. Brown, H. C. & Okamoto, Y. Electrophilic Substituent Constants. *J. Am. Chem. Soc.* **80**, 4979–4987 (1958).

114. Wayner, D. D. M.; Lusztyk, E.; Ingold, K.; Mulder, P.; Laarhoven, L.J.J.; Aldrich, H.S. Effects of Solvation on the Enthalpies of Reaction of tert-Butoxyl Radicals with Phenol and on the Calculated O-H Bond Strength in Phenol. *J. Am. Chem. Soc.* **117**, 8737–8744 (1995).

115. Lucarini, M., Mugnaini, V., Pedulli, G. F. & Guerra, M. Hydrogen-Bonding Effects on the Properties of Phenoxyl Radicals. An EPR, Kinetic, and Computational Study. *J. Am. Chem. Soc.* **125**, 8318–8329 (2003).

116. Abraham, M. H., Grellier, P. L., Prior, D. V., Morris, J. J. & Taylor, P. J. Hydrogen Bonding. Part 10.t A Scale of Solute Hydrogen-bond Basicity using log K Values for Complexation in Tetrachloromethane. *J. Chem. Soc. Perkins. Trans.* **2** 521 (1990).

117. Abraham, M. H.; Grellier, P.; Prior, D.; Duce, P.; Hydrogen bonding. Part 7. A scale of solute hydrogen-bond acidity based on log K values for complexation in tetrachloromethane. *J. Chem. Soc. Perkin Trans. 2* 699 (1989)

118. Steinberg, D., Parthasarathy, S., Carew, T. E., Khoo, J. C. & Witztum, J. L. Beyond Cholesterol. *N. Engl. J. Med.* **320**, 915–924 (1989).

119. Hangauer, M. J.; Viswanathan, V.; Ryan, M.; Bole, D.; Eaton, J.; Matov, A.; Galeas, J.; Dhruv, H.; Berens, M.; Schreiber, S.; McCormick, F.; McManus, M. Drug-tolerant persister cancer cells are vulnerable to GPX4 inhibition. *Nature* **551**, 247–250 (2017).

120. Jiang, Z.-Y., Woollard, A. C. S. & Wolff, S. P. Lipid hydroperoxide measurement by oxidation of Fe2+ in the presence of xylenol orange. Comparison with the TBA assay and an iodometric method. *Lipids* **26**, 853–856 (1991).

121. Rai, G.; Kenyon, V.; Jadhav, A.; Schultz, L.; Armstrong, M.; Jameson II, J.B.; Hoobler, E.; Leister, W.; Simeonov, A.; Holman, T.; Maloney, D. Discovery of Potent and Selective Inhibitors of Human Reticulocyte 15-Lipoxygenase-1. *J. Med. Chem.* **53**, 7392–7404 (2010).

122. Kenyon, V.; Rai, G.; Jadhav, A.; Schultz, L.; Armstrong, M.; Jameson II, J.B.; Perry, S.; Josh, N.; Bougie, J.; Leister, W.; Taylor-Fishwick, D.; Nadler, J.; Holinstat, M.; Simeonov, A.; Maloney, D.; Holman, T. Discovery of Potent and Selective Inhibitors of Human Platelet type 12-Lipoxygenase. *J. Med. Chem.* **54**, 5485–5497 (2011).

123. Jameson II, J. B.; Kantz, A.; Schultz, L.; Kalyanaraman, C.; Jacobson, M.; Maloney, D.; Jadhav, A.; Simeonov, A.; Holman, T. A High Throughput Screen Identifies Potent and Selective Inhibitors to Human Epithelial 15-Lipoxygenase-2. *PLoS ONE* **9**, e104094 (2014).

124. Berger, W., Chandt, M. T. M. D. & Cairns, C. B. Zileuton: clinical implications of 5-Lipoxygenase inhibition in severe airway disease. *Int. J. Clin. Pract.* **61**, 663–676 (2007).

125. Lu, P.; Schrag, M.; Slaughter, D.; Raab, C.; Shou, M.; Rodrigues, D. Mechanism-Based Inhibition of Human Liver Microsomal Cytochrome P450 1a2 by Zileuton, a 5-Lipoxygenase Inhibitor. *Drug Metab. Dispos.* **31**, 1352–1360 (2003).

126. McMillan, R. M., Masters, D. J., Sterling, W. W. & Bernstein, P. R. Biosynthesis of Leukotriene B4 in Human Leukocytes. in *Prostaglandins, Leukotrienes, and Lipoxins: Biochemistry, Mechanism of Action, and Clinical Applications* (Ed. Bailey, J. M.) 655–668 (Springer US, 1985).

127. Ishiura, S., Yoshimoto, T. & Villee, C. A. Reticulocyte lipoxygenase, ingensin, and ATP-dependent proteolysis. *FEBS Lett.* **201**, 87–93 (1986).

128. Whitman, S., Gezginci, M., Timmermann, B. N. & Holman, T. R. Structure−Activity Relationship Studies of Nordihydroguaiaretic Acid Inhibitors toward Soybean, 12-Human, and 15-Human Lipoxygenase. *J. Med. Chem.* **45**, 2659–2661 (2002).

129. Kemal, C., Louis-Flamberg, P., Krupinski-Olsen, R. & Shorter, A. L. Reductive inactivation of soybean lipoxygenase 1 by catechols: a possible mechanism for regulation of lipoxygenase activity. *Biochemistry* **26**, 7064–7072 (1987).

130. Lucas, D. R. & Newhouse, J. P. The Toxic Effect of Sodium L-Glutamate on the Inner Layers of the Retina. *AMA Arch. Ophthalmol.* **58**, 193–201 (1957).

131. Rothman, S. M. & Olney, J. W. Glutamate and the pathophysiology of hypoxic–ischemic brain damage. *Ann. Neurol.* **19**, 105–111 (1986).

132. Olney, J. W. Inciting Excitotoxic Cytocide Among Central Neurons. in *Excitatory Amino Acids and Epilepsy* (eds. Schwarcz, R. & Ben-Ari, Y.) 631–645 (Springer US, 1986).

133. Choi, D. W. Glutamate neurotoxicity and diseases of the nervous system. *Neuron* **1**, 623–634 (1988).

134. Murphy, T. H., Miyamoto, M., Sastre, A., Schnaar, R. L. & Coyle, J. T. Glutamate toxicity in a neuronal cell line involves inhibition of cystine transport leading to oxidative stress. *Neuron* **2**, 1547–1558 (1989).

135. Tan, S., Wood, M. & Maher, P. Oxidative Stress Induces a Form of Programmed Cell Death with Characteristics of Both Apoptosis and Necrosis in Neuronal Cells. *J. Neurochem.* **71**, 95–105 (1998).

136. Maher, P. & Davis, J. B. The Role of Monoamine Metabolism in Oxidative Glutamate Toxicity. *J. Neurosci.* **16**, 6394–6401 (1996).

137. Davis, J. B. & Maher, P. Protein kinase C activation inhibits glutamate-induced cytotoxicity in a neuronal cell line. *Brain Res.* **652**, 169–173 (1994).

138. Dixon, S. J. *et al.* Ferroptosis: An Iron-Dependent Form of Non-Apoptotic Cell Death. *Cell* **149**, 1060–1072 (2012).

139. Angeli, J. P. F., Shah, R., Pratt, D. A. & Conrad, M. Ferroptosis Inhibition: Mechanisms and Opportunities. *Trends Pharmacol. Sci.* **38**, 489–498 (2017).

140. Yang, W. S. *et al.* Regulation of Ferroptotic Cancer Cell Death by GPX4. *Cell* **156**, 317–331 (2014).

141. Küch, E.-M. *et al.* Differentially localized acyl-CoA synthetase 4 isoenzymes mediate the metabolic channeling of fatty acids towards phosphatidylinositol. *Biochim. Biophys. Acta BBA - Mol. Cell Biol. Lipids* **1841**, 227–239 (2014).

142. Soupene, E., Fyrst, H. & Kuypers, F. A. Mammalian acyl-CoA:lysophosphatidylcholine acyltransferase enzymes. *Proc. Natl. Acad. Sci.* **105**, 88–93 (2008).

143. Galluzzi, L. *et al.* Cell death modalities: classification and pathophysiological implications. *Cell Death Differ.* **14**, 1237–1243 (2007).

144. Kerr, J. F. R., Wyllie, A. H. & Currie, A. R. Apoptosis: A Basic Biological Phenomenon with Wide-ranging Implications in Tissue Kinetics. *Br. J. Cancer* **26**, 239–257 (1972).

145. Golstein, P. & Kroemer, G. Cell death by necrosis: towards a molecular definition. *Trends Biochem. Sci.* **32**, 37–43 (2007).

146. Bannai, S. Exchange of cystine and glutamate across plasma membrane of human fibroblasts. *J. Biol. Chem.* **261**, 2256–2263 (1986).

147. Fedorcsák, I., Harms-Ringdahl, M. & Ehrenberg, L. Prevention of sulfhydryl autoxidation by a polypeptide from red kidney beans, described to be a stimulator of RNA synthesis. *Exp. Cell Res.* **108**, 331–339 (1977).

148. Yant, L. J. *et al.* The selenoprotein GPX4 is essential for mouse development and protects from radiation and oxidative damage insults. *Free Radic. Biol. Med.* **34**, 496–502 (2003).

149. Roveri, A., Maiorino, M., Nisii, C. & Ursini, F. Purification and characterization of phospholipid hydroperoxide glutathione peroxidase from rat testis mitochondrial membranes. *Biochim. Biophys. Acta BBA - Protein Struct. Mol. Enzymol.* **1208**, 211–221 (1994).

150. Thomas, J. P., Geiger, P. G., Maiorino, M., Ursini, F. & Girotti, A. W. Enzymatic reduction of phospholipid and cholesterol hydroperoxides in artificial bilayers and lipoproteins. *Biochim. Biophys. Acta BBA - Lipids Lipid Metab.* **1045**, 252–260 (1990).

151. Ingold, I.; Berndt, C.; Schmitt, S.; Doll, S.; Poschmann, G.; Buday, K.; Roveri, A.; Peng, X.; Freitas, F.; Seibt, T.; Mehr, L.; Aichler, M.; Walch, A.; Lamp, D.; Jastroch, M.; Miyamoto, S.; Wurst, W.; Ursini, F.; Arnér, E.; Fradejas-Villar, N.; Schweizer, U.; Zischka, H.; Freidmann Angeli, J.P.; Conrad, M. Selenium Utilization by GPX4 Is Required to Prevent Hydroperoxide-Induced Ferroptosis. *Cell* **172**, 409-422.e21 (2018).

152. Doll, S.; Freitas, F.; Shah, R.; Aldrovandi, M.; Costa da Silva, M.; Ingold, I.; Grocin, A.; Xavier da Silva, T.; Panzilius, E.; Scheel, C.; Mourão, A.; Buday, K.; Sato, M.; Wanninger, J.; Vignane, T.; Mohana, V.; Rehberg, M.; Flatley, A.; Schepers, A.; Kurz, A.; White, D.; Sauer, M.; Sattler, M.; Tate, E.; Schmitz, W.; Schulze, A.; O'Donnell, V.; Proneth, B.; Popwicz,G.; Pratt, D.; Friedmann Angeli, J.P.; Conrad, C. FSP1 is a glutathione-independent ferroptosis suppressor. *Nature* **575**, 693–698 (2019).

153. Wu, G., Fang, Y.-Z., Yang, S., Lupton, J. R. & Turner, N. D. Glutathione Metabolism and Its Implications for Health. *J. Nutr.* **134**, 489–492 (2004).

154. Bannai, S., Tsukeda, H. & Okumura, H. Effect of antioxidants on cultured human diploid fibroblasts exposed to cystine-free medium. *Biochem. Biophys. Res. Commun.* **74**, 1582–1588 (1977).

155. Shi, Z. Z.; Osel-Frimpong, J.; Kala, G.; Kala, S.; Barrlos, R.; Hablb, G.; Lukin, D.; Danney, C.; Matzuk, M.; Lleberman, M. Glutathione synthesis is essential for mouse development but not for cell growth in culture. *Proc. Natl. Acad. Sci. U. S. A.* **97**, 5101–5106 (2000).

156. Yang, W. S. & Stockwell, B. R. Synthetic Lethal Screening Identifies Compounds Activating Iron-Dependent, Nonapoptotic Cell Death in Oncogenic-RAS-Harboring Cancer Cells. *Chem. Biol.* **15**, 234–245 (2008).

157. Weïwer, M.; Bittker, J.; Lewis, T.; Shimada, K.; Yang, W.S.; MacPherson, L.; Dandapani, S.; Palmer, M.; Stockwell, B.; Schreiber, S.; Munoz, B. Development of small-molecule probes that selectively kill cells induced to express mutant RAS. *Bioorg. Med. Chem. Lett.* **22**, 1822–1826 (2012).

158. Shimada, K.; Skouta, R.; Kaplan, A.; Yang, W.e.; Hayano, M.; Dixon, S.; Brown, L.; Valenzuela, C.; Wolpaw, A.; Stockwell, B. Global Survey of Cell Death Mechanisms Reveals Metabolic Regulation of Ferroptosis. *Nat. Chem. Biol.* **12**, 497–503 (2016).

159. Dolma, S., Lessnick, S. L., Hahn, W. C. & Stockwell, B. R. Identification of genotype-selective antitumor agents using synthetic lethal chemical screening in engineered human tumor cells. *Cancer Cell* **3**, 285–296 (2003).

160. Lachaier, E.; Louandre, C.; Godin, C.; Saidak, Z.; Baret, M.; Diouf, M.; Chauffert, B.; Galmiche, A. Sorafenib Induces Ferroptosis in Human Cancer Cell Lines Originating from Different Solid Tumors. *Anticancer Res.* **34**, 6417–6422 (2014).

161. Louandre, C.; Ezzoukhry, Z.; Godin, C.; Barbare, J.C.; Mazière, J.C.; Chauffert, B.; Galmiche, A. Iron-dependent cell death of hepatocellular carcinoma cells exposed to sorafenib. *Int. J. Cancer* **133**, 1732–1742 (2013).

162. Llabani, E.; Hicklin, R.; Lee, H.Y.; Motika, S.; Crawford, L.; Weerapana, E.; Hergenrother, P. Diverse compounds from pleuromutilin lead to a thioredoxin inhibitor and inducer of ferroptsis. *Nat. Chem.* **11**, 521–532 (2019).

163. Friedmann Angeli, J. P.; Schneider, M.; Proneth, B.; Tyurina, Y.; Tyurin, V.; Hammond, V.; Herbach, N.; Aichler, M.; Walch, A.; Eggenhofer, E.; Basavarajappa, D.; Radmark, O.; Kobayashi, S.; Seibt, T.; Beck, H.; Neff, F.; Esposito, I.; Wanke, R.; Förster, H.; Yefremova, O.; Heinrichmeyer, M.; Bornkamm, G.; Geissler, E.; Thomas, S.; Stockwell, B.; O'Donnell, V.; Kagan, V.; Schick, J.; Conrad, M. Inactivation of the ferroptosis regulator Gpx4 triggers acute renal failure in mice. *Nat. Cell Biol.* **16**, 1180–1191 (2014).

164. Fu, Y. & Koo, M. W. L. EGCG protects HT-22 cells against glutamate-induced oxidative stress. *Neurotox. Res.* **10**, 23–29 (2006).

165. Sagara, Y. Cellular Mechanisms of Resistance to Chronic Oxidative Stress. *Free Radic. Biol. Med.* **24**, 1375–1389 (1998).

166. Nam, T.; Rector, C.; Kim, H.Y.; Sonnen, A.; Meyer, R.; Nau, W.; Atkinson, J.; Rintoul, J.; Pratt, D.; Porter, N. Tetrahydro-1,8-naphthyridinol Analogues of α-Tocopherol as Antioxidants in Lipid Membranes and Low-Density Lipoproteins. *J. Am. Chem. Soc.* **129**, 10211–10219 (2007).

167. Shah, R., Shchepinov, M. S. & Pratt, D. A. Resolving the Role of Lipoxygenases in the Initiation and Execution of Ferroptosis. *ACS Cent. Sci.* **4**, 387–396 (2018).

168. Conlon, M.; Poltorack, C.; Forcina, G.; Wells, A.; Mallais, M.; Kahanu, A.; Magtanong, L.; Pratt, D.; Dixon, S. *A Compendium of Kinetic Cell Death Modulatory Profiles Identifies Ferroptosis Regulators*. http://biorxiv.org/lookup/doi/10.1101/826925 (2019) doi:10.1101/826925.

169. Shchepinov, M. S. Reactive Oxygen Species, Isotope Effect, Essential Nutrients, and Enhanced Longevity. *Rejuvenation Res.* **10**, 47–60 (2007).

170. Hill, S.; Lamberson, C.; Xu, L.; To, R.; Tsui, H.; Shmanai, V.; Bekish, A.; Awad, A.; Marbois, B.; Cantor, C.; Porter, N.; Clarke, C.; Shchepinov, M. Small amounts of isotope-reinforced polyunsaturated fatty acids suppress lipid autoxidation. *Free Radic. Biol. Med.* **53**, 893–906 (2012).

171. Cotticelli, M. G., Crabbe, A. M., Wilson, R. B. & Shchepinov, M. S. Insights into the role of oxidative stress in the pathology of Friedreich ataxia using peroxidation resistant polyunsaturated fatty acids. *Redox Biol.* **1**, 398–404 (2013).

172. Shchepinov, M. S.; Chou, V.; Pollock, P.; Langston, W.; Cantor, C.; Molinari, R.; Manning-Boğ, A. Isotopic reinforcement of essential polyunsaturated fatty acids diminishes nigrostriatal degeneration in a mouse model of Parkinson's disease. *Toxicol. Lett.* **207**, 97–103 (2011).

173. Wenzel, S. E.; Tyurina, Y.; Zhao, J.; St Croix, C.; Dar, H.; Mao, G.; Tyurin, V.; Anthonymu, T.; Kapralov, A.; Amoscato, A.; Mikulska-Ruminska, K.; Emlet, D.; Wen, X.; Minami, Y.; Qu, F.; Watkins, S.; Holman, T.; VanDemark, A.; Kellum, J.; Bahar, I.; Bayir, H.; Kagan, K. PEBP1 Wardens Ferroptosis by Enabling Lipoxygenase Generation of Lipid Death Signals. *Cell* **171**, 628-641.e26 (2017).

CHAPTER 2: Off-Target Activities of Lipoxygenase Inhibitors Confound the Role of Enzyme-Catalyzed (Phospho)Lipid Peroxidation in Ferroptosis

2.1 Introduction

First coined in 2012, ferroptosis is an iron dependent, apoptosis distinct, form of regulated cell death that is marked by an accumulation of oxidized lipids, specifically polyunsaturated phospholipids located within lipid membranes (PUFA-PL).[1] The introduction of polar groups along the lipophilic backbone disrupts lipid organization,[2] membrane integrity,[3] and permeability,[4] moreover, highly reactive electrophilic products are formed as byproducts of lipid peroxidation.[5] The identification and study of ferroptosis has provided key evidence linking lipid peroxidation to a number of human pathologies, such as neurodegenerative disorders[6,7], ischemia[8,9] and cancer.[10]

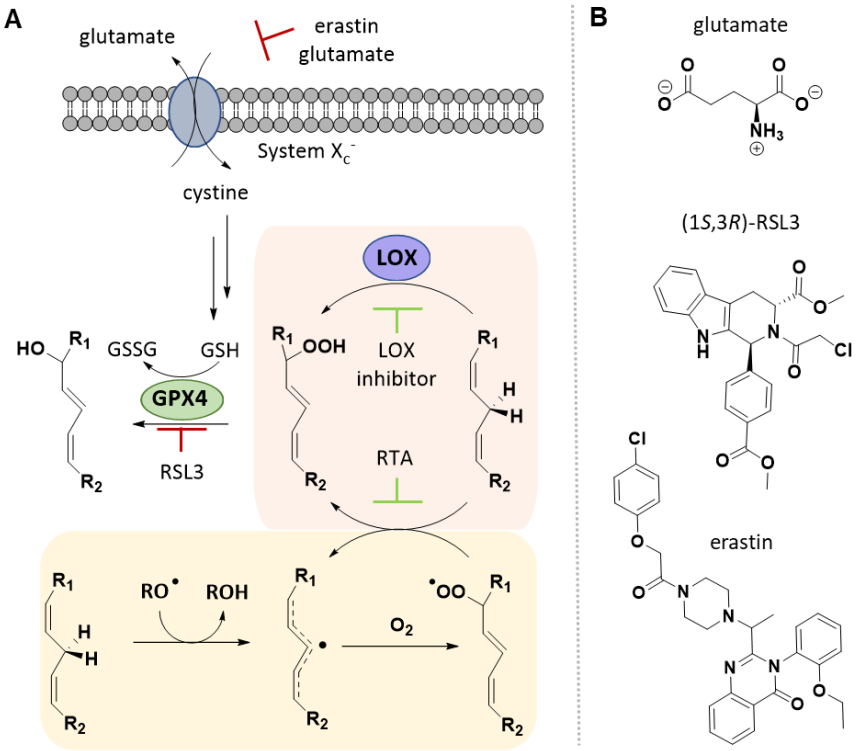

Figure 2.1 (**A**) Lipid hydroperoxides are the product of two pathways, radical mediated lipid peroxidation and enzymatically mediated LOX catalysis. Enzyme glutathione peroxidase 4 (GPX4) detoxifies lipid

hydroperoxides to the neutral alcohol. RSL3 directly inhibits GPX4 while erastin and glutamate inhibit system X_c^- which transports necessary precursor, cystine, required for glutathione biosynthesis. (**B**) Structures of common ferroptosis inducing agents.

The cell employs protective machinery, to manage the accumulation of lipid oxidation products. Most notably, selenoenzyme glutathione peroxidase 4 (GPX4) directly detoxifies lipid hydroperoxides to their non-reactive lipid alcohols[11–13] (**Figure 2.1)**. Endogenous antioxidants like α-tocopherol and tetrahydrobiopterin (BH4)[14] quench chain carrying radicals within the lipid membrane, and in parallel the recently characterized FSP1 pathway can inhibit lipid peroxidation through regeneration of enzyme Q10[15] (**Figure 2.2**). The redundancy of antioxidant machinery ensures cellular protection against lipid peroxidation. Pharmacologically, ferroptosis can be induced by small molecules that directly target these safeguards within the cell. RSL3 directly binds to and inhibits GPX4,[16,17] while erastin[18] and increased concentrations of glutamate[19,20] inhibit the cystine-glutamate antiporter, system X_c^-, suppressing the biosynthesis of glutathione, GPX4's reducing co-substrate (**Figure 2.1**).

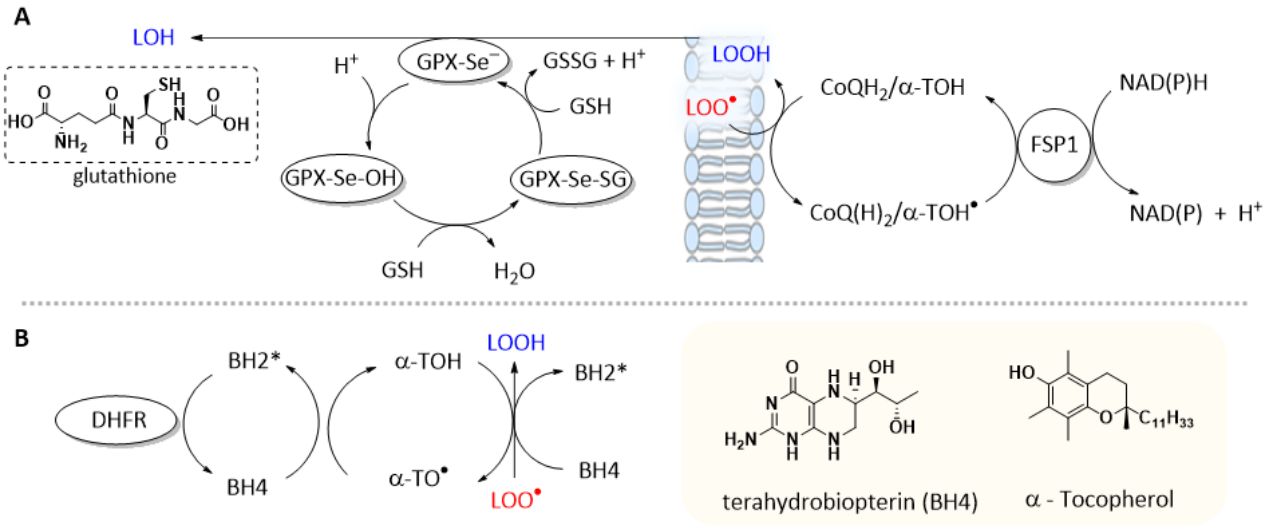

Figure 2.2 (**A**) Ubiquinol traps peroxyl radicals within lipid membranes and is regenerated by enzyme FSP1 (Ferroptosis suppressor protein 1). Peroxides are subsequently detoxified to the corresponding lipid alcohol by GPX4. (**B**) BH4 can directly quench lipid peroxyls, in parallel to regenerating endogenous antioxidant, α-tocopherol. DHFR: Dihydrofolate reductase

A key point of debate in the field concerns the origin of lipid hydroperoxides that accumulate in ferroptosis, and whether they are formed enzymatically or non-enzymatically (autoxidation) (**Figure 2.1**). Mechanistically, autoxidation describes H-atom transfer from bisallylic positions (k_p) on oxidizable substrate (LH) to radical species, followed by subsequent insertion of molecular oxygen to form lipid hydroperoxides (LOOH).[21] Radical trapping antioxidants (RTAs) are molecules with labile X-H bonds (generally aryl O-H or aryl N-H bonds) that can undergo H-atom transfer with propagating peroxyl radicals to form non-radicals products [1-2], effectively shutting down the autoxidation pathway.[22,23]

$$LOO^{\bullet} + ArOH \xrightarrow{k_{inh}} LOOH + ArO^{\bullet} \quad [1]$$

$$LOO^{\bullet} + ArO^{\bullet} \rightarrow \text{non-radical products} \quad [2]$$

Given ferroptosis is a purportedly regulated cell death process, its execution should be held under genetic control. As such, lipoxygenase enzymes, which directly catalyze the regio-and stereoselective dioxygenation of PUFAs to hydroperoxyeicosanoid products[24] (PUFA-OOH), are often implicated as likely culprits. In humans there exist six different isoforms of lipoxygenase, 15-LOX-2, eLOX3, 12R-LOX, 15-LOX-1, 12S-LOX, and 5-LOX (*ALOX15B, ALOXE3, ALOX12B, ALOX15, ALOX12, ALOX 5*), of which, certain isoforms can be selectively targeted pharmacologically and inhibited by small molecule LOX inhibitors.

Links between oxidative cell death and lipoxygenase have been made following earlier investigations into the toxic effects of glutamate in neurons. Increased concentrations of extracellular glutamate can trigger a form of oxidative cell death, 'oxytosis', that is marked by intracellular fluctuations of calcium, depletion of glutathione and an increase in ROS production. In one key experiment, treatment of mouse neuronal cells (HT-22) with glutamate was linked to 12/15 lipoxygenase activation as determined by immunodetection using human antiserum. Furthermore, HT-22 cells treated with specific 12/15-LOX-1 inhibitor baicalein and pan-LOX inhibitor NDGA were protected from glutamate toxicity.[25,26]

Additional investigations in 2008 by the Conrad group suggested that GPX4 and 12/15 LOX were key regulators of oxidative cell death. GPX4 knockout cells (MEFs) cultivated in the presence of LOX inhibitors NDGA, AA861, baicalein and PD146176 were protected, whereas cells grown without supplementation died within 24 hours.[27] However, it was later demonstrated that GPX4 and ALOX 15 double knockout cells were not protected from GPX4 deficiency, casting some doubt on the role of 15-LOX-1 in cell death.[28]

The first potent inhibitors of ferroptosis were discovered in high throughput cell-based screens. Liprostatin-1 (Lip-1) [28] was identified out of 40,000 compounds, as a potent inhibitor of TAM-induced Cre recombinase-mediated deletion of GPX4 MEF cells. Ferrostatin-1 (Fer-1) was discovered in a screen of 10,000 compounds subject to erastin challenge in HT-1080 cells.[29] Both compounds were effective at suppressing cellular lipid hydroperoxide formation as determined by BODIPY 581/591 C11, yet their mechanism of action was not known. In 2017, our group[30] demonstrated that Lip-1 and Fer-1 are good radical trapping antioxidants (RTAs). In fact, Lip-1 [k_{inh} (1.2 ± 0.1) x 10^4 $M^{-1}s^{-1}$] and Fer-1 [k_{inh} (4.6 ± 0.8) x 10^4 $M^{-1}s^{-1}$] exhibited more potent RTA activity than nature's best antioxidant, α-TOH [k_{inh} (4.7 ± 0.4) x 10^3 $M^{-1}s^{-1}$] in phospholipid bilayers. Conversely, they were found to be poor inhibitors (at best) of 15-LOX-1, suggesting that RTA activity, and not LOX inhibition, was fundamental to Lip-1 and Fer-1's anti-ferroptotic activity. This was key evidence in favour of radical mediated formation of lipid hydroperoxides within the cell driving ferroptotic cell death (**scheme 2.1**).

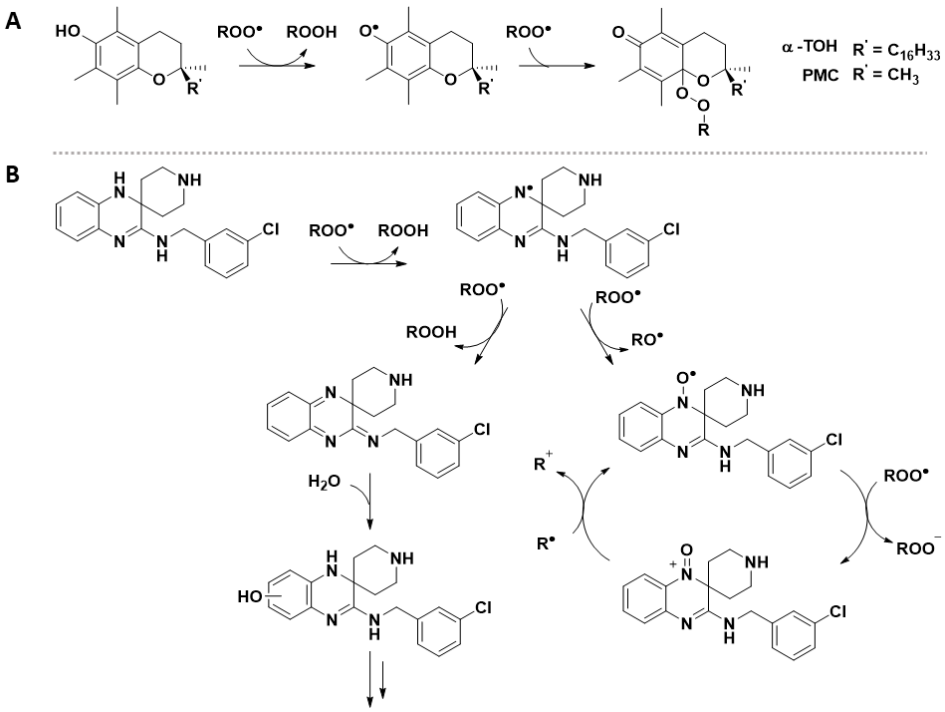

Scheme 2.1 Proposed mechanisms of (**A**) hindered phenolic and (**B**) diarylamine antioxidants (shown Lip-1). Scheme adapted from Zilka and Pratt (2017).[30]

In 2018, we followed this up by carrying out an in-depth investigation into the role of lipoxygenase in the execution of ferroptosis using human embryonic kidney cells (HEK) transfected to overexpress the 15-LOX-1, p12-LOX and 5-LOX isoforms.[31] Therein, canonical anti-ferroptotic agents, Lip-1 and Fer-1, were shown to be poor inhibitors of 12-LOX and 5-LOX (consistent with our previous observations with 15-LOX-1). Additionally, cytoprotective LOX inhibitors, Zileuton, NDGA and PD146176 were unequivocally established as RTAs, while non-cytoprotective 5-LOX inhibitors CAY10649 and CJ-13610 were discovered to be devoid of RTA activity (**Figure 2.3**). LOX overexpressing HEK cells could only be rescued by radical trapping antioxidants and redox active lipoxygenase inhibitors, thus prompting the conclusion that lipoxygenase catalysis is not required for the execution of ferroptosis.

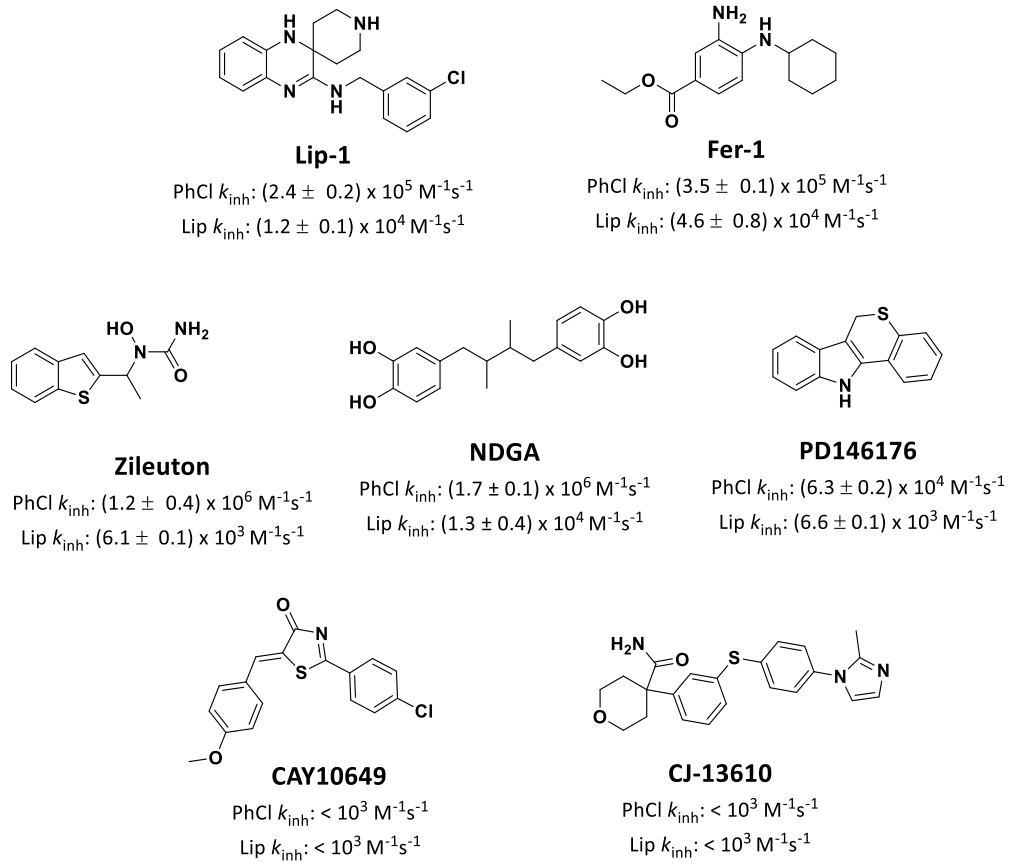

Figure 2.3 Inhibition rate constants for various LOX inhibitors measured in cumene co-autoxidations (PhCl) and in Egg PC liposomes (Lip) at 37˚C.

In this work, experiments were extended beyond transfected HEK cells, to include the cell models in which oxytosis and ferroptosis were originally established: HT-22 and HT-1080. To date, the HT-1080 fibrosarcoma cancer cell line has been used to screen oncogene RAS selective lethal compounds, prompting the discovery of system X_c^- inhibitor, erastin.[1] The cancer cell line has also served as a model for assaying the potency of small molecule GPX4 inhibitors, RSL3 and RSL5.[16] HT-1080 cells have been previously characterized to express 15-LOX-2 and eLOX-3 as determined by qPCR experiments.[32] The HT-22 mouse neuronal cell line was predominantly utilized in the study of glutamate induced neurotoxicity or, oxytosis. To date there is some ambiguity regarding LOX expression in HT-22 cells. HT-22 cells have been characterized in separate reports to express 15-LOX-1[25] and 15-LOX-2[33] by immunoblotting.

However, these attempts utilize an outdated method and a polyclonal antibody that has since been discontinued.

This work also builds on the 2017 and 2018 works by considering the other major LOX isoform, 15-LOX-2. As mentioned, 15-LOX-2 expression is linked to model cell lines HT-22 and HT-1080s, moreover, in a recent publication this isoform has been reported to complex with PEBP1, a RAF1 kinase inhibitory protein, altering the enzyme's substrate preference from free PUFA to PUFA-PL.[33] Molecular computational docking of 15-LOX-2/PEBP1 indicates a potential allosteric binding site for anti-ferroptotic agent, Fer-1 is formed following complexation,[34] which provides an alternative explanation for its RTA activity. Herein, we extend ferroptosis cell rescue experiments to 15-LOX-2 overexpressing HEK 293 to probe the role of 15-LOX-2 inhibition. Furthermore, we investigated both HT-22 and HT-1080 cells to assess 15-LOX-1, 15-LOX-2 and p12-LOX expression using monoclonal antibodies.

For this work, a small molecule library was modified from our previous work, to include LOX inhibitors, RTAs and LOX inhibitors with off-target RTA activity. The selection of the small molecule library is discussed in **chapter 2.2.1** and the characterization of each molecule for LOX inhibition and RTA activity are described in **chapters 2.2.3** & **2.2.6**. Following characterization of the small molecule library for LOX inhibition and RTA activity, compounds were subject to cell rescue assays in 15-LOX-2 overexpressing HEK 293 cells (**chapter 2.2.4**) and ferroptotic model cell lines (**chapter 2.2.5**). Presented herein, our results agree with previous conclusions from investigations into 12-LOX, 5-LOX and 15-LOX-1 overexpressing HEK cells[31] and fortify the conclusion that autoxidation remains the key modulator of ferroptotic cell death.

2.2 Results

2.2.1 Construction of Small Molecule Library

For the purpose of these experiments, a small molecule library was constructed, consisting of RTAs, lipoxygenase inhibitors and some LOX inhibitors that have been shown by our group to demonstrate off-target RTA activity (Baicalein, Zileuton, NDGA and PD146176) **(Figure 2.4)**.

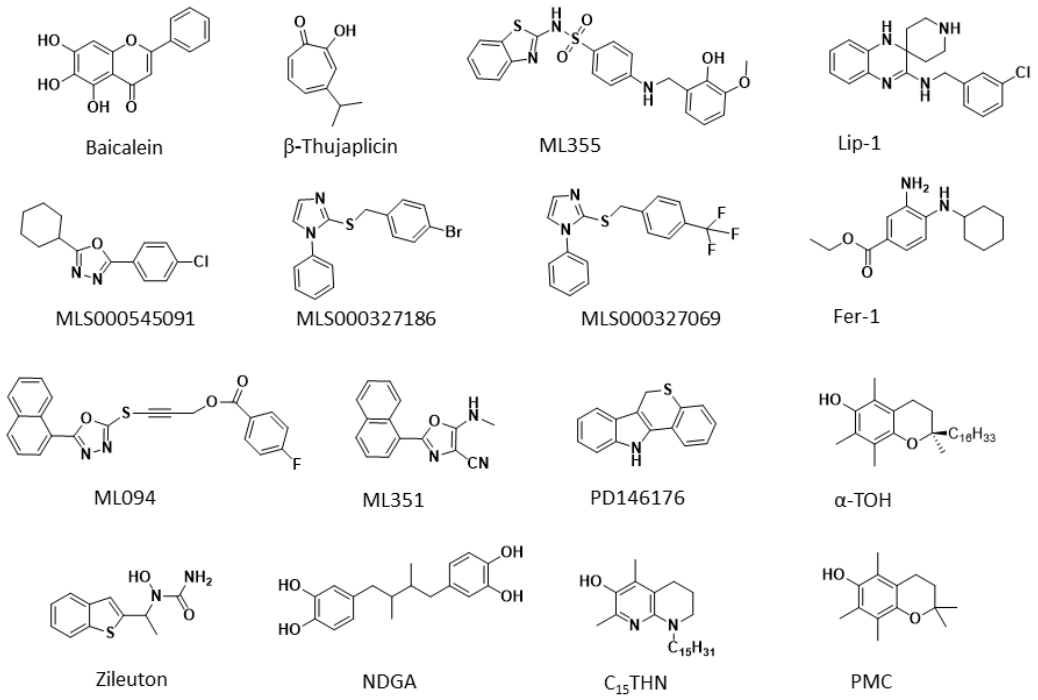

Figure 2.4 Molecular structures of selected RTAs and LOX inhibitors.

Alpha-Tocopherol, the most biologically active form of Vitamin E and nature's best antioxidant and its truncated analogue PMC were also examined as they represent the most common class of RTAs (**scheme 2.1.A**). Designer antioxidants such as the C_{15}THN were also included as they have been recorded as the most potent phenolic-like RTAs characterized to date [k_{inh} (8.8 ± 3.2) x 10^7 $M^{-1}s^{-1}$]. Additionally, the prototypical ferroptotic inhibitors Lip-1 and Fer-1 were selected as Zilka and Pratt have previously demonstrated both exhibit good RTA activity (**scheme 2.1.B**).[30] Of the antioxidants included in the small

molecule library, all have been shown previously to exhibit no lipoxygenase inhibition capacity.[31] Of the aforementioned RTAs, α-TOH and PMC were sourced commercially (**Chapter 2.5**), Lip-1 and Fer1 were synthesized by Ron Shah and C_{15}THN was synthesized by Omkar Zilka.

This library was modified from our previous work to include a broader range of LOX inhibitors; 15-LOX-1 inhibitors ML094 and ML351, 12-LOX inhibitors ML355 and β-Thujaplicin, and 15-LOX-2 inhibitors MLS000327186, MLS000327069, and MLS000545091. Previously, investigators have estimated their potencies using a common methodology that monitors the suppression of arachidonic acid LOX catalysis products (hydroperoxyeicosatetraenoic acid: HpETE) spectrophotometrically (234 nm), in the presence of varying concentrations of LOX inhibitor **(Figure 2.5A)**. Reported LOX inhibition measurements (**Figure 2.5B**) were collected from multiple sources over a broad period. To confirm these compounds do indeed inhibit isoform specific LOX, and, to adopt a more cohesive dataset, enzyme inhibition was measured in our own laboratory.

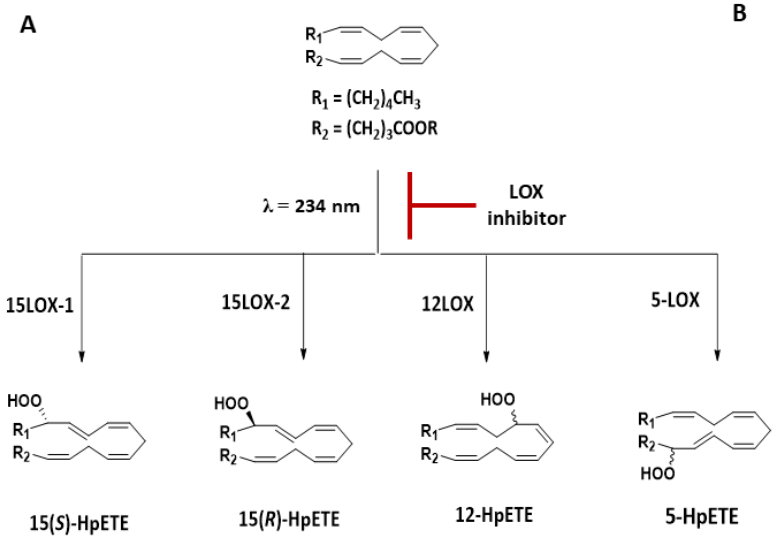

B

IC_{50} 15-LOX-1 (μM)	
PD146176	0.80
ML094	0.01
ML351	0.20
IC_{50} 15-LOX-2 (μM)	
MLS000327186	0.70
MLS000327069	0.90
MLS000545091	2.60
IC_{50} 12- LOX (μM)	
Baicalein	0.64 /1.6 (15-1)
β-Thujaplicin	0.10/>100 (15-1)
ML355	0.29/9.7 (15-1)
IC_{50} 5-LOX (μM)	
Zileuton	0.50
IC_{50} pan-LOX (μM)	
NDGA	0.20 (5), 0.11 (15-1) 5.1 (12) 11 (15-2)

Figure 2.5. Common experimental technique using purified LOX protein to measure LOX inhibition potency, described by IC_{50} value. **A**) Reported Enzyme inhibition values (IC_{50}) against varying isoforms of purified LOX protein: baicalein,[35] β-thujaplicin,[36] ML355,[37] PD146176,[38] ML094,[39] ML351,[40] NDGA,[41] Zileuton,[42] MLS000327069, MLS000327186 and MLS000545091.[43]

Of the LOX inhibitors selected for our compound library, ML094[39] and ML351[40] were synthesized as described in the literature. Whereas MLS000327069 and MLS000327186 were prepared in-house, in a single step, substitution reaction (**scheme 2.2**).

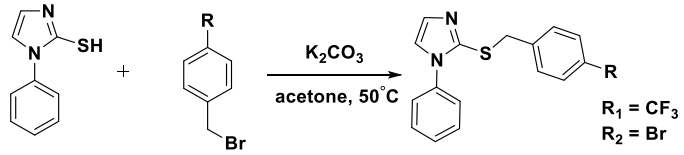

Scheme 2.2 . Synthesis of MLS000327069 (R_1) and MLS000327186 (R_2).

15-LOX-2 inhibitor MLS000545091 was also prepared in-house, in four synthetic steps. The 1,2,4 oxadiazole ring is typically accessed from cyclodehydration reactions of 1,2-diacylhydrazines (4) in an excess of dehydrating agent ($SOCl_2$, $POCl_3$).[44] The cyclodehydration reaction was instead based on work by Stabile et al., who report the synthesis of the des-chloro derivative under milder conditions, using TsCl and base.[45] The remaining LOX inhibitors (zileuton, NDGA, PD146176, β-thujaplicin, baicalein) were sourced commercially (**Chapter 2.5**).

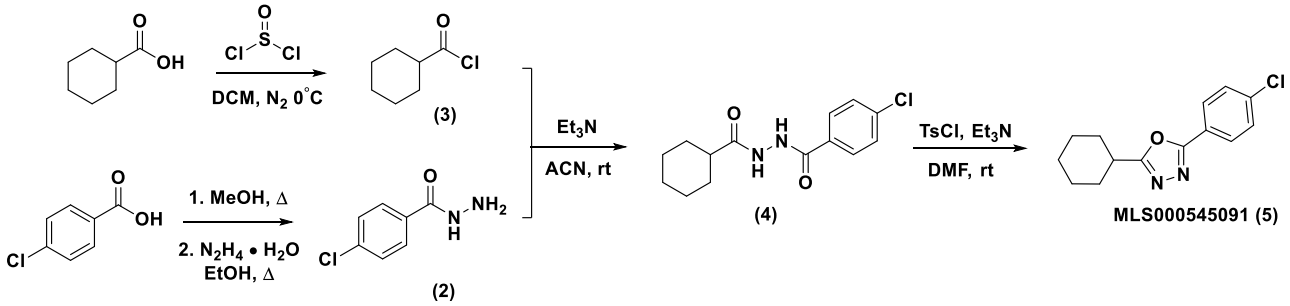

Scheme 2.3. Synthetic route of MLS000545091.

2.2.2 Generation and characterization of 15-LOX-2 overexpressing HEK 293 cells

Recent reports have suggested 15-LOX-2, upon complexation with PEBP1, a RAF1 kinase inhibitory protein, is capable of oxidizing PUFA-PL to 15-HPETE products that purportedly drive ferroptosis. To further investigate the role of 15-LOX-2 in ferroptosis, we sought to transfect HEK 293 cells to overexpress a recombinant pcDNA3/*alox15B* construct similarly to our previous studies with 5-LOX, p12-LOX and 15-LOX-1. Initial plasmid amplification in E. coli and transfection of HEK-293 cells were carried out by Ron Shah using 2.5 μg pcDNA3/15-LOX-2 plasmid in the presence of cationic lipids (Lipofectamine reagent) to facilitate the uptake of plasmid DNA. To select for cells that stably express the transfected DNA, cells were treated with 0.1 g/L of antibiotic, geneticin, as the pcDNA3/15-LOX-2 vector includes an antibiotic resistance tag. The stable transfection of 15-LOX-2 plasmid was confirmed by immunoblotting using an anti-15-LOX-2 monoclonal antibody and goat anti-rabbit IgG (H+L) secondary antibody [HRP]. Additionally, 15-LOX-2 activity was confirmed by dosing 15-LOX-2 HEK 293 cell lysate, suspended in Tris buffer (pH 7.4), with arachidonic acid and monitoring 15-HETE product formation by UPLC-ESI-MS/MS. The LC-MS method used for enzyme activity experiments was previously developed by Ron Shah[31] (**Figure 2.6**).

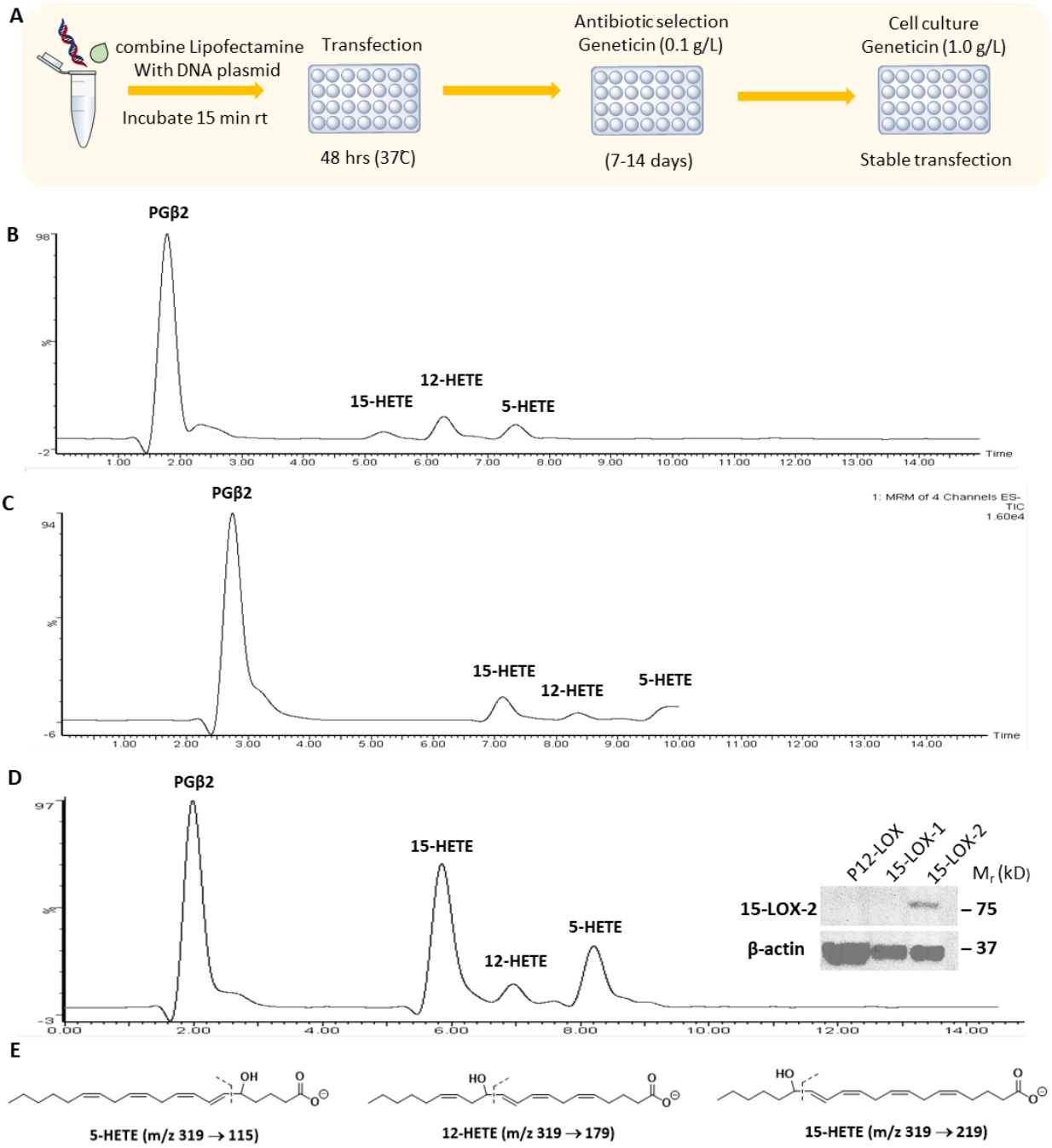

Figure 2.6 (**A**) Transfection method scheme. (**B**) LC-MS/MS chromatogram of HEK 293 cell lysate dosed with 70 μM AA (**C**) LC-MS/MS chromatogram of 15-LOX-2 HEK 293 cell lysate, selected with 0.1 g/L geneticin, dosed with 70 μM AA. N.b. A drift in elution time by ~1 min is observed. (**D**) LC-MS/MS chromatogram of 15-LOX-2 HEK 293 cell lysate, cultured in 1.0 g/L geneticin, dosed with 70 μM AA. 15-LOX-2 expression was confirmed by immunoblotting with anti-15-LOX-2 monoclonal antibody (**E**) Determination of regioisomeric products by UPLC/ESI$^-$/MS/MS based on each isomer's unique ms/ms transitions relative to internal standard prostaglandin β2. (15-1 HETE (319 → 219), 12 HETE (319 → 179), 5 HETE (319 → 115), and PGβ2 (333 → 235)).

It was noted that the proportion of 15-HETE produced in UPLC-MS/MS enzyme activity assays with transfected 15-LOX-2 HEK 293 cells was only marginally higher when compared with WT HEK 293 cells (compare **Figure 2.6B** with **2.6C**). Although the transfected cells stably expressed the 15-LOX-2 protein, as determined by immunoblotting, it was especially evident that 15-LOX-2 expression levels were considerably lower than those found in HEK 293 cells similarly transfected to overexpress the genes encoding the p12, 15-1 and 5-LOX isoforms.[31] Initial selection was performed with 0.1 g/L geneticin to improve cell survival during antibiotic selection. Freshly transfected 15-LOX-2 HEK 293 cells treated with concentrations of geneticin greater than 0.1 g/L were unable to survive the screening period, as plasmid uptake was very low. Ideally, screening should be carried out at 1.0 g/L (**Figure 2.7.A**) to remove all WT HEK 293 cells that have not successfully taken up the pcDNA3/15-LOX-2 vector. To improve plasmid uptake, transfection parameters such as the ratio of DNA plasmid-to-cell, the amount of Lipofectamine reagent and cell density were adjusted. Cells subject to these transfection conditions were still unable to survive antibiotic selection above 0.1 g/L. (**Figure 2.7.B 2-4**). Instead, freshly transfected HEK 293 cells selected with 0.1 g/L geneticin, were subsequently cultured in medium with gradually increasing geneticin until 1.0 g/L was reached. These cells were subsequently lysed, treated with arachidonic acid, and subjected to analysis by LC-MS/MS, where 15-HETE production was noticeably increased (**Figure 2.6D**). The expression of 15-LOX-2 was confirmed by immunoblotting using the same monoclonal antibody as before (**Figure 2.6.D**).

A

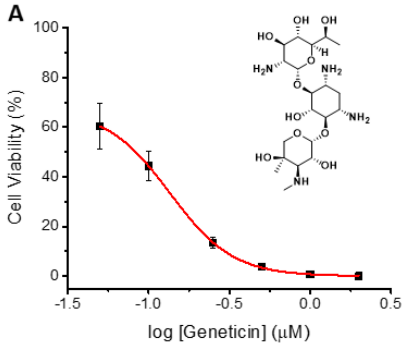

B

No.	Plate size (well)	Cell density (cell/well)	DNA/well (ng)	Lipofectamine/well (μL)	PLUS rgnt /well (μL)	[Geneticin] g/L
1	6	7.8×10^5	2500	3.75, 7.5	2.5	0.1 → 1.0
2	6	1×10^5	2500	5, 7.5, 10, 12.5	3.0	0.25, 1.0
3	96	1000	100	0.3	1	0.375, 0.5
4	96	2000	100	0.3	1	0.25, 0.375, 0.5

Figure 2.7 (**A**) Geneticin kill curve for WT HEK 293. 1000 cells/100uL were plated in a 96 well plate and cultured in varying concentrations of geneticin over 8 days. Cell viability was assessed by fluorescence intensity with Aquabluer assay (540 ex/590 em). (**B**) transfection optimization table.

The expression of 15-LOX-2 by HEK 293 cells was further probed pharmacologically, by monitoring inhibition of 15-HETE production using MLS000327069, a known 15-LOX-2 inhibitor.[43] The quantity of 15-HETE product was assessed by UPLC/ESI^-/MS/MS, wherein, increasing amounts of MLS000327069 effectively decreased the formation of 15-HETE product (**Figure 2.8**). Given these results, the 15-LOX-2 expressing HEK 293 cells were considered a suitable model to probe enzyme activity of the small molecule library as detailed in **Chapter 2.2.3.**

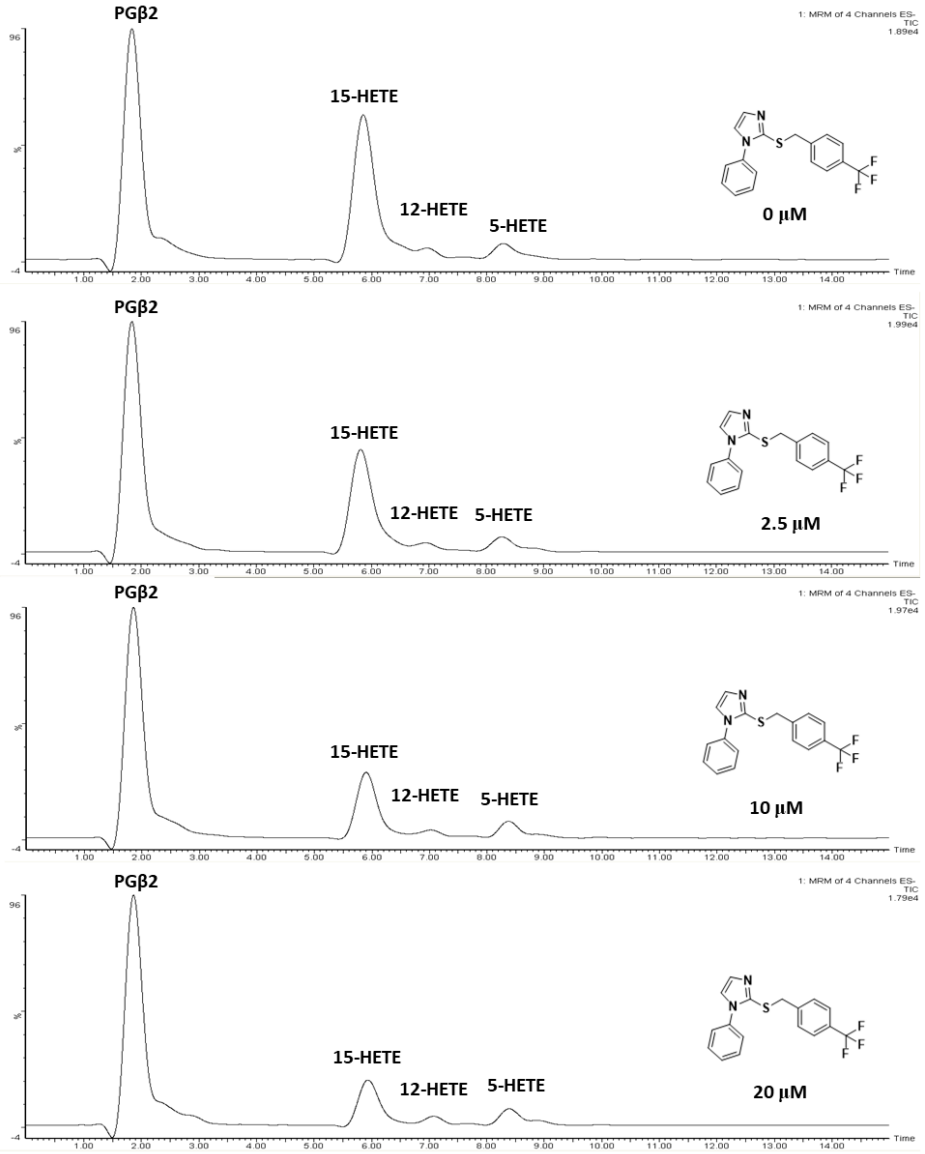

Figure 2.8 Representation chromatogram from UPLC/ESI$^-$/MS/MS analysis following treatment of 15-LOX-2 HEK 293 lysate with 70 μM arachidonic acid and increasing concentration of MLS000327069 (0-20 μM). 5 μL Aliquots were injected onto UPLC/ESI/MS/MS, and regioisomeric products were separated on an Acquity C18 column in an isocratic mobile phase of (acetonitrile, methanol, water and acetic acid 42:25:33:0.007) over 10 minutes at 0.15 mL/min. Quantification of 15-HETE peaks was carried out in its respective m*z*/m*z* transition channel (319→219).

2.2.3 Characterization of LOX inhibition activity

To date, considerable insight into the molecular mechanisms of ferroptosis has been provided from studies with compounds which induce or inhibit cell death. In this context, cytoprotective effects of LOX inhibitors have implicated enzymatic lipid oxidation in ferroptosis. To probe the role of LOX in cell death, we have selected the following inhibitors: β-thujaplicin, ML355, baicalein, ML351, ML094, MLS000327069, MLS000327186, MLS000545091 to add to the LOX inhibitors we examined in our previous work. These molecules have been previously characterized for their enzyme inhibition potency, summarized in **Figure 2.5.B**, however these values are sourced from multiple laboratories, and use different methods. To construct a more cohesive dataset, LOX inhibitors were screened for their ability to inhibit p12-LOX, 5-LOX, 15-LOX-1 and 15-LOX-2 in house.

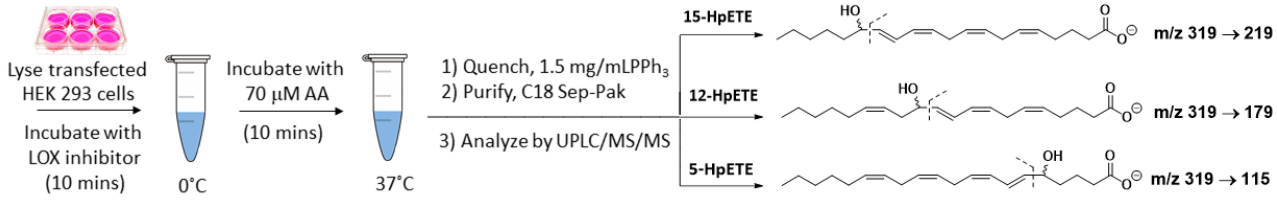

Figure 2.9 Enzyme activity reaction scheme. Determination of regio-isomeric products by UPLC/ESI$^-$/MS/MS based on each isomer's unique ms/ms transitions. (15-1 HETE (319 → 219), 12 HETE (319 → 179), 5 HETE (319 → 115), and PGβ2 (333 → 235)).

This was accomplished by monitoring arachidonic acid oxidation products (HETE), of transfected HEK-293 cell lysate, by UPLC/ESI$^-$/MS/MS (**Figure 2.9**).[30,31] Thus, lysed transfected HEK-293 cells were incubated with varying concentrations of LOX inhibitor and AA substrate at 37˚C for 10 minutes. Afterwards, HpETE (-OOH) products were reduced to the corresponding HETE (-OH) with triphenylphosphine (PPh_3) and purified samples were analyzed by UPLC-ESI-MS/MS. Quantification of HETE regioisomers were carried out relative to 10 μM PGβ2 (Prostaglandin β-2) internal standard, following integration of peaks in respective *m/z* transition channels. Following transfection, it was observed by LC-MS/MS that LOX activity appeared greater in p-12 and 15-LOX-1 overexpressing cells

compared to 5-LOX and 15-LOX-2 overexpressing cells based on relative HETE product formation (**figure 2.10 B-E**). The relatively poor activity of the latter likely results from the relatively poor expression of 15-LOX-2 as indicated in the corresponding Western blot.

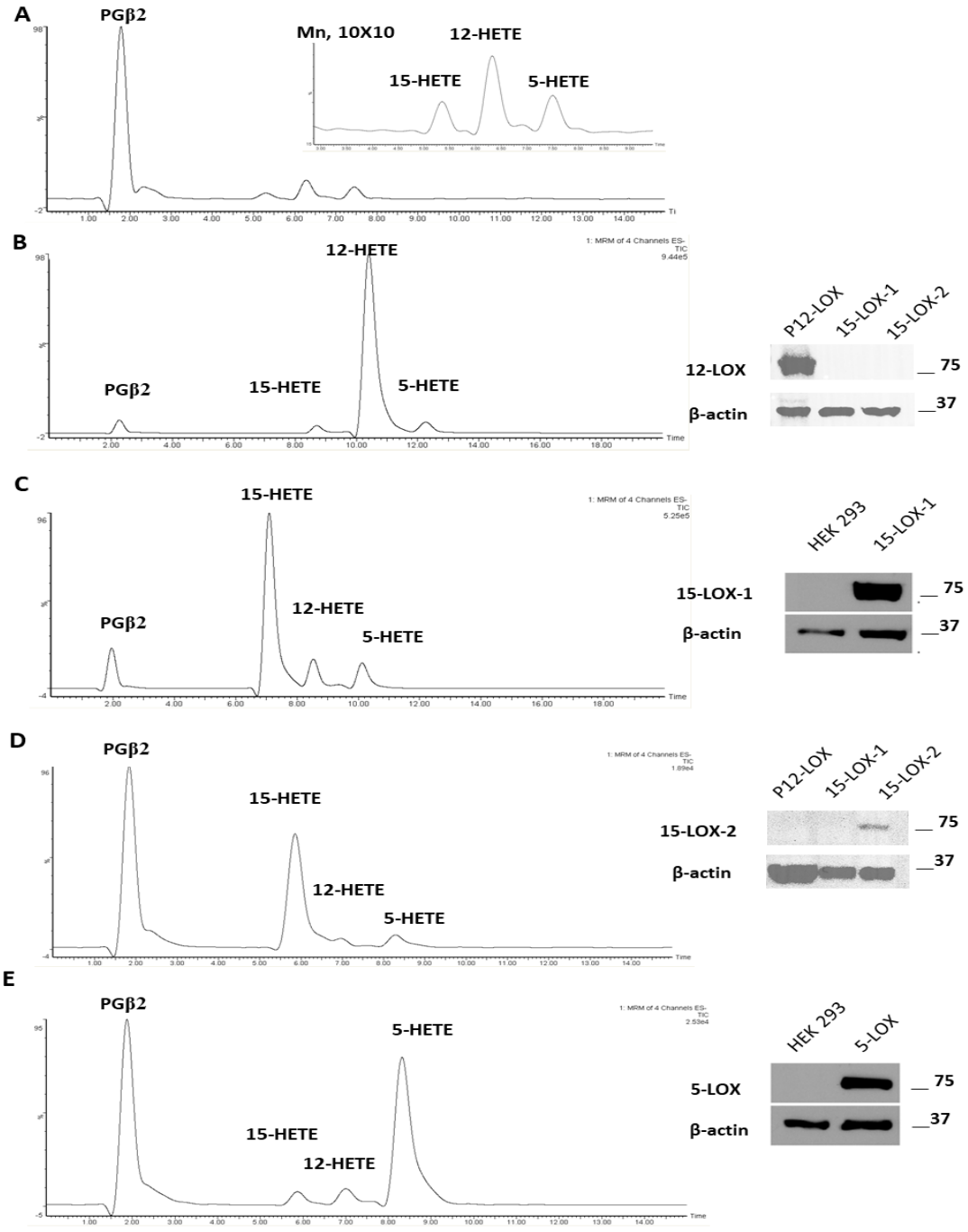

Figure 2.10. (**A**) LC-MS/MS chromatogram of HEK 293 cell lysate dosed with 70 μM AA and magnification (X10) of peaks in the region of 3 min -9 min. LOX over-expressing HEK 293 cell lysate dosed with 70 μM

AA were subject to analysis by UPLC/MS/MS (**B**) p12 -LOX overexpressing HEK 293 cell lysate. 12-LOX expression was confirmed by immunoblotting with anti-12LOX monoclonal antibody. (**C**) 15-LOX-1 overexpressing HEK 293 cell lysate. 15-LOX-1 expression was previously confirmed by immunoblotting with anti-15-LOX-1 monoclonal antibody.[31] (**D**) 15-LOX-2 overexpressing HEK 293 cell lysate. 15-LOX-2 expression was confirmed by immunoblotting with anti-15-LOX-2 monoclonal antibody (**E**) 5 -LOX overexpressing HEK 293 cell lysate. Expression was previously demonstrated using an anti 5-LOX monoclonal antibody.[31]

In this context, enzyme inhibition is given as a percentage of HETE formation (%), as determined by quantifying HETE peaks in the corresponding *m*/*z* transition channel, with respect to a control without LOX inhibitor (**Figure 2.10**). A summary of the results of enzyme activity assays is included in **Figure 2.12**. First, the potency of purportedly redox inactive 15-LOX-1 inhibitors, ML094 and ML351 were assessed against 15-LOX-1 overexpressing HEK293 cell lysate in triplicate. ML094 has been reported as a very effective inhibitor of the 15-LOX-1 isoform as determined spectrophotometrically (IC_{50} = 0.01 μM)[39] and, on average, is an order of magnitude more potent than most inhibitors in our compound library. In our investigations, ML094 was confirmed as an effective inhibitor, after near suppression of 15(*S*)-HETE product was achieved, but at much lower potency. It is also observed that ML094, also suppressed non-specific autoxidation products (12-HETE, 5-HETE). Representative chromatograms have been included for illustrative purposes (**Figure 2.11**).

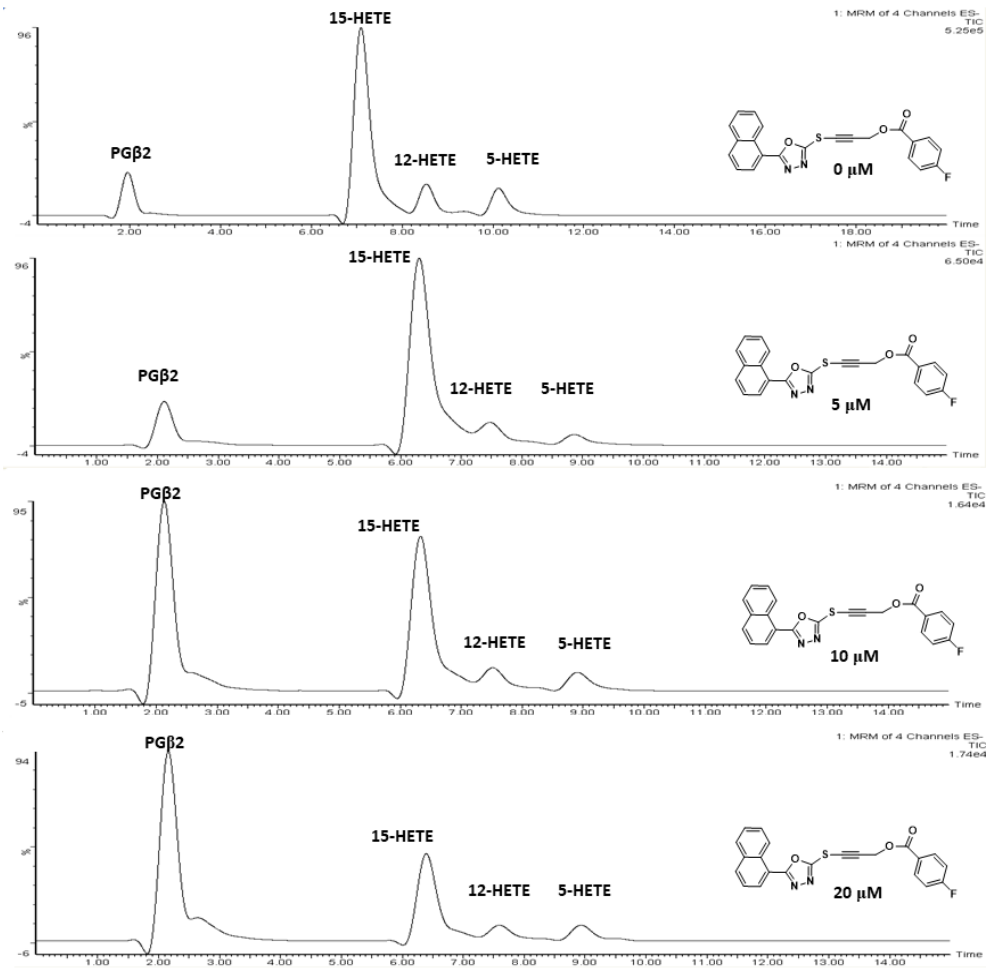

Figure 2.11 Representation chromatogram from UPLC/ESI$^-$/MS/MS analysis following treatment of 15-LOX-1 HEK 293 lysate with 70 μM arachidonic acid and increasing concentration of ML094 (0-20 μM). 5 μL Aliquots were injected onto UPLC/ESI/MS/MS, and regioisomeric products were separated on an Acquity C18 column in a isocratic mobile phase of (acetonitrile, methanol, water and acetic acid 42:25:33:0.007) over 10 minutes at 0.15 mL/min. Quantification of 15-HETE peaks was carried out in its respective m*z*/m*z* transition channel (319→219).

Selective LOX inhibitor ML351, is reported to potently inhibit 15-LOX-1 with an IC_{50} value of 0.2 μM.[40] Our investigations revealed ML351, does indeed exhibit 15-LOX-1 inhibition activity and suppressed 15(*S*)-HETE formation by 53 % at a concentration of 20 μM. It is apparent that ML094 is still a more potent inhibitor of 15-LOX-1 and is in agreement with reported results.[39,40] Furthermore, both inhibitors were screened against p12-LOX, 5-LOX and 15-LOX-2 overexpressing HEK293 cell lysate to assess for selectivity

in isoform inhibition. It was determined that ML351 and ML094 do not inhibit p-12-LOX or 15-LOX-2 isoforms given the lack in 12-HETE and 15(*R*)-HETE suppression.

As for 5-LOX, ML094 was observed to be an ineffective inhibitor of 5-LOX following a single trial, and will be repeated again to obtain triplicate results. In contrast, ML351 was a potent suppressor of 5-HETE using our LC-MS method – more so than against its intended target 15-LOX-1. Previous investigations into ML351 suggested excellent isoform selectivity, using the traditional UV-vis approach with purified 5-LOX (IC_{50} > 50 μM).[40]

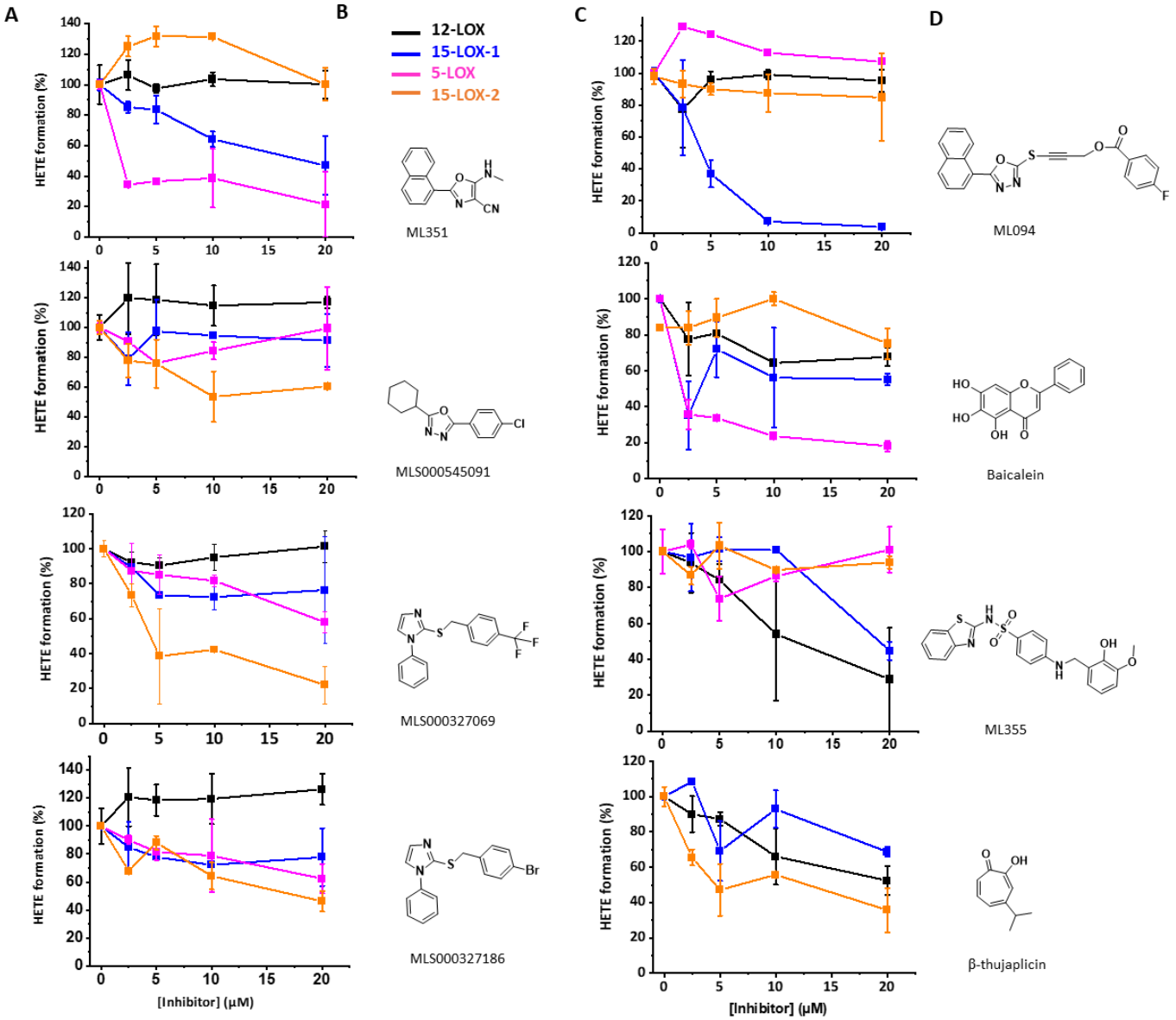

Figure 2.12 p12-LOX (blue), 15-LOX-1 (orange), 5-LOX (grey) and 15-LOX-2 (yellow) over-expressing HEK 293 cell lysate was dosed with 70 μM AA in the presence of varying concentration of LOX inhibitor. Enzyme inhibition was modelled with respect to suppression of arachidonic acid oxidation products of interest (HETE) as monitored by UPLC/ESI^-/MS/MS. Quantification was determined following integration of targeted HETE peak in corresponding m*z*/m*z* channel relative to internal standard prostaglandin β2 (12-HETE: 319→179/ 15-HETE: 319→219) 5 HETE (319 → 115), and PGβ2 (333 → 235)).

The efficacy of p12-LOX inhibitors, baicalein, ML355, and β-thujaplicin were then investigated in p12-LOX HEK 293 cells. All three inhibitors were observed to suppress 12-HETE formation, with ML355 being most potent, followed by β-thujaplicin and then baicalein. Again, the compounds were much less potent in our hands than the EC50s found in the literature (see above). Of interest, it has been reported in previous investigations that 12-LOX inhibitors baicalein,[35] ML355,[37] and to a much lesser degree, β-thujaplicin[36] also inhibit 15-LOX-1. Our results are consistent with these observations, however, baicalein was demonstrably more potent towards inhibition of 15-LOX-1 than p12-LOX, which is contrary to prior publication (p12-LOX IC_{50} : 0.64 μM/15-LOX-1 IC_{50} : 1.6 μM)[35]. It was also observed that β-thujaplicin suppressed formation of 15(*S*)-HETE, though not as effectively as baicalein and ML355, which aligned with literature results (15-LOX-1 IC_{50} > 100 μM).[36]

As for the 15-LOX-2 isoform, baicalein and ML355 were ineffective at inhibiting 15-LOX-2, whereas β-thujaplicin inhibited 15(*R*)-HETE production by 64%. There are no prior investigations into β-thujaplicin as an inhibitor of 15-LOX-2. Rather unexpectedly, 5-LOX overexpressing HEK 293 lysate treated with β-thujaplicin resulted in an impressive increase in 5-HETE formation (**Figure 2.13)**. This result was confirmed on a separate occasion using freshly prepared stocks.

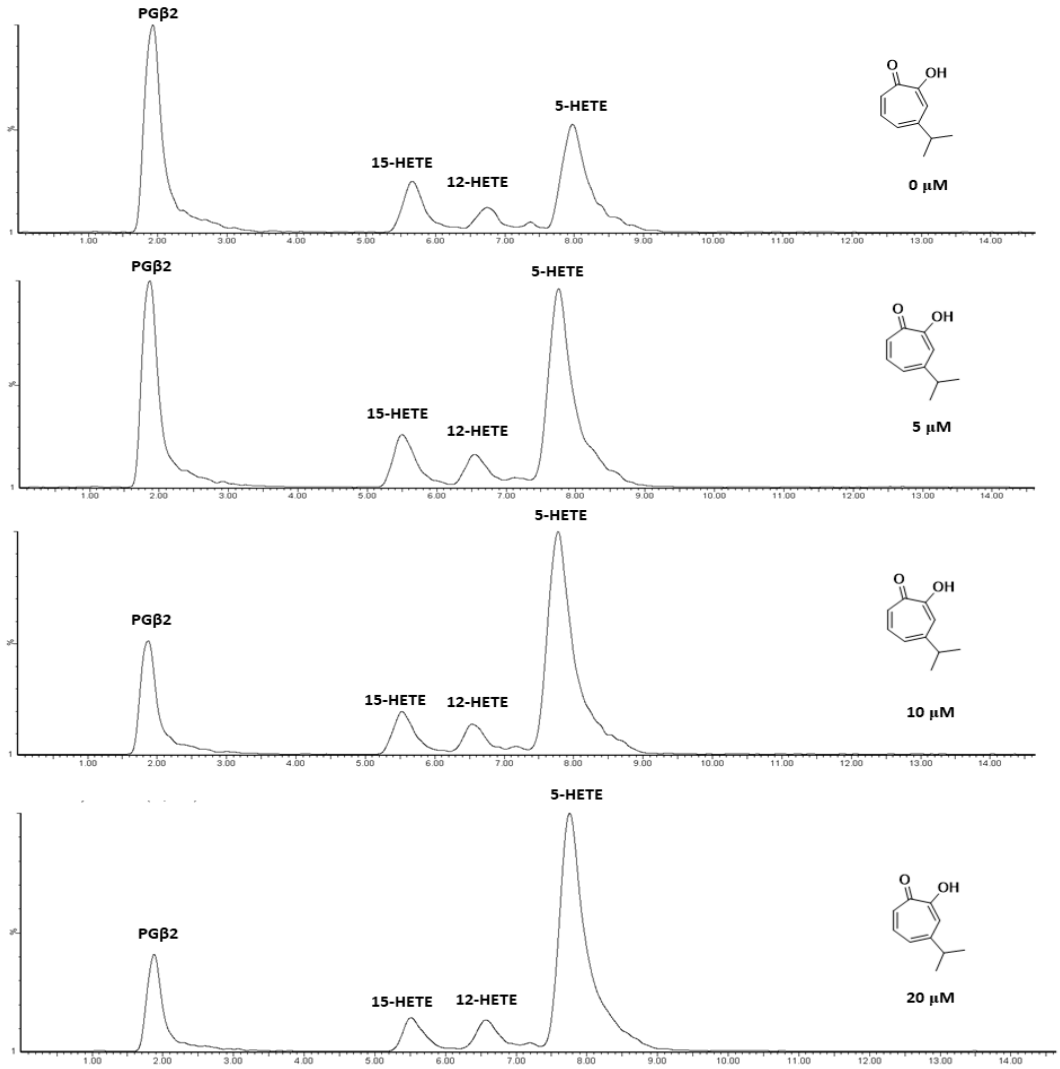

Figure 2.13. Representation chromatogram from UPLC/ESI-/MS/MS analysis following treatment of 5-LOX HEK 293 lysate with 70 μM arachidonic acid and increasing concentration of β-thujaplicin (0-20 μM). 5 μL Aliquots were injected onto UPLC/ESI/MS/MS, and regioisomeric products were separated on an Acquity C18 column in an isocratic mobile phase of (acetonitrile, methanol, water and acetic acid 42:25:33:0.007) over 10 minutes at 0.15 mL/min. Quantification of 5-HETE peaks was carried out in its respective mz/mz transition channel (319→115) relative to internal standard, prostaglandin PGβ2 (333 → 235).

If LOX activation occupied a central role in ferroptosis, then perhaps β-thujaplicin could sensitize 5-LOX expressing cells to RSL3 induced cell death. Varying concentrations of β-thujaplicin were administered to 5-LOX overexpressing HEK 293 cells treated with GPX4 inhibitor, RSL3. Under these circumstances, β-thujaplicin did not sensitize cells to ferroptosis, but instead rescued 5-LOX cells from

oxidative cell death (**Figure 2.14.B**). The remainder of the small molecule library was subject to cell rescue assays in **Chapter 2.2.4 and Chapter 2.2.5**

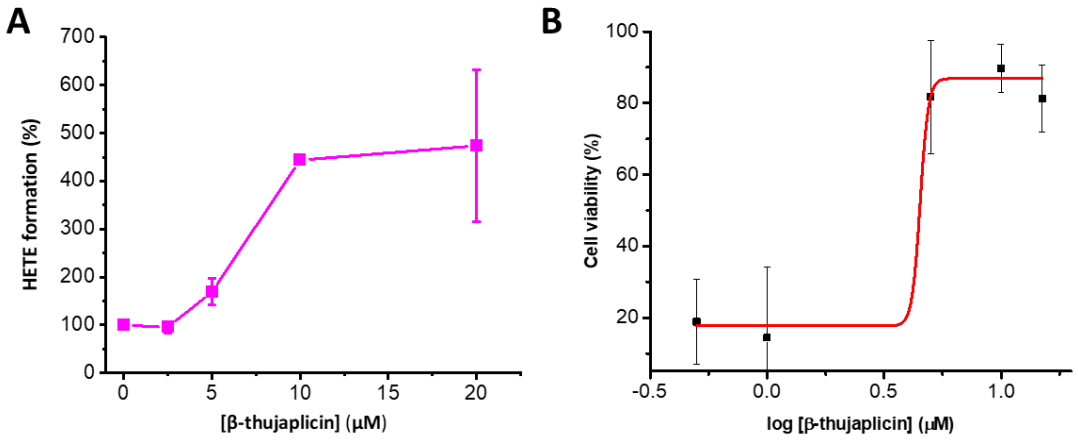

Figure 2.14 (**A**) 5-LOX (grey) over-expressing HEK 293 cell lysate was dosed with 70 μM AA in the presence of varying concentration of β-thujaplicin. Enzyme inhibition was modeled with respect to suppression of arachidonic acid oxidation products (HETE) as monitored by UPLC/ESI$^-$/MS/MS. Quantification was determined following integration of targeted HETE peak in corresponding m*z*/m*z* channel (5 HETE (319 → 115) relative to PGβ2 (333 → 235). (**B**) 5-LOX cells (3000 cells/100 μL) were incubated at 37˚C for 4 hours with 5.5 μM RSL3 and varying concentrations of β-thujaplicin. Cell viability was assessed using Aquabluer assay, wherein, fluorescence intensity (540 ex/ 590 em) of treated cells was compared to a live cell control.

15-LOX-2 inhibitors MLS000327186, MLS000327069, and MLS000545091 were also screened for enzyme inhibition against each of the transfected cell lines. All three compounds inhibited 15-LOX-2 activity. MLS000327069 suppressed 15(*R*)-HETE formation by 78%, MLS000327186 by 54%, and MLS000545091 by 40%. Initial investigations observed MLS000327186 (IC_{50}: 0.7 μM) to be more potent than MLS000327069 (IC_{50}: 0.9 μM).[43] Although these compounds had no inhibitory effects against 12-HETE formation, it was observed that MLS000327186 and MLS000327069 did inhibit 15-LOX-1 and 5-LOX by approximately 20%. This is consistent with reports observing IC_{50} > 50 μM for both compounds against 15-LOX-1.[43] It is worth noting, that the direct comparison of IC_{50} values obtained from enzyme inhibition studied in-house against literature values is inappropriate. The reported IC_{50} values were measured using a different assay, and are dependent on several factors, such as, the concentration of reagents (i.e.

arachidonic acid, RTA, LOX inhibitor), lipoxygenase to inhibitor ratio, and whether the experiment uses purified enzyme or cell lysate.

2.2.4 15-LOX-2 Overexpressing HEK 293 cells are rescued from ferroptosis by RTAs and some LOX inhibitors

Given the recent implication of 15-LOX-2 in ferroptosis, we sought to determine the effectiveness of RTAs and LOX inhibitors from our compound library in cell rescue assays. First, 15-LOX-2 overexpressing HEK 293 cells were screened for sensitization towards ferroptotic induction. In the 2018 work, it was demonstrated that LOX overexpressing cells were sensitized to GPX4 inhibition and GSH depletion as compared to their wild type counterparts. To assess the sensitivity of 15-LOX-2 overexpressing HEK 293 cells to ferroptosis, cells were treated with varying concentrations of the GPX4 inhibitor, RSL3, and system X_c^- inhibitor, erastin. It was observed that 15-LOX-2 overexpressing HEK 293 cells were sensitized to RSL3 induced ferroptosis, as compared to wild type HEK 293 (15-LOX-2 LD_{50} : 3.4 μM, WT LD_{50}: 6.8 μM [31]). 15-LOX-2 sensitization was less prominent as compared to HEK 293 cells transfected to overexpress other LOX isoforms (p12-LOX: 0.4 μM, 15-LOX-1: 0.5 μM, 5-LOX: 0.6 μM), reflecting the relatively lower expression of 15-LOX-2, as compared with p-12-LOX and 15-LOX-1.

Similarly, 15-LOX-2 HEK 293 were slightly sensitized to erastin induced oxidative cell death as compared to wild type HEK 293 cells (15-LOX-2 LD_{50} : 4.9 μM**,** WT LD_{50}: 6.6 μM[31]). Again, 15-LOX-2 cells were less sensitive to erastin treatment compared with other LOX expressing HEK 293 cells (p12-LOX: 0.9 μM, 15-LOX-1: 1.7 μM, 5-LOX: 1.4 μM) consistent. We previously speculated that LOX expression renders HEK293 more susceptible to ferroptosis due to the initiation of non-enzymatic lipid peroxidation. An initial increase in oxidized lipid product (HpETE) can undergo Fenton-like one electron reduction to form hydroxyl/alkoxyl species that are capable of initiating autoxidation (**Figure 2.15.A**).

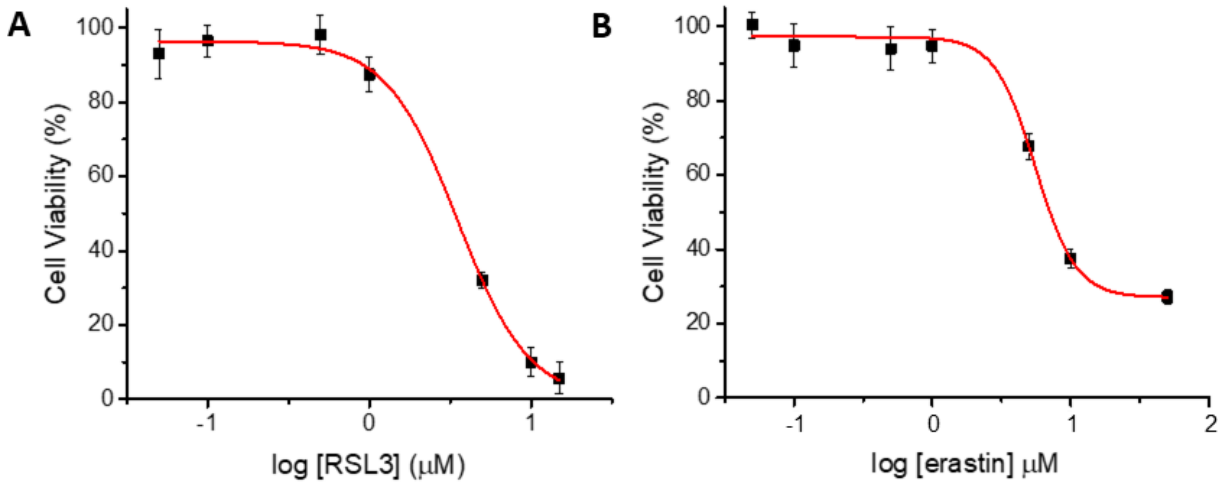

Figure 2.15 (**A**) RSL3 cytotoxicity curve with 15-LOX-2 transfected HEK 293 cells LD_{50}: 3.4 μM (**B**) Erastin cytotoxicity curve with transfected 15-LOX-2 HEK 293 cells LD_{50}: 4.9 μM

To assess the potency of our compound library in transfected 15-LOX-2 HEK 293, cells were subject to recue assays. The night prior, 3000 cells/ 100 μL were aliquoted into 96 well plates and left to adhere overnight. The following morning, culture medium was removed and replaced with medium containing 5.5 μM RSL3. To each well, varying concentrations of compound library were administered and 4 hours later, cell viability was assessed with using Aquabluer. Prior to the addition of Aquabluer solution, the experimental medium was removed. Viable cells will reduce redox indicator, Aquabluer, to its fluorescent form, which can be monitored at 540 ex/590 em. Cell viability is determined by comparing the fluorescence intensity of treated cells relative to a negative cell control (**Figure 2.16**).

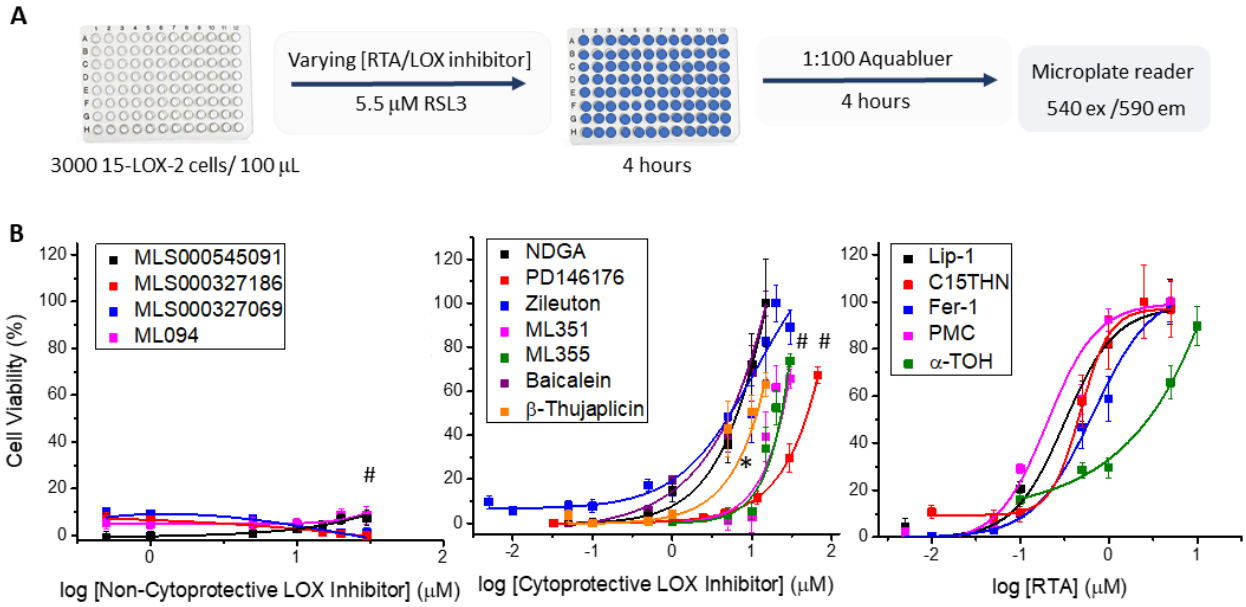

C

LOX inhibitors	EC_{50} RSL3 (nM)
MLS000545091	NR
MLS000327186	NR
MLS000327069	NR
ML094	NR

LOX inhibitors	EC_{50} RSL3 (nM)
NDGA	4730
PD146176	NR
Zileuton	6460
ML351	NR
ML355	NR
Baicalein	NR
β-Thujaplicin	NR

RTAs	EC_{50} RSL3 (nM)
Lip-1	316
C_{15}-THN	477
Fer-1	667
PMC	202
α-TOH	2460

Figure 2.16 (**A**)15-LOX-2 cells (3000 cells /100 µL) were incubated at 37˚C for 4 hours with 5.5 µM RSL3 and varying concentrations of RTA/LOX inhibitors. Cell viability was assessed using Aquabluer assay, wherein, fluorescence intensity (540 ex/ 590 em) of treated cells was compared to a live cell control. (**B**) Cell survival curves plotted as the average of triplicate trials. (**C**) Respective EC_{50} (nM) values were derived from dose-response curves. Complete rescue could not be achieved as (*) the compound became cytotoxic or (#) the compound surpassed its maximum solubility in solution.

Prototypical ferroptosis inhibitors Lip-1 (EC_{50}: 316 nM) and Fer-1 (EC_{50}: 667 nM) were moderately potent at rescuing 15 LOX-2 HEK 293 cells from RSL3 induced ferroptosis, although previously, rescue was achieved with a lower administered dosage in p12LOX (Lip EC_{50}: 20 nM Fer EC_{50}: 103 nM), 15-LOX-1 (Lip EC_{50}: 15 nM Fer EC_{50}: 40 nM) and 5-LOX (Lip EC_{50}: 12 nM Fer EC_{50}: 46 nM) overexpressing HEK293 cells.[31] Additionally, RTAs, α-TOH (EC_{50}: 2460 nM), C15THN (EC_{50}: 477 nM) and truncated analog, PMC (EC_{50}: 202

nM) were good anti-ferroptotic agents. It is worth noting that PMC outperforms α-TOH by an impressive margin, presumably, since α-TOH is slower to diffuse into the cell.

Of the LOX inhibitors, 15-LOX-2 inhibitors, MLS00045091, MLS000327069 and MLS000327186 and 15-LOX-1 inhibitor, ML094 were unsuccessful at rescuing 15-LOX-2 HEK 293 cells from RSL3 induced ferroptosis at concentrations upwards of 30 μM. Rather, pan-LOX inhibitor, NDGA (EC_{50}: 4730 nM) and Zileuton (EC_{50}: 6460 nM) proved to be most effective, followed by LOX inhibitors, baicalein, β-thujaplicin, PD146176, ML355, and ML351. It was not possible to derive an EC_{50} value for β-thujaplicin, as it became cytotoxic at increased concentrations, and ML355, ML351 and PD146176 surpass their solubility threshold in experimental cell media. In the 2018 work, PD146176 was notably more potent in overexpressing p12-LOX (EC_{50}: 705 nM), 15-LOX-1 (EC_{50}: 691 nM) and 5-LOX (EC_{50}: 620 nM) HEK 293 cells. The decrease in efficacy is suspected to be caused by a less potent stock solution of PD146176, which we have noted undergoes autoxidation upon storage.

2.2.5 Model cell lines are rescued from ferroptosis by RTAs and some LOX inhibitors

To probe the role of LOX-catalyzed lipid peroxidation beyond transfected HEK 293 cells, we sought model cell lines that are well established in the study of ferroptosis, such as HT-22s and HT-1080s. To assess glutamate lethality to HT-22 cells under our laboratory conditions, HT-22 cells were treated with varying concentrations of the neurotransmitter over the span of 24 hours, followed by an assessment of cell viability using Aquabluer. Viable cells reduce the redox indicator, Aquabluer, to its fluorescent form, which can be monitored at 540 ex/590 em. Cell viability is determined by comparing the fluorescence intensity of treated cells relative to untreated cells as a negative control. The results are shown in **Figure 2.17A**, from which the LD_{50} was determined to be 6 mM. Subsequent investigations to assess the potency of cytoprotective agents were therefore carried out at a concentration of 10 mM.

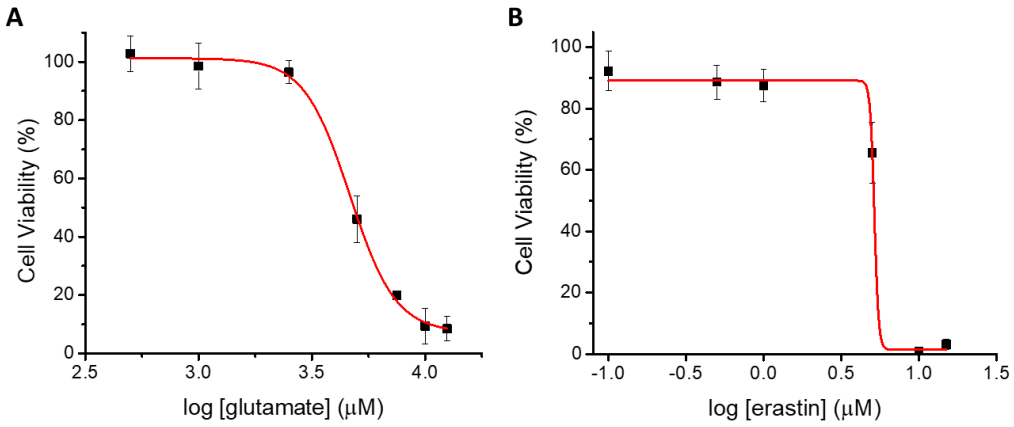

Figure 2.17 (**A**) Lethal dosage (LD_{50}) of glutamate in HT-22 cells. 3000 cells/100 μL were dosed with varying concentrations of glutamate in glutamine-free media over 24 hours. Cell viability was recorded on a Synergy microplate reader (LD_{50} : 4.6 mM). (**B**) Lethal dosage (LD_{50}) of erastin in HT-1080 cells. 3000 cells/100 μL were dosed with varying concentrations of erastin over 24 hours. Cell viability was recorded on a Synergy microplate reader (LD_{50} : 5.2 μM).

To evaluate the effectiveness of our compound library against glutamate induced cell death, HT-22 cells were dosed with glutamate and varying concentrations of RTA/LOX inhibitor and following 24 hours, experimental medium was removed and replaced with an Aquabluer solution in glutamine-free media. It is important to note that glutamine renders HT-22s cells immune to glutamate challenge. The relationship between glutamine and glutamate and its effect on cytotoxicity has been documented in glial cells by Simantov, who observed glutamine deficiency instead inhibited glutamate cytotoxicity![46] Evidently, the type of neuronal cell and its role in the glutamine-glutamate cycle may determine its relationship to neurotransmitter cytotoxicity. HT-22 cell rescue experiments against (1*S*,3*R*) RSL3 challenge were performed in parallel by Spencer Short and the corresponding EC_{50} (μM) values have been included for comparison (**Figure 2.18B**).

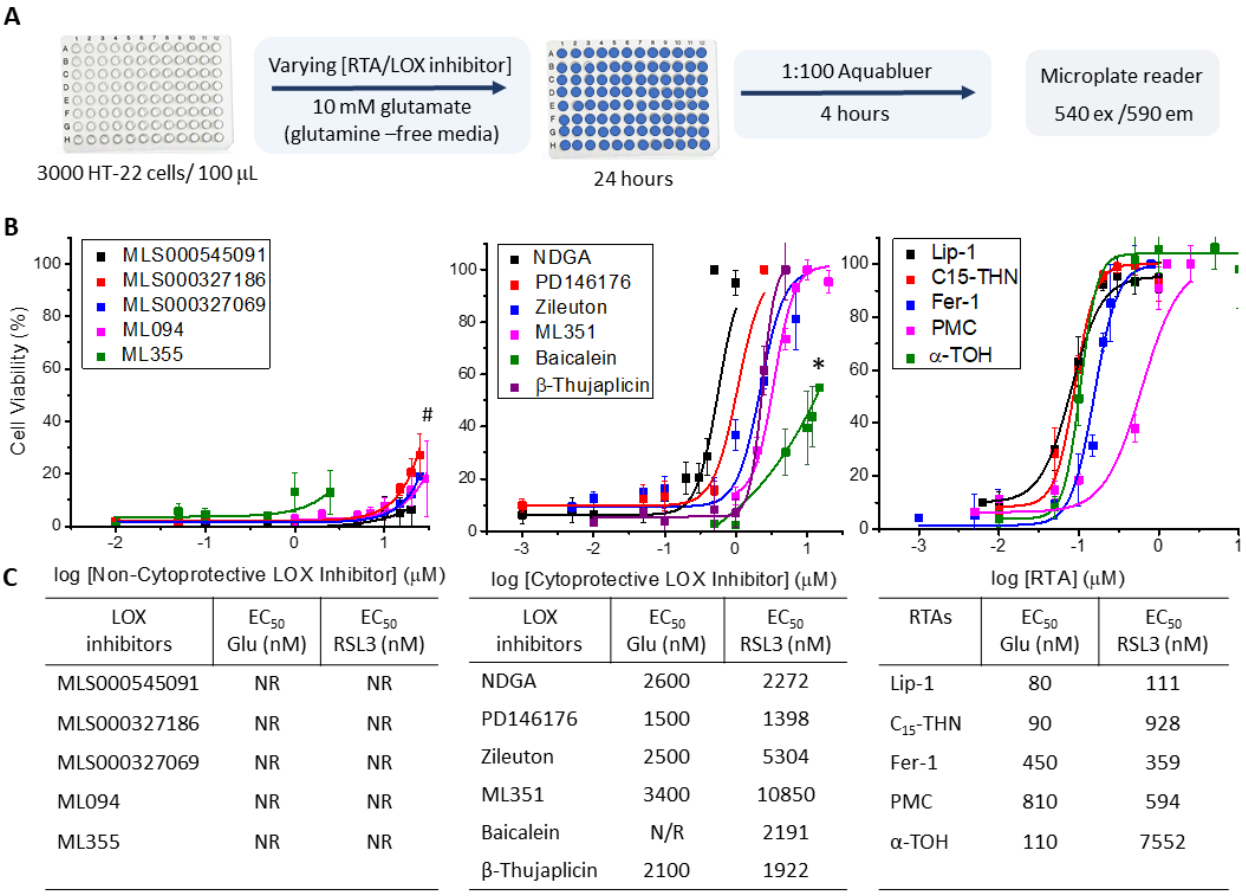

C

LOX inhibitors	EC_{50} Glu (nM)	EC_{50} RSL3 (nM)
MLS000545091	NR	NR
MLS000327186	NR	NR
MLS000327069	NR	NR
ML094	NR	NR
ML355	NR	NR

LOX inhibitors	EC_{50} Glu (nM)	EC_{50} RSL3 (nM)
NDGA	2600	2272
PD146176	1500	1398
Zileuton	2500	5304
ML351	3400	10850
Baicalein	N/R	2191
β-Thujaplicin	2100	1922

RTAs	EC_{50} Glu (nM)	EC_{50} RSL3 (nM)
Lip-1	80	111
C_{15}-THN	90	928
Fer-1	450	359
PMC	810	594
α-TOH	110	7552

Figure 2.18 (**A**) HT-22 cells (3000 cells /100 µL) were incubated at 37˚C for 24 hours with 10 mM glutamate in glutamine-free media and varying concentrations of RTA/LOX inhibitors. Cell viability was assessed using Aquabluer assay, wherein, fluorescence intensity (540 ex/ 590 em) of treated cells was compared to a live cell control. (**B**) Cell survival curves plotted as the average of triplicate trials. (**C**) Respective EC_{50} (nM) values were derived from dose-response curves. Complete rescue could not be achieved as (*) the compound became cytotoxic or (#) the compound surpassed its maximum solubility in solution.

The corresponding cell rescue data was separated into LOX inhibitors and RTAs, and further into non-/cytoprotective LOX inhibitors (**Figure 2.18**). RTAs proved to be potent inhibitors of both RSL3 and glutamate induced cell death, however, it was remarked that a higher dosage of RTA (nM) is required to achieve rescue against RSL3 challenge compared with glutamate. Notably, Lip-1 was an exceptionally potent anti-ferroptotic agent at low nanomolar concentrations (Glu EC_{50} 80 nM : RSL3 EC_{50} 111 nM) and its reactivity is comparable with previous studies in transfected HEK 293 (RSL3 EC_{50} 9-20 µM)[31].

Furthermore, α-TOH was observed to be nearly 68 fold more potent over 24 hour experiments in glutamate than in RSL3 (Glu EC_{50} 110nM : RSL3 EC_{50} 7552 nM), presumably since α-TOH requires more time to diffuse into the cell. Experiments with truncated chain derivative, PMC, featured increased potency over shorter, 4 hour investigations with RSL3.

It was observed that a diverse range of LOX inhibitors, NDGA (pan-LOX), PD146176 (15-LOX-1), Zileuton (5-LOX), ML351 (15-LOX-1/5-LOX) and B-thujaplicin (12-LOX/15-LOX-1/15-LOX-2) restored HT-22 viability against glutamate and RSL3 challenge, in fact, the therapeutic dosage for most of the aforementioned LOX inhibitors was similar between experimental conditions. It has been previously demonstrated by Shah and Pratt[31] that LOX inhibitors NDGA, PD146176 and Zileuton were cytoprotective in transfected HEK 293 cells due to their RTA activity. 12-LOX/15-LOX-2 and 5-LOX inhibitor baicalein was demonstrated to be competent against RSL3 challenge, but complete rescue could not be achieved in glutamate treated cells, as baicalein becomes cytotoxic at higher concentrations.

LOX inhibitors ML094 (15-LOX-1) and ML355 (12-LOX/15-LOX-1) as well as 15-LOX-2 inhibitors, MLS000327186, MLS000327069, MLS000545091, were unsuccessful at rescuing HT-22 from both RSL3 and glutamate induced cell death. There is a noted gradual increase in cell viability towards 20%, however, this is soon met with the solubility limit of these compounds in cell culture buffer. It is an intriguing observation that all 15-LOX-2 inhibitors performed poorly in cell rescue experiments, given the purported role of 15-LOX-2/PEBP1 in ferroptosis and the purported role of 15-LOX-2 in oxytosis in HT-22 cells.

Similar cell rescue investigations were carried out in HT-1080 fibrosarcoma cells subjected to erastin induced cell death. Erastin lethality was evaluated over 24 hours (LD_{50} 5.2 μM) and a dosage of 10 μM was deemed sufficient to kill cells within the experimental time frame (**Figure 2.17B**). The night prior, 3000 cells/100 uL were aliquoted in a 96 well plate and left to adhere overnight. The following morning culture medium was removed and replaced with 10 μM erastin in culture medium. Varying concentrations

of LOX inhibitor/RTA were administered to HT-1080 cells and 24 hours later, cell viability was assessed on the Synergy microplate reader. In parallel, Spencer Short performed the corresponding experiments with (1*S*,3*R*) RSL3 challenge, EC_{50} values are included for comparison (**Figure 2.19B**).

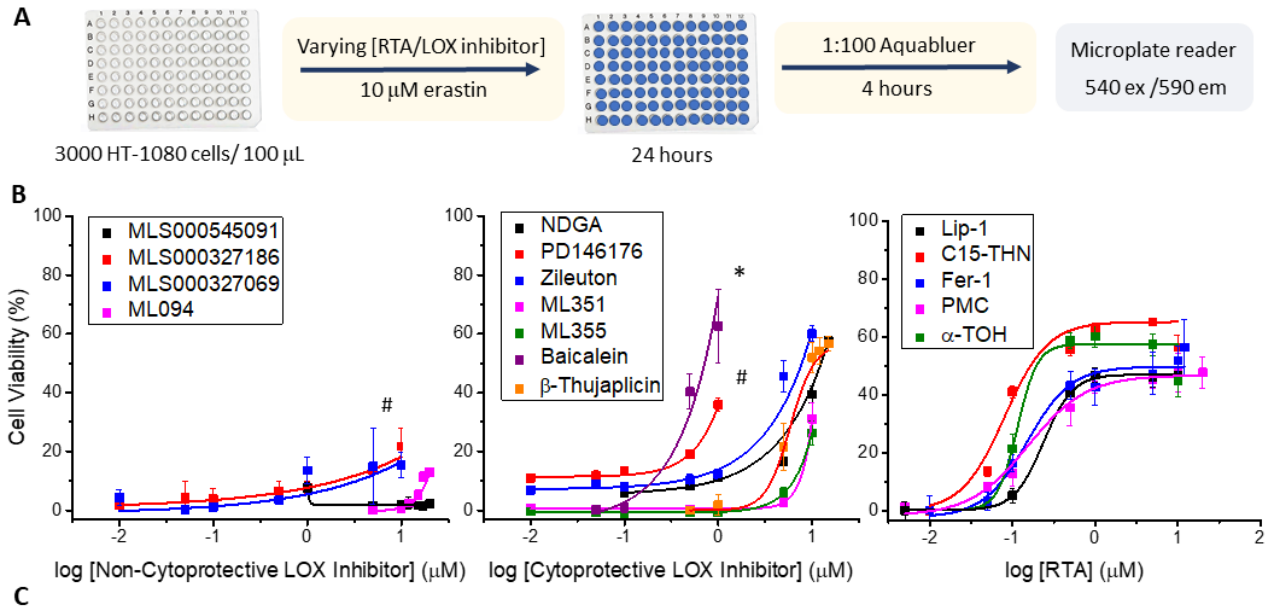

C

LOX inhibitors	EC_{50} Eras (nM)	EC_{50} RSL3 (nM)
MLS000545091	NR	NR
MLS000327186	NR	NR
MLS000327069	NR	NR
ML094	NR	NR

LOX inhibitors	EC_{50} Eras (nM)	EC_{50} RSL3 (nM)
NDGA	1710	1324
PD146176	NR	1705
Zileuton	2840	1153
ML351	NR	6310
ML355	NR	34450
Baicalein	NR	930
β-Thujaplicin	5830	1531

RTAs	EC_{50} Eras (nM)	EC_{50} RSL3 (nM)
Lip-1	227	28
C_{15}-THN	45	273
Fer-1	127	178
PMC	155	288
α-TOH	107	1422

Figure 2.19 (**A**) HT-1080 cells (3000 cells /100 µL) were incubated at 37˚C for 24 hours with 10 µM erastin and varying concentrations of RTA/LOX inhibitors. Cell viability was assessed using Aquabluer assay, wherein, fluorescence intensity (540 ex/ 590 em) of treated cells was compared to a live cell control. (**B**) Cell survival curves plotted as the average of triplicate trials. (**C**) Respective EC_{50} (nM) values were derived from dose-response curves. Complete rescue could not be achieved as (*) the compound became cytotoxic or (#) the compound surpassed its maximum solubility in solution.

In HT-1080 cells, a similar trend emerges, wherein all RTAs and some LOX inhibitors are successful at rescuing cells from both RSL3 and erastin induced ferroptosis (**Figure 2.19**). Fer-1 remains an exceptionally potent anti-ferroptotic agent (Eras EC_{50} 45 nM : RSL3 EC_{50} 178 nM), as observed previously

in HT-22 and transfected HEK 293 cell lines. Again, α-TOH was significantly less potent (RSL3 EC_{50} 1422 nM) during shorter, 4 hour, RSL3 investigations as compared to its truncated analog, PMC (RSL3 EC_{50} 288 nM). Shorter experiments provide a narrower window for α-TOH to diffuse into the cell and exert its antioxidant activity. Upon further inspection, it was observed that HT-1080 cells required, on average, 2-5 times less RTA to achieve cell rescue as compared with HT-22 cells.

LOX inhibitors, NDGA (pan-LOX), zileuton (5-LOX) and β-thujaplicin (12-LOX/15-LOX-1/15-LOX-2) are good anti-ferroptotic agents towards both erastin and RSL3 challenge. Whereas, LOX inhibitors, ML355 (12-LOX/15-LOX-1), ML351 (15-LOX-1/5-LOX), PD146176 (15-LOX-1) and Baicalein (12-LOX/15-LOX-1/5-LOX) cannot fully restore cell viability following erastin treatment, therefore EC_{50} values for these compounds could not be derived. As demonstrated in **Figure 2.19** Baicalein and PD146176 reach a cytotoxic threshold in the cell before establishing complete rescue, while ML355 is limited by its solubility in cell culture buffer. Furthermore, LOX inhibitors, ML094 (15-LO-1), MLS000327069 (15-LOX-2), MLS000327186 (15-LOX-2), and MLS000545091 (15-LOX-2) do not rescue nor do they suppress the onset of oxidative cell death, which again, is interesting considering HT-1080 cells have been characterized as 15-LOX-2 expressing cells.[47]

Intriguingly, HT-1080 cells in the presence of erastin were only restored to 60% viability following treatment with any cytoprotective agent. Therefore, HT-1080 cell viability was monitored over a 40 hour period following dosage with 10 μM erastin and treatment with (red) and without (black) 10 μM of Fer-1 (**Figure 2.20**). Results indicate that Fer-1 only improves cell viability by a certain threshold, but does not completely restore viability to 100%. Additionally, over the 30 hours, cell viability decreases with time, presumably coinciding with the consumption of Fer-1 by peroxyl radicals. It is possible that complete restoration of viability is not possible, as additional cell death mechanisms may be triggered following erastin treatment.

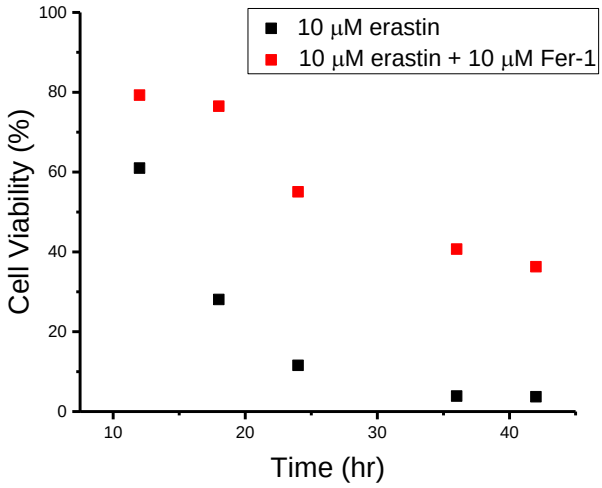

Figure 2.20 HT-1080 (3000 cells / 100 μL) cells were dosed with 10 μM erastin (black) and 10 μM Fer-1 (red) at regular time intervals and cell viability was recorded spectroscopically using Aquabluer assay.

2.2.6 Radical Trapping Antioxidant Compounds are Potent Anti-Ferroptotic Agents

In our previous work,[31] it was discovered that only certain LOX inhibitors, pan-LOX NDGA, 5-LOX inhibitor Zileuton, 15-LOX-1 inhibitor PD146176, and 15-LOX-2 inhibitor baicalein were capable of rescue across cell lines transfected to express *ALOX5*, *ALOX15A*, and *ALOX12*. These data were inconsistent regarding the relationship between inhibition of specific lipoxygenase isoforms and cytoprotection. In the same study, radical-trapping antioxidants, such as α-tocopherol and its water soluble analog PMC, were shown to be potent anti-ferroptotic agents. NDGA, Zileuton, PD146176 and baicalein were later identified to possess RTA activity, while non-cytoprotective 5-LOX inhibitors CAY10649 and CJ-13610 were demonstrated to lack any significant RTA activity. To provide more insight into the cytoprotective nature of LOX inhibitors, the expanded compound library was probed for antioxidant activity (**Figure 2.21-Figure 2.22**).

Radical-trapping antioxidant activity is best quantified from inhibited autoxidation data. Co-autoxidations of STY-BODIPY and an oxidizable substrate (e.g. a hydrocarbon such as cumene or phospholipid such as egg phosphatidylcholine) can be used for this purpose. In an assay developed by our

group,[48] STY-BODIPY consumption, by peroxyl addition to the phenylbutadiene moiety ($k_{STY\text{-}BODIPY}$ = 894 M^{-1} s^{-1}), can be monitored by loss of absorbance at 565 nm over time (**Figure 2.21A**). The addition of redox active agents can retard and, in some cases, inhibit dye consumption by quenching peroxyl radicals preventing chain-propagation. The inhibition rate constant, k_{inh}, which is the rate constant for the reaction of inhibitors with chain-carrying peroxyl radicals, is determined from the initial rate of the inhibited reaction as in equation (1). The number of radical chains broken by a compound is given by its stoichiometry, *n*, as described by equation (2) (**Figure 2.21B**).

The panel of compounds was first subjected to inhibited autoxidation experiments in cumene to determine inherent RTA activity, as some medium can exhibit kinetic solvent effects (ie: H-bonding). Previous work by Ingold has shown that H-bonding can retard the rate of H atom transfer.[49]

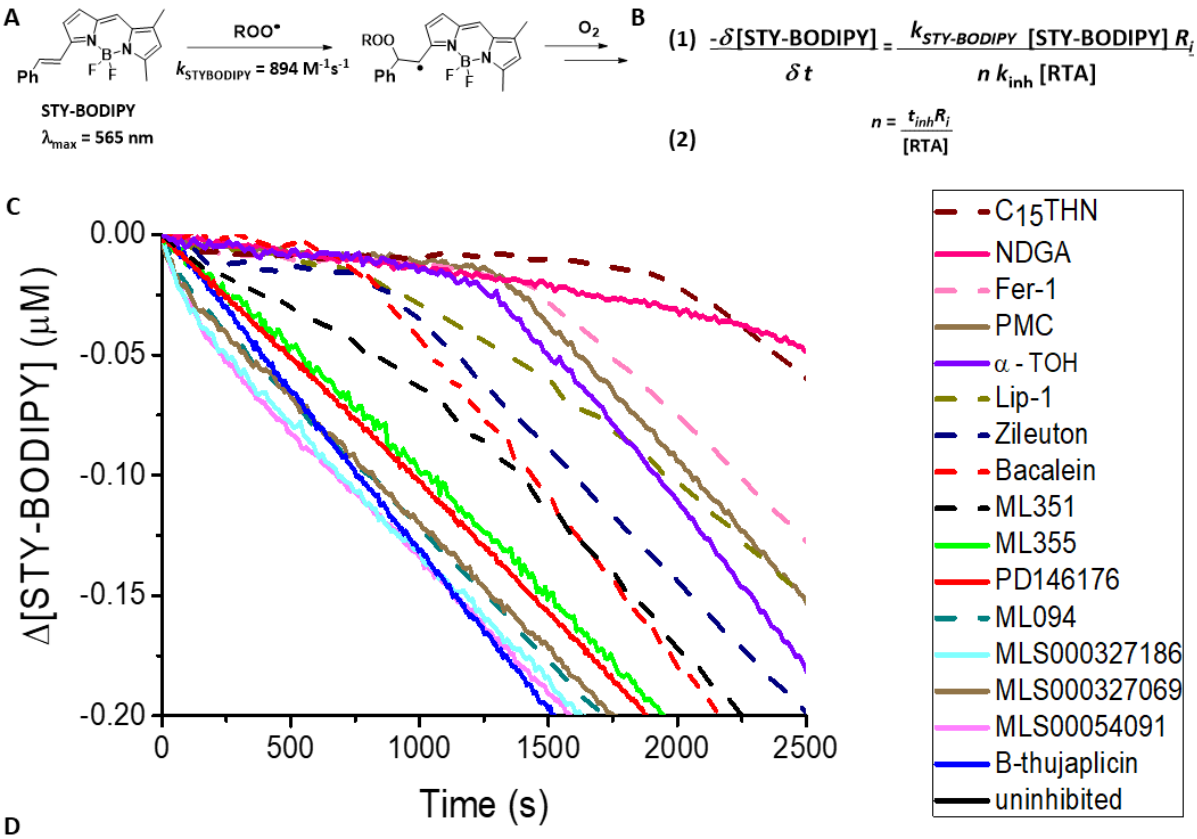

D

LOX inhibitors	PhCl k_{inh} ($M^{-1}s^{-1}$)
ML094	< 10^3
MLS000327186	< 10^3
MLS000327069	< 10^3
MLS000545091	< 10^3
β-Thujaplicin	< 10^3

LOX inhibitors	PhCl k_{inh} ($M^{-1}s^{-1}$)
ML355	(7.7 ± 0.1) x 10^3
ML351	(3.1 ± 0.02) x 10^4
PD146176	(6.3 ± 0.2) x 10^4
Baicalein	(1.0 ± 0.2) x $10^{6\,a}$
Zileuton	(1.1 ± 0.4) x 10^5
NDGA	(1.7 ± 0.1) x $10^{6\,a}$

RTAs	PhCl k_{inh} ($M^{-1}s^{-1}$)
Lip-1	(1.6 ± 0.3) x 10^5
Fer-1	(3.1 ± 0.3) x 10^5
C_{15}-THN	(8.8 ± 3.2) x $10^{7\,b}$
α-TOH	(3.6 ± 0.1) x $10^{6\,b}$
PMC	(1.6 ± 0.1) x 10^5

Figure 2.21 (**A**) Peroxyl radical formation is monitored by consumption of STY-BODIPY (monitored at 565 mn). (**B**) (1) The initial rate of inhibition can be imputed to derive *k* inhibition rate constant, k_{inh} . (2) The time of inhibition, $t_{inh,}$ can be imputed to derive reaction stoichiometry, *n*, (2) (**C**) Co-Autoxidation of cumene (3.6 M) and STY-BODIPY (10 μM) at 37˚C initiated by AIBN (6 mM) and inhibited by 2 μM RTA or LOX inhibitor. The data for the uninhibited rate of autoxidation coincides with that that observed in the presence of β-thujaplicin. **(D)** Respective inhibition rate constants k_{inh} calculated in cumene (PhCl). *a* measured previously at 37˚C in cumene,[31] *b* measured previously at 37˚C in styrene at 37˚C.[30]

Using this assay, the RTA activity of the panel of compounds was evaluated. Our group has previously measured the RTA activity of phenolic antioxidants, α-TOH, PMC and C15THN. Furthermore,

Anti-ferroptotic agents Lip-1 [k_{inh} (1.6 ± 0.3) x 10^5 $M^{-1}s^{-1}$] and Fer-1 [k_{inh} (3.1 ± 0.3) x 10^5 $M^{-1}s^{-1}$] were again confirmed to exhibit good antioxidant activity in organic solution as both compounds feature an arylamine moiety that has been extensively demonstrated as a good RTA scaffold.[50,51] Again, pan LOX inhibitor NDGA, 5-LOX inhibitor Zileuton, 15-LOX-1 inhibitor PD146176, and 12-LOX/15-LOX-1/5-LOX inhibitor baicalein were shown to exhibit moderate to good RTA activity in cumene co-autoxidations, as consistent with previous reports. NDGA and baicalein are polyphenols that feature multiple labile O-H bonds,[52] Zileuton, a hydroxamic acid group (O-H bond)[53] and PD146176, a diarylamine (N-H bond). These results were all consistent with previous reports.

Cytoprotective LOX inhibitors ML351 [k_{inh} (3.1 ± .02) x 10^4 $M^{-1}s^{-1}$], and ML355 [k_{inh} (7.7 ± 0.1) x 10^3 $M^{-1}s^{-1}$] exhibit moderate RTA activity in organic solution. However, cytoprotective agent, β-thujaplicin was indistinguishable from the uninhibited control, indicating no significant RTA activity [k_{inh} < 10^3 $M^{-1}s^{-1}$]). The reactivity of ML351 may be ascribed to the *N*-methyl oxazolamine scaffold (N-H bond) and in ML355 to the phenol (O-H bond) and arylamine (N-H) functional groups. The remaining LOX inhibitors, MLS000327069, MLS000327186, MLS000545091, and ML094 were indistinguishable from the uninhibited control, and are therefore devoid of any significant RTA activity (< 10^3 M^{-1} s^{-1}).

Next, the RTA activity of the compound library was determined in biologically relevant Egg PC liposomes suspended in PBS buffer (pH 7.4) (**Figure 2.22**). This medium is more representative of the environmental conditions found within the cell (ie: H-bonding, biphasic environments). Rate constants measured in H-bonding medium are often slower than those measured in organic medium, as RTAs that undergo strong H-bonding with phospholipid head group cannot participate in inhibiting radical mediated lipid peroxidation.[49,54]

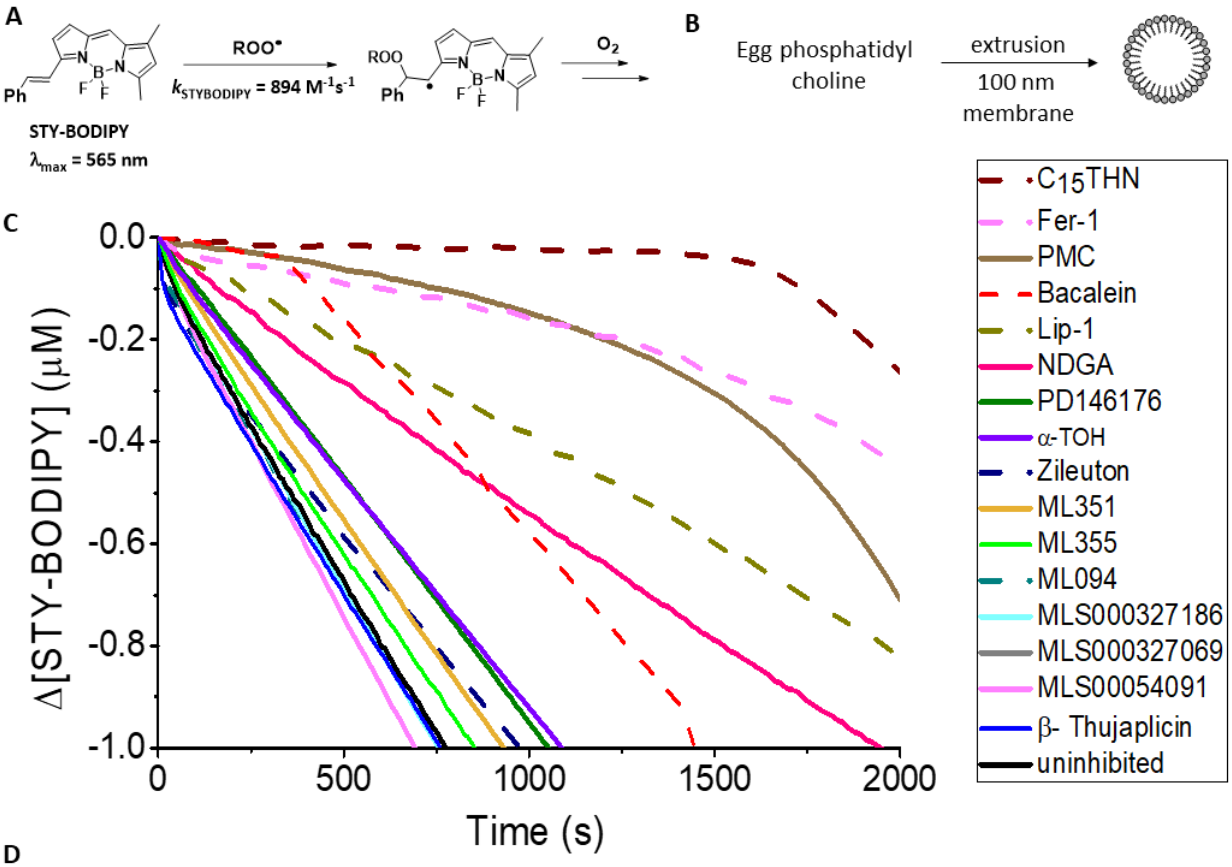

D

LOX inhibitors	Liposome k_{inh} ($M^{-1}s^{-1}$)
ML094	< 10^3
MLS000327186	< 10^3
MLS000327069	< 10^3
MLS000545091	< 10^3
β-Thujaplicin	< 10^3

LOX inhibitors	Liposome k_{inh} ($M^{-1}s^{-1}$)
ML355	(5.2 ± 0.2) x 10^3
ML351	(9.4 ±0.2) x 10^3
PD146176	(1.5 ± 0.5) x 10^4
Baicalein	(3.2 ± 0.3) x 10^4 [c]
Zileuton	(6.8 ± 0.5) x 10^3
NDGA	(1.1 ± 0.2) x 10^4

RTAs	Liposome k_{inh} ($M^{-1}s^{-1}$)
Lip-1	(1.7 ± 0.4) x 10^4
Fer-1	(4.1 ± 0.5) x 10^4
C_{15}-THN	(1.0 ± 0.6) x 10^5
α-TOH	(4.7 ± 0.4) x 10^3 [c]
PMC	(3.5 ± 0.1) x 10^4

Figure 2.22. (**A**) Peroxyl radical formation is monitored by consumption of STY-BODIPY (monitored at 565 mn). (**B**) Liposomes are prepared from Egg Phosphatidyl choline, and extruded through 100 nm membrane to form unilamellar liposomes (**C**) Co-Autoxidation of Egg PC liposomes (1 mM) suspended in PBS buffer (7.4 pH) and STY-BODIPY (10 μM) at 37˚C initiated by MeOAMVN (0.2 mM) and inhibited by of 2 μM RTA or LOX inhibitors. (**D**) Respective inhibition rate constants k_{inh} calculated Egg PC liposomes (Lip). *c* measured previously in Egg PC liposomes at 37˚C.[30]

Anti-ferroptotic agents Lip-1 [k_{inh}(1.7 ± 0.4) x 10^4 $M^{-1}s^{-1}$], and Fer-1 [k_{inh} (4.1 ± 0.5) x 10^4 $M^{-1}s^{-1}$] exhibit good antioxidant activity in both biologically relevant liposomes. Although, the measured k_{inh} is

approximately an order of magnitude slower in aqueous buffer. Additionally, pan LOX inhibitor NDGA, 5-LOX inhibitor Zileuton, 15-LOX-1 inhibitor PD146176, and 12-LOX/15-LOX-1/5-LOX inhibitor baicalein were shown to exhibit moderate to good RTA activity in Egg PC liposome co-autoxidations, as consistent with previous reports carried out in Egg PC liposomes.[31]

Of the newly studied cytoprotective LOX inhibitors, only ML351 and ML355 were shown to exhibit moderate RTA activity [ML351: k_{inh} (9.4 ± .02) x 10^3 $M^{-1}s^{-1}$; ML355: k_{inh} (5.2 ± 0.2) x 10^3 $M^{-1}s^{-1}$] whereas, β-thujaplicin was indistinguishable from the uninhibited control, indicating no significant RTA activity [k_{inh} < 10^3 $M^{-1}s^{-1}$]. A rationale for the cytoprotective activity of β-thujaplicin has been provided in the discussion. The remaining newly studied LOX inhibitors, MLS000327069, MLS000327186, MLS000545091, ML094 were indistinguishable from the uninhibited control, and are therefore devoid of any significant RTA activity (< 10^3 M^{-1} s^{-1}).

2.2.7 Characterization of Lipoxygenase Protein in Model Cell Lines (HT-22, HT-1080)

Characterization of LOX expression in HT-22 cells is fairly ambiguous up to this point. Early reports indicate that HT-22s express 12/15 LOX (aka 15-LOX-1) based on detection of the LOX protein using human antiserum.[25] More recent reports, indicate HT-22s instead express high levels of 15-LOX-2, as determined by western blotting,[33] though, it is not possible to replicate these exact experiments as the polyclonal antibody used in those experiments was discontinued in 2016. To date, the HT-1080 cell line has been classified as expressing high levels of ALOX15B and ALOXE3 as determined by qPCR.[32]

First, monoclonal antibodies for 15-LOX-1, p12-LOX and 15-LOX-2 were tested for isoform specificity. Cell lysate of HEK 293 over-expressing 15-LOX-1, p12-LOX and 15-LOX-2 were electrophoretically separated by SDS-PAGE gel, subsequently transferred to PVDF membrane and probed with the respective monoclonal antibody for chemiluminescent imaging (**Figure 2.23**). Herein, we

confirmed that each monoclonal antibody binds to their advertised LOX isoform. Due to the low protein loading from the 15-LOX-1 transfected cells probed with anti-15LOX-2, we cannot say unequivocally that the antibody is specific to 15-LOX-2.

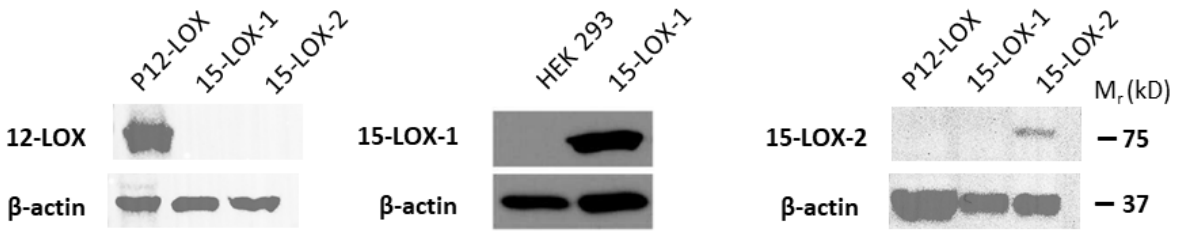

Figure 2.23 p12-LOX, 15-LOX-1 and 15-LOX-2 transfected HEK 293 cell lysate (1 million cells) were probed with respective monoclonal antibody to assess binding specificity of antibody. The western blot probed with 15-LOX-1 antibody was previously prepared by Shah and Pratt.[31]

Next, increasing counts of HT-22 and HT-1080 cell lysate were loaded onto an SDS-PAGE gel for protein separation. The gels were subsequently transferred to PVDF membrane and each membrane was washed with either p12-LOX, 15-LOX-1 or 15-LOX-2 monoclonal antibody (**Figure 2.24**). Upon visualization, we observed that neither HT-22 nor HT-1080 cell lysate contained 12-LOX, 15-LOX-1 or 15-LOX-2 protein. Whereas, clear bands for LOX protein were visible for transfected LOX HEK293 cell lysate included as a positive control.

To corroborate this observation, LOX enzyme activity was monitored by UPLC/ESI-/MS/MS. HT-22 and HT-1080 cell lysate were incubated with 70 μM arachidonic acid at 37˚C for 10 minutes, followed by reduction of potential HpETE product to HETE with PPh_3 in MeOH. Analysis of purified samples, demonstrated minimal formation of HETE products, in both HT-1080 and HT-22 cell lysate (**Figure 2.24**) as compared with HEK 293 cell control (**Figure 2.10.A**). Upon closer inspection, there is slight formation of 15-HETE and 5-HETE peaks in HT-22 cell lysate. Although this proportion of HETE must be correlated with extremely low expression levels of lipoxygenase, as no LOX protein could be detected by immunoblotting with sample containing upwards of 3 million HT-22 cell lysate. The detected HETE

products are more likely a result of background autoxidation of arachidonic acid, as minimal amounts of HETE products are also detected in treated WT HEK 293 cells. It was previously demonstrated that WT HEK 293 cells do not express p12-LOX, 15-LOX-1 or 5-LOX by immunoblotting.[2] It is noted that β-actin bands for control lanes did not visualize properly, this is believed to be a consequence of long-term cold storage of LOX overexpressing lysate samples.

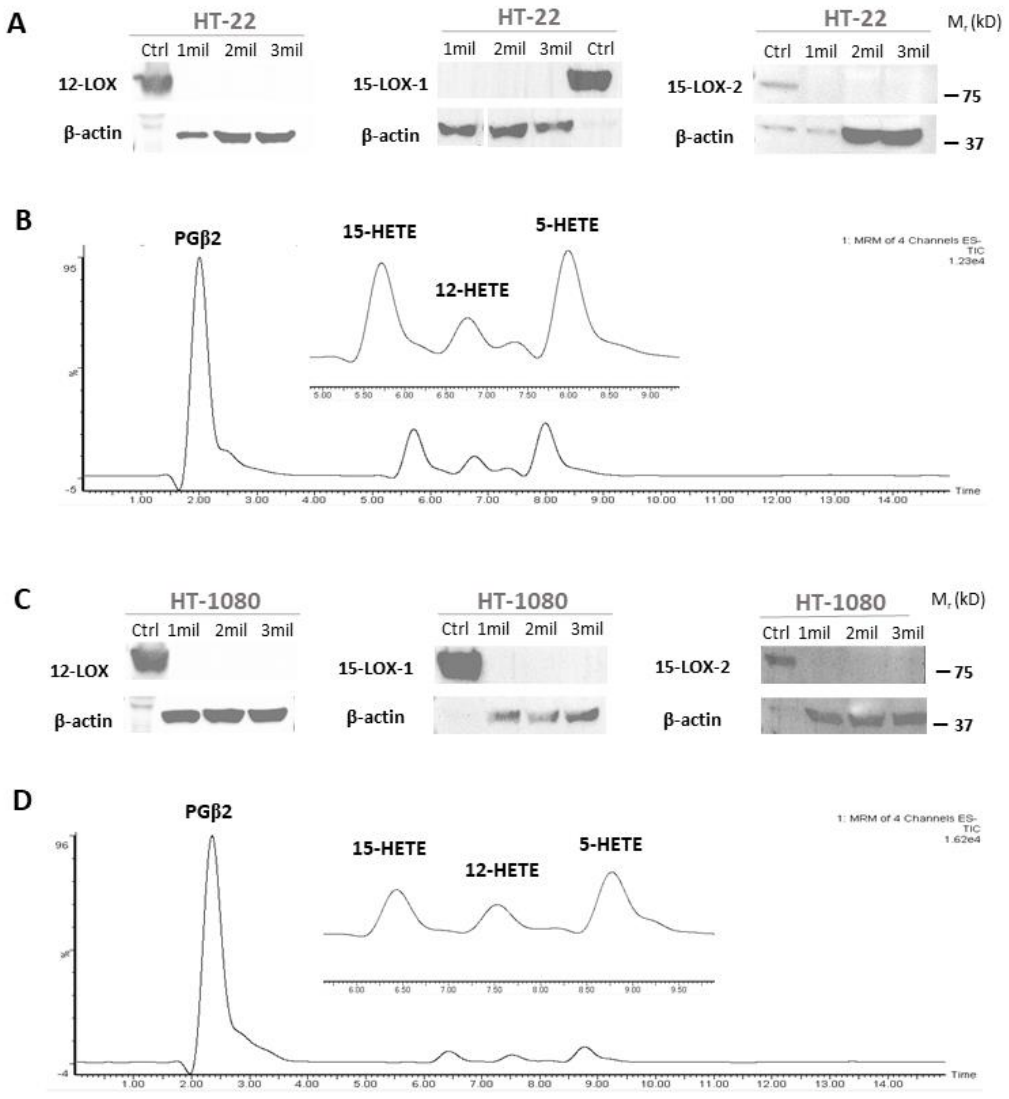

Figure 2.24 (**A**) Increasing counts of HT-22 cells (1 million-3 million) were prepared in 300 μL loading buffer and denatured at 100˚C for 10 minutes. Protein was separated by SDS-PAGE gel electrophoresis and transferred to PVDF membrane for subsequent immunoblotting. (**B**) LC-MS/MS chromatogram of HT-22 cell lysate dosed with 70 μM AA. (**C**) Increasing counts of HT-1080 cells (1million-3million) were prepared

in 300 μL loading buffer and denatured at 100˚C for 10 minutes. Protein was separated by SDS-PAGE gel electrophoresis and transferred to PVDF membrane for subsequent immunoblotting. (**D**) LC-MS/MS chromatogram of HT-1080 cell lysate dosed with 70 μM AA.

We considered the possibility that LOX expression may be induced/increased under circumstances of cellular stress and sought to induce ferroptotic stress in model cell lines following treatment with RSL3 and glutamate, over brief time intervals (**Figure 2.25**). HT-22 cells were dosed with glutamate containing medium over 4 hours, sufficient time to induce a cellular response to stress, but avoid killing the cell.[55] Likewise, HT-1080 cells were dosed with RSL3 for 10 minutes, as previous studies monitoring viability in transfected HEK-293 cells showcased decreased viability from this time point onwards.[31] Although, it is difficult to confidently dictate whether HT-1080 cells respond effectively to RSL3 in only 10 minutes. Therefore, HT-1080 cells were also exposed to erastin for 4 hours prior to analysis by immunoblotting. Probing the stressed HT-22 and HT-1080 cell lysate with p12-LOX, 15-LOX-1 and 15-LOX-2 monoclonal antibody again revealed no lipoxygenase protein could be detected.

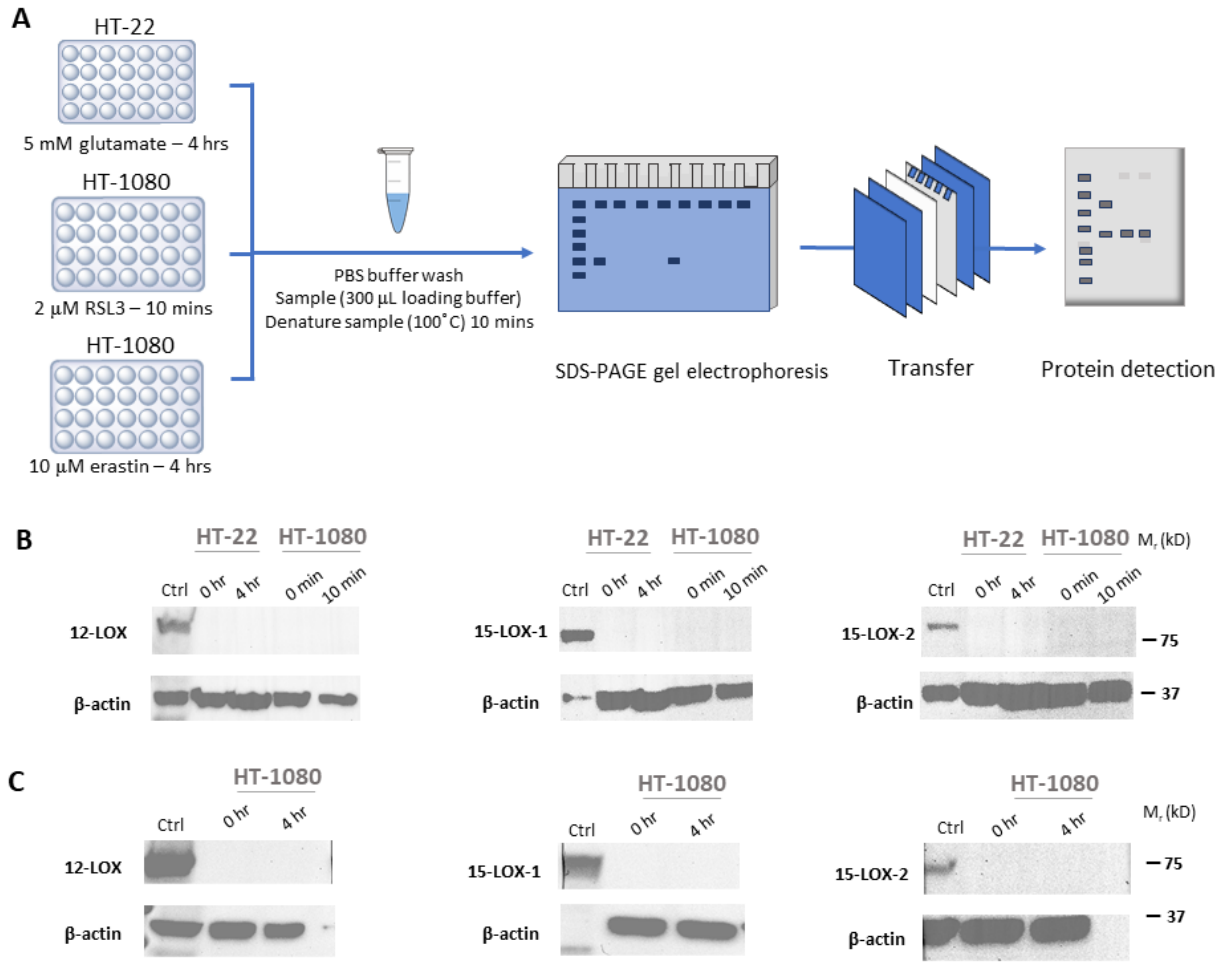

Figure 2.25 (**A**) HT-22 and HT-1080 cells were stressed with ferroptosis inducing agents, followed by preparation of sampled for SDS-PAGE gel electrophoresis and subsequent protein detection by immunoblotting. (**B**) HT-22 (1 million) cells treated with glutamate and HT-1080 (1 million) cells treated with RSL3 were probed with p-12LOX, 15-LOX-1 and 15-LOX-2 monoclonal antibody. (**C**) HT-1080 (1 million) cells treated with erastin were probed with p-12LOX, 15-LOX-1 and 15-LOX-2 monoclonal antibody.

The lack of detected LOX protein implies that they are not expressed to a significant extent in the cell lines wherein ferroptosis and oxytosis were first characterized. This underscores the foregoing cell rescue results which imply that LOX catalysis cannot be the primary source of the lipid hydroperoxides associated with ferroptosis execution.

2.3 Discussion

Ferroptosis is a form of regulated cell death marked by an accumulation of lipid hydroperoxides. Oxidized lipids disrupt membrane packing, organization and permeability and lead to reactive electrophilic byproducts. To date, the source of lipid hydroperoxides has remained a contested point of debate in the literature. Evidence in support of lipoxygenase as a key ferroptotic regulator is primarily based on pharmacological mediation with small molecule LOX inhibitors and genetic intervention of LOX. For example, Seiler et al. demonstrated that GPX4 knockout MEFs could be rescued when cultivated in the presence of NDGA, baicalein and PD146176.[27] In the same paper, 12/15 Knockout MEF cells, were shown to be highly resistant to GSH depletion. Later work by Yang et al. focused on BJeLR and HT-1080 cells lines, which were characterized to express ALOX15B and ALOXE3.[47] Both cells were treated with a pool of siRNA targeting both ALOX genes, and were rescued from erastin induced cell death.

Previous work by Shah and Pratt[31] demonstrated that overexpression of 5-LOX, p12-LOX or 15-LOX-1 in transfected HEK-293 cells marginally sensitized cells to ferroptosis. Furthermore, it was also established that RTAs and redox active LOX inhibitors, such as NDGA, zileuton, PD146176 and baicalein were good anti-ferroptotic agents, independent of their isoform selectivity. Redox inactive LOX inhibitors of 5-LOX such as CAY10649 and CJ-13610 could not rescue cells treated with GPX4 inhibitor, RSL3. This was a crucial piece of evidence that suggested that autoxidation is key to the execution of ferroptotic cell death. In the current work, we extended the 2018 investigations to include investigation of redox inactive inhibitors of 15-LOX-1 and p12-LOX. Once again, redox inactive inhibitors were incapable of subverting ferroptosis.

Shah and Pratt's original work also failed to include investigations with cells transfected to overexpress the 15-LOX-2 isoform. Intervening work by the Kagan group has implicated the 15-LOX2/PEBP1 complex as a key player in ferroptosis.[33,34] The purported role of 15-LOX-2 in ferroptosis was

investigated in HEK 293 cells transfected to express *ALOX15B*. The presence of 15-LOX-2 protein was demonstrated using a monoclonal antibody with established isoform selectivity. In cell rescue experiments, we observed RTAs (i.e. Lip-1, Fer-1, C15THN, PMC, α-TOH), redox active LOX inhibitors (i.e. NDGA, Zileuton, PD146176) and β-thujaplicin successfully restored cell viability, but not redox inactive 15-LOX-2 inhibitors (MLS000327186, MLS000327069, MLS000545091). A literature search reveals β-thujaplicin is an excellent ferric/ferrous iron chelator.[56] It has been well documented in the literature that iron chelators such as DFOM can possess potent anti-ferroptotic activity[16], although the speciation of iron that participates in ferroptosis, free or enzyme bound is currently unknown.

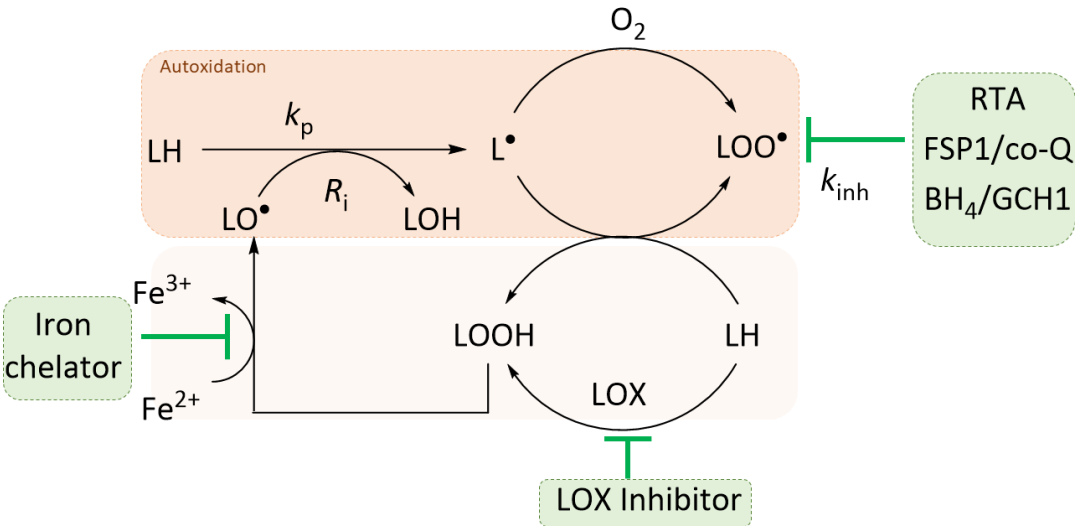

Figure 2.26 kinetic scheme illustrating radical mediated oxidation of unsaturated lipid (LH) by peroxyl/alkoxyl species (LOO•/ LO•). RTA quench radicals in solution to form non-radicals products. If present, LOX catalyze dioxygenation of unsaturated lipid substrate to contribute to cellular pool of LOOH. Low valent metals, such as iron promoted the decomposition of lipid hydroperoxide to alkoxyl/hydroxyl products.

An exceptional increase in 5-HPETE production was observed following administration with increasing concentration of β-thujaplicin in 5-LOX overexpressing HEK 293 cells. The 5-LOX isoform plays a critical role in the leukotriene biosynthesis pathway by catalyzing the first two steps. Following liberation of arachidonic acid from phospholipids by cytosolic phospholipase $A_2\alpha$ ($CPLA_2\alpha$), arachidonic acid is swiftly

taken up by 5-LOX to catalyze the formation of unstable epoxide intermediate leukotriene A_4 (LA_4).[24] From here, LA_4 is transformed to many leukotrienes and lipoxins (**figure 1.12**). For instance, glutathione S-transferase II (LTC4S), catalyzes the first step of cysteinyl leukotriene biosynthesis. It is possible β-thujaplicin inhibits the formation of epoxide intermediate leukotriene A_4 or even inhibits an enzyme downstream of 5-LOX, such as LTC4S, halting consumption of 5-HPETE, that would otherwise fuel leukotriene biosynthetic pathways.

It was also demonstrated in 15-LOX-2 overexpressing cell rescue experiments that redox inactive 15-LOX-2 inhibitors MLS000327186, MLS000327069, and MLS000545091 were unable to extend cell viability past 10 %. If 15-LOX-2 were an essential piece of ferroptosis machinery, we would expect pharmacological inhibition of LOX to maintain cell viability. The PEPB1/15-LOX-2 was reported as a key payer in ferroptotic cell death, as it favours the oxidation of AA-PE.[33] It was previously demonstrated by our group that HEK cells express PEBP1, by immunodetection.[31] However, the poor performance of 15-LOX-2 inhibitors at rescuing 15-LOX-2 expressing HEK 293 cells from RSL3 induced ferroptosis does not support the role of the 15-LOX-2/PEBP1 complex as a central mediator of ferroptotic lipid peroxidation.

Furthermore, it was observed that 15-LOX-2 overexpressing HEK 293 cells were sensitized to ferroptosis. In previous work by Shah and Pratt, 15-LOX-1, p12-LOX and 5-LOX transfected HEK 293 cells were also sensitized to both RSL3 and erastin induced ferroptosis as compared to wild type HEK 293. The following observations can be rationalized to a broader statement, that any piece of machinery that increases the cellular concentration of lipid hydroperoxides (LOOH), such as lipoxygenase, will increase the rate of initiation of lipid autoxidation, R_i. For example, iron (II) can catalyze the decomposition of lipid hydroperoxides to alkoxyl radicals. These reactive intermediates serve to generate additional lipid chains that directly re-source the cellular concentration of lipid hydroperoxide product. Likewise, ACLS4, a key enzyme in the biosynthesis of esterified lipids, increases the pool of lipid peroxidation substrate, both increasing R_i. Analogously, the reverse statement is also true, where any agent that decreases the

concentration of LOOH, will decrease R_i. For example, GPX4 directly detoxifies the cellular lipid hydroperoxides to the corresponding neutral alcohol, eliminating the cellular pool of LOOH. Additionally, endogenous antioxidants, including the recently characterized FSP1/co-Q[15] and BH4/GCH1[14] pathways, remove reactive radical species to non-destructive pathways.

In HT-22 and HT-1080 cell lines which were used in the initial characterization of oxytosis and ferroptosis, respectively, we again observed that RTAs and iron chelators were effective anti-ferroptotic agents, regardless of the mode of initiation (glutamate, erastin and RSL3). Notably, Lip-1, Fer-1, and designer antioxidant, C15-THN were especially potent over 24 hour experiments following treatment with glutamate and erastin. Furthermore, LOX inhibitors with RTA activity, especially, Zileuton, NDGA and PD146176 proved to be good-to-moderate anti-ferroptotic agents, whereas, redox inactive LOX inhibitors, in particular 15-LOX-2 inhibitors, held little-to-no impact on cell viability. At the time, this was an interesting revelation as both HT-22 and HT-1080 cells were reported to express 15-LOX-2. 15-LOX-2 has garnered attention in the literature as a favourable source of lipid hydroperoxides within a ferropotiotic cell. However, characterizing these cell lines in our own hands by immunoblotting yielded an unexpected result.

Established cell lines used in the study of ferroptosis, HT-22 and HT-1080s cell lysate did not appear to express p12-LOX, 15-LOX-1 nor 15-LOX-2 by immunoblotting**.** These results were corroborated by monitoring the corresponding arachidonic acid oxidation (HETE) products of both cell lines by UPLC/ESI^-/MS/MS which showed very minimal and non-regiospecific HETE production. This was especially interesting given the purported role of 15-LOX-2 in ferroptosis. It is plausible that LOX expression may be promoted during episodes of cellular stress. As a result, HT-22 and HT-1080s were incubated with ferroptotic inducers over shortened periods to generate cellular stress, yet, LOX protein could still not be detected by immunoblotting. Previous characterization of HT-22 cells by immunoblotting detected 15-LOX-2 protein, however this attempt made use of a polyclonal antibody, that has since been

discontinued.[33] The lack of LOX protein present in model cell lines fortified our previous observation, that LOX is not an integral part of ferroptosis and prompted the following conclusion. If present, LOX can contribute to the cellular concentration of lipid hydroperoxides, yet autoxidation is the key mediator of ferropototic cell death.

Consistent with previous work, we have demonstrated that RTAs rescue cells from ferroptotic activity, however, some RTAs perform better than others in the context of restoring viability in cell rescue assays. Previously our group studied the relationship between RTA activity and anti-ferropototic potency and found an excellent correlation exists when measuring RTA activity using the FENIX method.[52] The FENIX method uses a lipophilic initiator DTUN, in place of the classic initiator MeOAMVN. When plotting the log of EC_{50} (M) values measured in glutamate treated HT-22 cells and erastin treated HT-1080 cells against the log of k_{inh} measured in liposomes, against MeOAMVN, (k_{inh} $M^{-1}s^{-1}$), a poor correlation is observed (**Figure 2.27 C - D**).

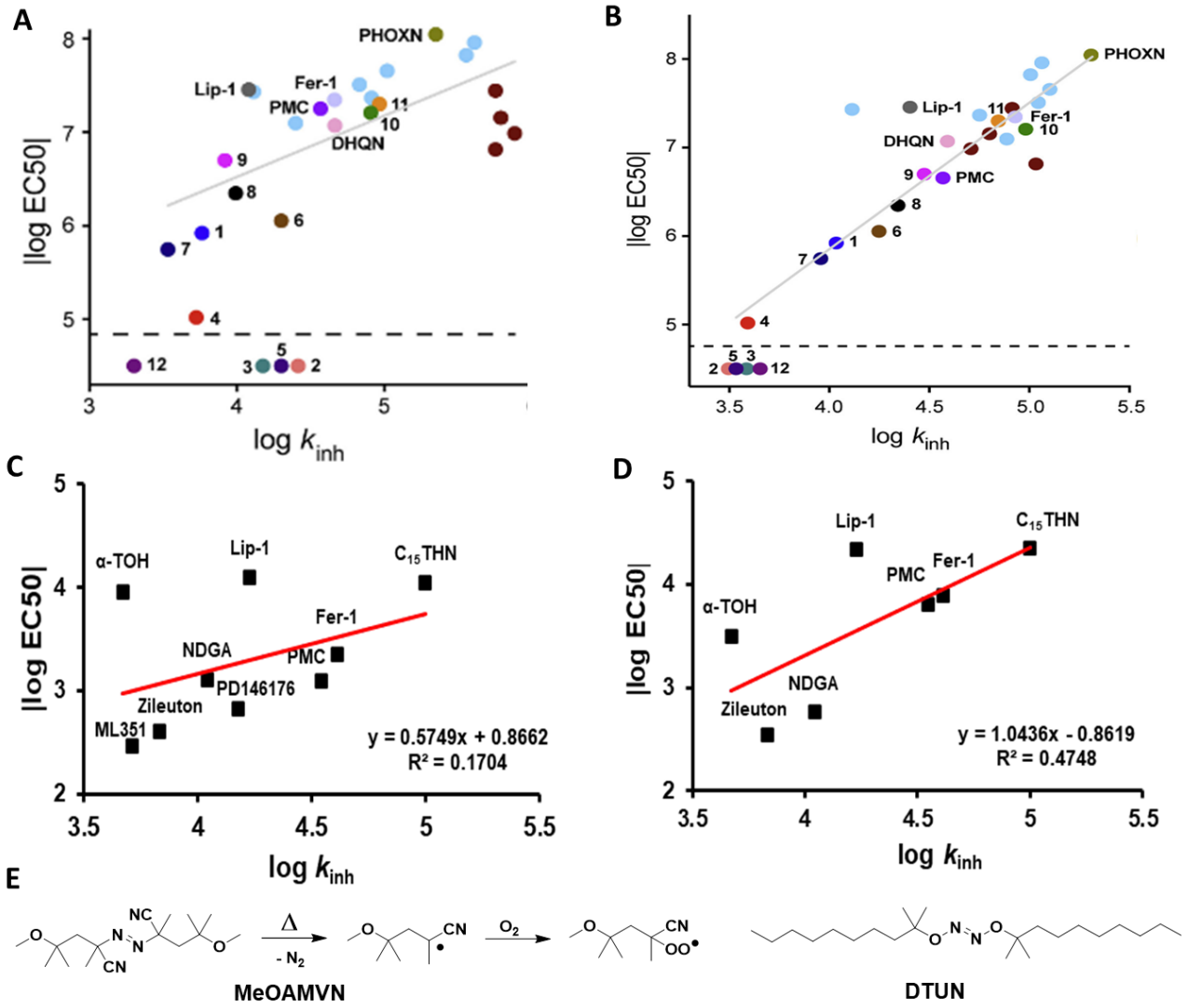

Figure 2.27 The log of *k* inhibition rate constants measured against MeOAMVN in liposomes (Lip k_{inh} $M^{-1}s^{-1}$) were plotted against the log of EC_{50} (M) values determined in (**A**) RSL3 treated Pfa1 MEFs. (**B**) The log of *k* inhibition rate constants measured against DTUN in liposomes (Lip k_{inh} $M^{-1}s^{-1}$) were plotted against the log of EC_{50} (M) values determined in RSL3 treated Pfa1 MEFs. Plots were used from publication, with consent [52] (**C**) The log of *k* inhibition rate constants measured against MeOAMVN in liposomes (Lip k_{inh} $M^{-1}s^{-1}$) were plotted against the log of EC_{50} (M) values determined in glutamate treated HT-22's and (**D**) erastin treated HT-1080 cells. (**E**) Molecular structures of classic aza-initiator MeOAMVN and newly developed lipophilic imitator DTUN.[54]

Previously, Shah and co-workers demonstrated a poor correlation exists between k_{inh} measured against MeOAMVN in Egg PC liposomes and cell rescue in Pfa1 cells treated with RSL3 (**Figure 2.27.A**). MeOAMVN overestimates the reactivity of water soluble RTAs, as it is amphiphilic and resides at the lipid-

aqueous interface. At low concentrations of lipid, water soluble RTAs will react directly with MeOAMVN derived radicals prior to inhibiting lipid peroxidation, competing with initiation of lipid peroxidation. Instead, Shah and coworkers demonstrated that lipophilic, hyponitrite initiator DTUN is mechanistically more similar to ferroptotosis execution and provides excellent correlations between RTA potency and cell based assays.

Targeting lipid peroxidation suppresses a downstream pathway of ferroptosis, where RTA concentration must be continuous to ensure cell survival. This is visualized in **Figure 2.18** wherein HT-1080 treated with erastin and an initial dose of Fer-1, undergo a decrease in cell viability from 100 → 40% over a 40 hour period. Following consumption of RTA, the cell is once again vulnerable to lipid peroxidation and must rely on endogenous systems like FSP1 and DHFR pathways. For future therapies, it is worth investigating upstream pathways that mediate the genesis of lipid peroxidation initiation. Perhaps, this is where the role of iron in "ferro"-ptosis will become more transparent. Iron is an essential element for life, that exists in two forms, ferric (II) and ferrous (III) and plays a key role in cellular respiration, DNA synthesis, enzyme cofactors.

Consistent with previous investigations,[16,30,31] we have again demonstrated in investigations pharmacologically targeting both lipoxygenase and radical mediated lipid peroxidation, that RTAs and iron chelators are cytoprotective agents. Furthermore, investigations into monitoring HETE detection by UPLC/ESI^-/MS/MS and immunoblotting, it has been shown that the cell lines which were used in the initial characterization of ferroptosis (HT-1080) and oxytosis (HT-22) do not produce significant amounts of lipoxygenase enzymes. These results support our earlier contention that lipoxygenase catalysis is not necessary for ferroptosis, and moreover, that lipid autoxidation is the key mediator of ferroptosis execution. If lipoxygenases are expressed to a significant extent, they simply contribute to the cellular pool of lipid hydroperoxides. The next questions that remains to be answered are the role and speciation (free or enzyme bound) of iron, and the link between lipid accumulation and cell death. These answers

may provide insight and potential therapeutic solutions to a number of human pathologies linked to oxidative stress such as neurodegenerative diseases (Alzheimer's, Parkinson's disease), diabetes and ischemia.

2.4 Conclusion and Perspective

In summary, ferroptosis is a novel form of regulated cell death marked by an accumulation of lipid hydroperoxides. The work carried out by Zilka, Shah, and Pratt and the work outlined in this document have contributed to elucidating the origin of lipid hydroperoxides during ferroptosis initiation and execution. Herein, we have demonstrated in rescue experiments across transfected and model cell lines that radical trapping antioxidants (Lip-1, Fer-1, PMC, A-TOH and C15-THN), LOX inhibitors with RTA activity (NDGA, Zileuton, PD146176) and iron chelating compounds (β-thujaplicin) are effective at halting ferroptotic cell death. Mechanistically, antioxidants quench reactive radical species within the lipid membrane that otherwise catalyze lipid peroxidation. Moreover, metal chelators coordinate to iron, inhibiting its capacity to undergo 1 electron chemistry. LOX inhibitors (Baicalein, ML351, ML355) were successful at suppressing lipid peroxidation, but were unable to fully restore cell viability across multiple cell lines. Baicalein reaches a cytotoxic threshold within the cell, and ML351 and ML355 reach the point of solubility in experimental media before complete cell viability can be attained. LOX inhibitors with no RTA activity (ML094, MLS000545091, MLS000327186, MLS000327069) are completely deficient at suppressing the onset of ferroptotic death.

Given the recent implication of 15-LOX-2 as a key mediator in ferroptosis, cell rescue experiments were also carried out in 15-LOX-2 transfected HEK 293 cells. Although expression in transfected cell lines was low, it was observed that 15-LOX-2 expressing cells were still sensitized to oxidative cell death, as lipoxygenase can contribute to the cellular pool of lipid hydroperoxides, increasing R_i. In cell rescue experiments, again, only RTAs (Lip-1, Fer-1, PMC, A-TOH and C15-THN, NDGA, Zileuton) and iron chelators

(β-thujaplicin), were successful at rescuing ferroptotic cells. Moreover, 15-LOX-2 inhibitors had no impact on cell viability. Results in both transfected and model cell lines suggest the role of lipoxygenase in ferroptosis initiation and execution is minimal.

Further investigation towards characterizing ferroptotic model cell lines, HT-22 and HT-1080, revealed these cellular models do not express p12-LOX, 15-LOX-1 and 15-LOX-2 as determined by immunoblotting with monoclonal antibody detection. This was corroborated by autoxidation chromatograms carried out by LC/MS/MS. Model cells were stressed with ferroptotic inducing agents, glutamate, RSL3 and erastin and still, lipoxygenase protein could not be detected. These observations prompted the suggestion that the presence of lipoxygenase is not a requisite for ferroptotic initiation and execution. Moreover, if present, lipoxygenase can contribute to the cellular pool of lipid hydroperoxides, yet it is radical mediated lipid peroxidation that drive ferroptosis.

In the context of this work, some experiments remain to be completed. First, known RTAs (αTOH, PMC, Lip-1, Fer-1 and C_{15}THN) will also be subjected to 15-LOX-2 enzyme activity experiments. In our previous work, these compounds were not determined to exhibit p12-LOX, 5-LOX or 15-LOX-1 inhibitory activity. However, a recent publication has suggested that following complexation of 15-LOX-2 and PEPB1, an inhibitory binding site for Fer-1 is formed.[33] Furthermore, an initial objective for this work was to test our compound library in cell models that naturally express high levels of lipoxygenase. Previously, our investigations into overexpressing LOX cells have been carried out in HEK 293 cells transfected to overexpress different isoforms of LOX. Following the selection of HT-22 and HT-1080 model cell lines, it was later determined that neither express substantial amounts of LOX. Therefore, support for our hypothesis would be strengthened by extending investigations in cells which do, in fact, express high levels of LOX, beyond transfected HEK-293 cells.

The scope of future work for this project can be extended to a wider lens. There is great utility in compiling characterization data such as RTA activity (k_{inh}) and cell potency (EC_{50}) and constructing predictive tools to identify potential potent anti ferroptotic candidates. In our group, anti-ferropototic potency is primarily measured in cell rescue assays, although a greater amount of information could be generated by testing RTA drug candidates in animal models and clinical trials. To date, a considerable number of antioxidants have failed in clinical trials[57] however, not all RTAs can efficiently inhibit (phospho)lipid peroxidation. For example, Shah and coworkers have demonstrated that water-soluble RTAs and lipophilic RTAs that undergo strong H bonding with phospholipid head groups are not efficient anti-ferroptotic agents (e.g. phenols).[54]

The application of RTAs in ferroptosis is a solution to a downstream process, and once an RTA is consumed lipid peroxidation will resume until the cell dies or, until the RTA is regenerated. Future work, in the study of ferroptosis, relies on identifying upstream targets, such as genes and their subsequent gene products. For instance, elucidating the role of iron regulation in ferroptosis. These advances rely on the application of genetic tools and the development of chemical probes to observe the outplay of ferroptosis in tissue and entire organisms. Once a detailed blueprint of ferroptosis is assembled, coupled with the identification of potential biomarkers, the occurrence of ferroptosis in disease will become more clear. To date, ferroptosis has been linked to a number of human pathologies including cancer, ischemia, diabetes and neurodegenerative disorders, Alzheimer's, Parkinson's and Huntington's diseases. Providing further insight into the biochemical, morphological and genetic mechanism of ferroptosis could bridge the way towards future therapies and pathological mediation.

2.5 Experimental

All chemicals and solvents were purchased from Sigma Aldrich Co. LLC and used as received unless otherwise stated. BHT and PPh_3 were recrystallized from hexanes prior to use. ML351[40] and ML094[39] were synthesized according to literature protocol. Synthetic procedures for MLS000327069, MLS000327186

and MLS000545091 are described within. Erastin,[30,58] RSL3,[28,29] Fer-1,[29] Lip-1[28] were synthesized according to literature protocol and was graciously provided by Ron Shah. C15THN[59] was synthesized according to literature protocol and were graciously provided by Omkar Zilka. Egg phosphatidylcholine, AIBN, MeOAMVN, Arachidonic Acid, NDGA, Zileuton, PD146176, Baicalein, β-thujaplicin, ML355, α-TOH and PMC were purchased from commercial sources and used as received. pcDNA15-LOX-2 plasmid was generously provided by Professor Alan Brash (Vanderbilt University). OptiMEM, DMEM and MEM media with/without phenol red, Dulbecco's phosphate buffered saline (DPBS), fetal bovine serum (FBS), penicillin-streptomycin, Lipofectamine LTX reagent with PLUS reagent, and AquaBluer were purchased from commercial sources and used as received. SiliaPrep SPE cartridges C18 (17%) poly were purchased from SiliCycle and used as received. Antibodies: Beta-actin antibody (AC-15) NB600-501, 15-Lipoxygenase 1 Antibody (OT13G8) NBP2-01740, 15-Lipoxygenase 2 Antibody NBP2-58984, 12-Lipoxygenase Antibody (1C3) NBP2-46512, Goat anti-rabbit igG (H+L) Secondary antibody [HRP] NB7160 and Goat anti-Mouse IgG (H+L) SecondaryAntibody [HRP] NB7539 were purchased from Novus biologicals and used as received.

Cumene Co-autoxidations. Cumene was washed with 1.0 M NaOH (X3), brine (X1), dried over $MgSO_4$ and then distilled under vacuum. The resulting distillate was then run over a column of basic alumina (2/3) silica (1/3) and the purified cumene could be used over 7 days. To each quartz cuvette, 1.25 mL (3.6 M) cumene and 1.18mL (4.65 M) chlorobenzene were added and left to equilibrate for 5 minutes at 37˚C. The solution was blanked, after which 12.5 μL of STY-BODIPY (2 mM solution in 2,3,5-trichlorobenzene) was added followed by 50 μL of AIBN (0.3 M stock in chlorobenzene), ensuring the solution was completely mixed. After 45 minutes, 10 μL of compound (500 μM RTA or LOX inhibitor stock in chlorobenzene) was added to the cuvette and again mixed thoroughly. The loss in absorbance at 565 nm was followed with three technical replicates, and inhibition rate constants (k_{inh}) and stoichiometry (n) were determined per equations 1-2 (**Figure 2.22**). Kinetics are reported as the mean ± standard deviation.

Egg PC liposome Co-autoxidations. To each quartz cuvette, 2.3 mL of liposome buffer (10 mM PBS, pH 7.4) and 125 μL of freshly extruded liposomes (10 mM stock in PBS buffer, pH 7.4, preparation of liposome described herein[28]) were added and equilibrated in the cuvette at 37˚C for 5 minutes. The solution was blanked, afterwhich 10 μL of STY-BODIPY (2 mM stock in DMSO) was added followed by 10 μL of MeOAMVN (0.05M stock in ACN), ensuring the solution was completely mixed. After 5 minutes, 10 μL of compound (500μM RTA or LOX inhibitor stock in DMSO) was added to the cuvette and again mixed thoroughly. The loss in absorbance at 565 nm was followed with three technical replicates, and inhibition rate constants (k_{inh}) and stoichiometry (n) were determined per equations 1-2 (**Figure 2.22**). Kinetics are reported as the mean ± standard deviation.

Cell culture. All cell lines were cultured at 37˚C in an atmosphere of 5% CO_2. HT-22 and HT-1080 cells were grown in DMEM, 10% FBS, 1 mM glutamine and 1% penicillin-streptomycin. HEK 293 cells were grown in MEM 10% FBS, 1 mM sodium pyruvate, 1% 100X non-essential amino acids and 1% penicillin-streptomycin. Transfected cell lines 15-LOX-1 HEK293 and p12-LOX HEK 293 were grown in MEM 10% FBS, 1 mM sodium pyruvate, 1% 100X non-essential amino acids, 1 g/L geneticin. Transfected cell line 15-LOX-2 HEK 293 cells were grown in MEM 10% FBS, 1 mM sodium pyruvate, 1% 100X non-essential amino acids and 0.1 g/L geneticin. Cells were passaged using 1X solution of 0.05% Trypsin, 0.02% EDTA in PBS buffer at 37˚C every two to three days. Cells were cultured for a maximum of 25 passages.

***(1S,3R) RSL3 (inhibition of GPX4) induced ferroptosis*.** The night prior, 15-LOX-2HEK293 cells HT-22 or HT-1080 (3000 cells per 100 μL) were seeded in a 96 well plate. The following morning, culture medium was removed, washed with PBS buffer and replaced with fresh culture medium. Cells were dosed with *(1S,3R)* RSL3 (0.8 μM HT-22, 2 μM HT-1080, 5.5 μM 15-LOX-2HEK293) and incubated for 4 hours at 37˚C. To determine cell viability, experimental medium was then removed and replaced with a 1/100 dilution of Aquabluer, following manufacturer's instructions. Cell data were normalized using untreated cells as a blank. 3 Technical replicates were performed using n = 6 wells as one replicate. Cell viability plots were

fitted with the dose-response function in Microcal Origin (upper and lower bounds were not fixed) from which EC_{50}values were derived. EC_{50} values are reported as the mean ± standard deviation.

Glutamate (inhibition of system X_c^-) induced ferroptosis. The night prior, HT-22 cells (3000 cells per 100 μL) were seeded in a 96 well plate. The following morning, culture media was removed, washed with PBS buffer and replaced with experiment medium (DMEM 10% FBS, 1% penicillin & streptomycin). Cells were dosed with 10 mM glutamate and were incubated for 24 hours at 37˚C. To determine cell viability, experimental media was then removed and replaced with a 1/100 dilution of Aquabluer (no glutamine), following manufacturer's instructions. Cell data were normalized using untreated cells as a blank. Three Technical replicates were performed using n = 6 wells as one replicate. Cell viability plots were fitted with the dose-response function in Microcal Origin (upper and lower bounds were not fixed) from which EC_{50}-values were derived. EC_{50} values are reported as the mean ± standard deviation.

Erastin (inhibition of system X_c^-) induced ferroptosis. The night prior, HT-1080 cells (3000 cells per 100 μL) were seeded in a 96 well plate. The following morning, culture medium was removed, washed with PBS buffer and replaced with experimental medium (DMEM, 10% FBS, 1mM glutamine, 1% penicillin & streptomycin and 10 μM erastin) and were left to incubate for 24 hours at 37˚C. To determine cell viability, experimental medium was then removed and replaced with a 1/100 dilution of Aquabluer, following manufacturer's instructions. Cell data were normalized using untreated cells as a blank. Three Technical replicates were performed using n = 6 wells as one replicate. Cell viability plots were fitted with the dose-response function in Microcal Origin (upper and lower bounds were not fixed) from which EC_{50}values were derived. EC_{50} values are reported as the mean ± standard deviation.

Inhibition of (1S,3R) RSL3 (inhibition of GPX4) induced ferroptosis. The night prior, 15-LOX-2HEK293 cells HT-22 or HT-1080 (3000 cells per 100 μL) were seeded in a 96 well plate. The following morning, culture media was removed, washed with PBS buffer and replaced with fresh culture medium. Cells were treated

with a range of RTA or LOX inhibitor concentrations and were left to incubate for 30 minutes at 37˚C. Following incubation, cells were dosed with *(1S,3R)* RSL3 (0.8 μM HT-22, 2 μM HT-1080, 5.5 μM 15-LOX-2HEK293) and incubated for 4 hours at 37˚C. To determine cell viability, experimental media was then removed and replaced with a 1/100 dilution of Aquabluar, following manufacturer's instructions. Cell data was normalized using untreated cells as a blank. 3 Technical replicates were performed using n = 6 wells as one replicate. EC_{50} values are reported as the mean ± standard deviation.

***Inhibition of glutamate (inhibition of system X_c^-) induced ferroptosis*.** The night prior, HT-22 cells (3000 cells per 100μL) were seeded in a 96 well plate. The following morning, culture medium was removed, washed with PBS buffer and replaced with experiment medium (DMEM 10% FBS, 1% penicillin & streptomycin). Cells were treated with a range of RTA or LOX inhibitor concentrations and left to incubate for 30 minutes at 37˚C. Following incubation, cells were dosed with 10 mM glutamate and were incubated for 24 hours at 37˚C. To determine cell viability, experimental medium was then removed and replaced with a 1/100 dilution of Aquabluer (no glutamine), following manufacturer's instructions. Cell data were normalized using untreated cells as a blank. Three Technical replicates were performed using n = 6 wells as one replicate. Cell viability plots were fitted with the dose-response function in Microcal Origin (upper and lower bounds were not fixed) from which EC_{50}values were derived. EC_{50} values are reported as the mean ± standard deviation.

***Inhibition of erastin (inhibition of system X_c^-) induced ferroptosis*.** The night prior, HT-1080 cells (3000 cells per 100 μL) were seeded in a 96 well plate. The following morning, culture medium was removed, washed with PBS buffer and replaced with experimental medium (DMEM, 10% FBS, 1 mM glutamine, 1% penicillin & streptomycin and 10 μM erastin). Cells were treated with a range of RTA or LOX inhibitor concentrations and were left to incubate for 24 hours at 37˚C. To determine cell viability, experimental medium was then removed and replaced with a 1/100 dilution of Aquabluer, following manufacturer's instructions. Cell data were normalized using untreated cells as a blank. Three technical replicates were

performed using n = 6 wells as one replicate. Cell viability plots were fitted with the dose-response function in Microcal Origin (upper and lower bounds were not fixed) from which EC_{50} values were derived. EC_{50} values are reported as the mean ± standard deviation.

Bacterial transformation and cell transfection. For transformation, freshly thawed E. coli were incubated with pcDNA *alox15B* plasmid (45 μg/mL) (graciously provided by Professor Alan Brash from Vanderbilt University) on ice for 30 minutes, followed by heat shock for 45 seconds (42˚C) and immediate return to ice for 2 minutes. E coli/DNA mixture was added to LB broth (1 mL) and incubated at 37˚C for 30 minutes in a shaking incubator . An aliquot of broth (10 μL) was plated on agarose (loaded with ampicillin) culture dishes and incubated overnight at 37˚C. The following morning, single colonies were transferred to fresh LB broth (2 mL) containing (100 μL/mL) ampicillin and were grown in a shaking incubator at 37˚C overnight. The next day, DNA plasmid was extracted from bacterial cells using the Monarch plasmid DNA miniprep kit, following manufacturer's instructions. For transfection, HEK 293 cells were plated to 50-80% confluency in a 6 well plate and then transfected with pcDNA3 *alox15B* construct using Lipofectamine 3000 & PLUS reagent according to manufacturer's recommendations. Cells were passaged to a new 6 well plate after one day and screened using 0.1→1 g/L geneticin. Stable transfection was verified every few passages.

***Determination of H(P)ETES by UPLC/MS/MS*.** Once confluent, transfected LOX HEK 293 cells were tryspinized, transferred to a 50 mL falcon tube and spun at 1000 rpm for 4 minutes. The culture medium was removed and replaced with Tris buffer (7.4 pH). Cells were lysed with 1% protease inhibitor cocktail and the resulting solution was incubated with 70 μM Arachidonic Acid for 10 minutes at 37˚C. The reactions were terminated with 1 volume of 1.5 mg/mL PMC in MeOH and left to quench for 90 minutes at room temperature, ensuring all HPETE are reduced to HETE. For inhibition studies LOX inhibitors were incubated with cell lysate on ice for 10 minutes prior to addition of arachidonic acid. After quenching, samples were purified on Silicycle C18 solid phase extraction columns, following manufacturer's

instruction. The eluent in methanol were dried (MeOH was removed under vacuum) and resuspended in 80 μL MeOH and 20 μL of Prostaglandin β2 (50 μM stock in MeOH). For separation and quantification of HETE products, 5 μL aliquots were injected onto a Waters UPLC/MS system using an Acquity C18 reverse phase column (2.1 mm X 50 mm, 1.7 μM particle size). HETE products were eluted isocratically in a mobile phase consisting of acetonitrile, methanol, water and acetic acid (42:25:33:0.007) over 10 minutes (flow rate: 0.15 mL/min). HETE detection was performed on negative ion mode for multiple reaction monitoring of *m/z* 333→235 (PGβ2), *m/z* 319→115 (5-HETE), *m/z* 319→179 (12-HETE) and, *m/z* 319→219 (15-HETE). Each experiment was performed in technical replicate.

Antibody specificity immunoblotting. Transfected LOX HEK293 cells were lysed with protein loading buffer (62.5 mM Tris pH 6.8, 25% glycerol, 2% SDS, 0.1% bromophenol blue, 5% 2-mercaptoethanol), and 20 μL aliquots were separated by SDS-PAGE (10%) gel electrophoresis (180 V). Following separation, the SDS-PAGE gel was transferred onto PVDF membrane, and blocked in milk protein (Tris pH 7.4) for 30 minutes on a rotating platform. The membrane was subjected to either, 15-LOX-1, p12-LOX, or 15-LOX-2 primary monoclonal antibody wash (2 μL primary antibody in 5% dry milk in Tris pH 7.4) overnight at 4˚C in the dark, and again with beta-actin primary antibody. The blot was then washed with 5% dry milk in Tris buffered saline, pH 7.4 (x3) and was subsequently treated with corresponding secondary antibody conjugated to horseradish peroxidase. LOX protein was detected by chemiluminescence on a BioRad ChemiDoc imaging system.

LOX expression of HT-22 and HT-1080 as determined by immunoblotting. HT-22 and HT-1080 cells were lysed with protein loading buffer (62.5 mM Tris pH 6.8, 25% glycerol, 2% SDS, 0.1% bromophenol blue, 5% 2-mercaptoethanol), and 20 μL aliquots were separated by SDS-PAGE (10%) gel electrophoresis (180 V). Following separation, the SDS-PAGE gel was transferred onto PVDF membrane, and blocked in milk protein (Tris 7.4 pH) for 30 minutes on a rotating platform. The membrane was subjected to either, 15-LOX-1, p12-LOX, or 15-LOX-2 primary monoclonal antibody wash (2 μL primary antibody in 5% dry milk in

Tris buffered saline, pH 7.4) overnight at 4˚C in the dark, and again with beta-actin primary antibody. The blot was then washed with 5% dry milk in Tris buffered saline, pH 7.4 (x3) and was subsequently treated with corresponding secondary antibody conjugated to horseradish peroxidase. LOX protein was detected by chemiluminescence on a BioRad ChemiDoc imaging system.

***LOX expression of stressed HT-22 as determined by immunoblotting*.** HT-22 cells (1 million at confluency) plated in 60 mm plates were treated with 5 mM glutamate over 4 h in DMEM, 10% FBS, 1% penicillin streptomycin. The experimental media was removed, cells were washed with PBS buffer and subsequently lysed with protein loading buffer (62.5 mM Tris pH 6.8, 25% glycerol, 2% SDS, 0.1% bromophenol blue, 5% 2-mercaptoethanol). 20 μL aliquots were separated by SDS-PAGE (10%) gel electrophoresis (180 V). Following separation, the SDS-PAGE gel was transferred onto PVDF membrane, and blocked in milk protein (Tris pH 7.4) for 30 minutes on a rotating platform. The membrane was subjected to either, 15-LOX-1, p12-LOX, or 15-LOX-2 primary monoclonal antibody wash (2 μL primary antibody in 5% dry milk in Tris buffered saline, pH 7.4) overnight at 4˚C in the dark, and again with beta-actin primary antibody. The blot was then washed with 5% dry milk in Tris buffered saline, pH 7.4 (x3) and was subsequently treated with corresponding secondary antibody conjugated to horseradish peroxidase. LOX protein was detected by chemiluminescence on a BioRad ChemiDoc imaging system.

***LOX expression of stressed HT-1080 as determined by immunoblotting*.** HT-1080 cells (1 million at confluency) plated in 60 mm plates were treated with 2 μM *(1S,3R)* RSL3 over 10 minutes in DMEM, 10% FBS, 1 mM glutamine, 1% penicillin & streptomycin. The experimental medium was removed, cells were washed with PBS buffer and subsequently lysed with protein loading buffer (62.5 mM Tris pH 6.8, 25% glycerol, 2% SDS, 0.1% bromophenol blue, 5% 2-mercaptoethanol). 20 μL aliquots were separated by SDS-PAGE (10%) gel electrophoresis (180 V). Following separation, the SDS-PAGE gel was transferred onto PVDF membrane, and blocked in milk protein (Tris 7.4 pH) for 30 minutes on a rotating platform. The membrane was subjected to either, 15-LOX-1, p12-LOX, or 15-LOX-2 primary monoclonal antibody wash

(2 μL primary antibody in 5% dry milk in Tris buffered saline, pH 7.4) overnight at 4˚C in the dark, and again with beta-actin primary antibody. The blot was then washed with 5% dry milk in Tris buffered saline, pH 7.4 (x3) and was subsequently treated with corresponding secondary antibody conjugated to horseradish peroxidase. LOX protein was detected by chemiluminescence on a BioRad ChemiDoc imaging system.

Synthesis of LOX Inhibitors :

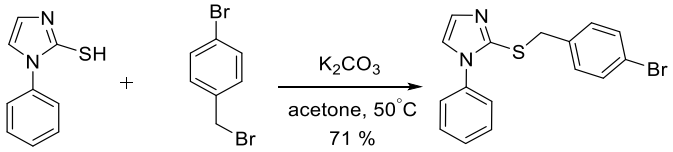

Scheme 2.4. Synthetic route of MLS000327186

Synthesis of MLS000327186: Potassium carbonate (1.568 g, 11 mmol, 5 equiv.) was added to a 100 mL two-necked round bottom flask, equipped with a stir bar, containing 20 mL dry acetone. The vessel was fitted with a refluxing condenser, was subjected to a nitrogen atmosphere and was heated to 50˚C. To this, 1,3-dihydro-1-phenyl-2*H*-imidazole-2-thione (0.400 g, 2.2 mmol, 1 equiv.) and 1-bromo-4-(bromomethyl)-benzene (0.550 g, 2.2 mmol, 1 equiv.) were added and the reaction was stirred overnight (24 h). The following morning, the reaction vessel was cooled and filtered. The filtrate was collected and concentrated *in vacuo*. The crude material was purified by silica gel chromatography 80:15:5 $CHCl_3$:EtOAc:Hex (0.539 g, 70.9%). ^{1}H NMR (400 MHz, $CDCl_3$) δ 7.45 (d, *J* = 8.0 Hz, 2H), 7.36-7.40 (m, 3H), 7.26 (d, *J* = 6.8, 2.5 H), 7.21 (d, J = 1.6 Hz, 1H), 7.09 (m, 3.0H), 4.27 (s, 2H). ^{13}C NMR (400 MHz, $CDCl_3$) δ 141.7, 140.8, 137.0, 130.0, 129.2, 128.4, 125.5, 125.4, 125.3, 122.7, 38.3. HRMS (ESI, [M + H^+]): m/z calc. for $C_{17}H_{13}F_3N_2S$, 344.9983 found, 344.9981.

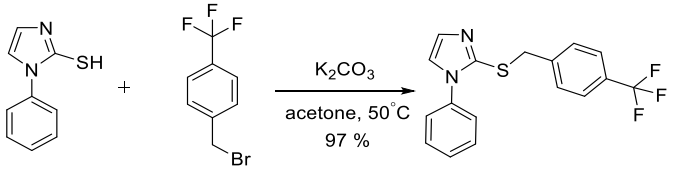

Scheme 2.5 Synthetic route of MLS000327069.

***Synthesis of MLS000327069*:** Potassium carbonate (1.568 g, 11 mmol, 5 equiv.) was added to a 100 mL two-necked round bottom flask, equipped with a stir bar, containing 20 mL dry acetone. The vessel was fitted with a refluxing condenser, was subject to a nitrogen atmosphere and was heated to 50˚C. To this, 1,3-dihydro-1-phenyl-2*H*-imidazole-2-thione (0.400 g, 2.2 mmol, 1 equiv.) and 1-(bromomethyl)-4-(trifluoromethyl)-benzene (0.526 g, 2.2 mmol, 1 equiv.) were added and the reaction was stirred overnight (24 h). The following morning, the reaction vessel was cooled and filtered. The filtrate was collected and concentrated *in vacuo*. The crude material was purified by silica gel chromatography 80:15:5 $CHCl_3$:EtOAc:Hex (0.711 g, 96.7 %). ^{1}H NMR (400 MHz, $CDCl_3$): δ 7.46 (d, *J* = 8.0 Hz, 2H), 7.36-7.40 (m, 3H), 7.26 (d, *J* = 8.0, 2.0H), 7.21 (d, *J* = 1.3 Hz, 1H), 7.09 (m, 3.0H), 4.26 (s, 2H). ^{13}C NMR (400 MHz, $CDCl_3$) δ 141.7, 140.8, 137.0, 130.0, 129.2, 129.2, 128.4, 125.5, 125.4, 125.3, 122.7, 38.31. HRMS (ESI, [M + H^+]): m/z calc. for $C_{17}H_{13}F_3N_2S$, 334.0752 found, 334.0767.

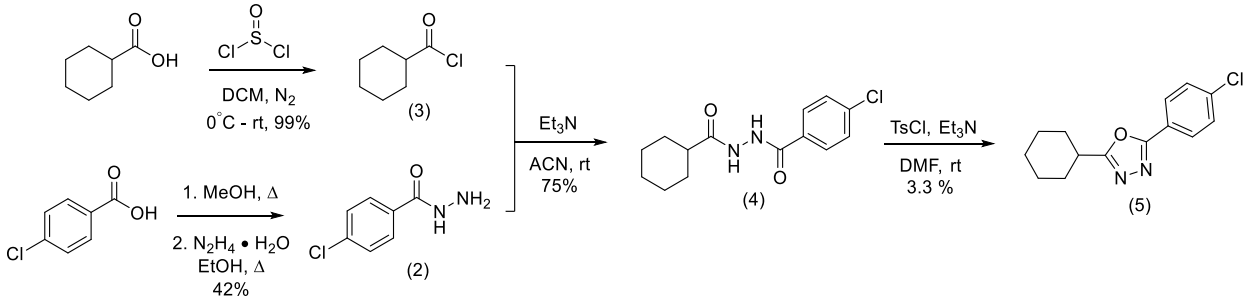

Scheme 2.6. Synthetic route of MLS000545091.

***Synthesis of MLS000545091*:**

The synthesis of MLS000545091 was based on previous work by Hung et al., who report the preparation of the 2-(4-bromophenyl)-5-(4-tert-butylphenyl)-1,3,4-oxadiazole derivative.[44] Therein, the 1,3,4 oxadiazole ring is accessed following reflux of the dihydrazide precursor in $POCl_3$. To avoid such harsh reaction conditions, the cyclodehydration reaction was performed instead in the presence of TsCl and base, as described by Stabile et al. [45]

4-chlorobenzoic acid (1): 4-chloro-benzoic acid (2.0 g, 12.7 mmol, 1 equiv.) was dissolved in 150 mL dry methanol in a nitrogen flushed round bottom flask, equipped with a water condenser. Sulfuric acid was added dropwise to the stirring reaction vessel (5 mL, 0.6 M) and the reaction was further stirred at reflux overnight. The following morning, the vessel was cooled, and the crude was concentrated *in vacuo*, diluted with water, and neutralized with saturated $NaHCO_3$ solution. The crude was then extracted with DCM (x 3), washed with 5% $NaHCO_3$ (x 3), brine (x 1), dried over $MgSO_4$ and filtered. The filtrate was concentrated *in vacuo* and carried on. (1.45 g, 67.2 %) ^{1}H NMR (400 MHz, $CDCl_3$) 7.93-7.98 (dt, *J* = 12, *J* = 4, 2H) 7.37-7.42 (dt, *J* = 12, *J* = 4, 2H) 3.90 (s, 3H).

4-chloro-hydrazide benzoic acid (2): 4-chloro-benzoate (1.45 g, 8.5 mmol, 1 equiv.) was dissolved in 100 mL ethanol in a two-neck round bottom flask, equipped with a water condenser. To this, hydrazine hydrate (2.25 mL, 34 mmol, 4 equiv.) was added dropwise to the reaction vessel and was left to stir overnight at reflux. The following morning, the reaction vessel was cooled, diluted with cold water and the resulting precipitate was collected by filtration. The precipitate was washed with cold hexanes and water. (923 mg, 63.4 %). ^{1}H NMR (400 MHz $CDCl_3$) 12.96 (s, 2H) 10.43 (s, 1H) 7.07-7.12 (dt, *J* = 12, *J* = 4, 2H) 6.81-6.86 (dt, *J* = 12, *J* = 4, 2H).

cyclohexanecarbonyl chloride (3): Cyclohexanecarboxylic acid (500 mg, 3.5 mmol, 1 equiv.) was dissolved in 50 mL dry dichloromethane in a round bottom flask and cooled to 0 ˚C. To this, a catalytic amount of DMF (12.0 μL, 0.005 equiv.) and thionyl chloride (751 μL, 3.85 mmol, 1.1 equiv.) were added dropwise to a stirring solution. The reaction ran for three hours, warming to room temperature. An additional equivalent of thionyl chloride (751 μL, 3.85 mmol, 1.1 equiv.) was added to push the reaction to completion, as monitoring by TLC. Afterwards, the reaction mixture was concentrated under vacuum (collected solvent was quenched with ice water and NaOH solution) and the resulting acid chloride (light yellow liquid).

4-chloro-2-(cyclohexylcarbonyl) hydrazide benzoic acid (4): Hydrazide (200 mg, 1.17 mmol, 1 equiv.) was dissolved in 25mL dry acetonitrile with triethylamine (293 μL, 2.1 mmol, 1.8 equiv.) in a round bottom flask equipped with a stirring bar at room temperature. To this, cyclohexanecarbonyl chloride (3) (1701 μL, 1.17 mmol, 1.0 equiv.) was added dropwise to the solution and a white precipitate is formed. Following complete addition of (3), the solution was filtered and precipitate was washed with several volumes of ether. The collected precipitate was collected and dried under vacuum. (0.246 g, 75 %). ^{13}C NMR (400 MHz, DMSO-d_6) δ 175.0, 164.9, 137.1, 131.8, 129.8, 129.0, 45.2, 29.5, 25.8, 25.6. HRMS (ESI, [M + H^+]): m/z calc. for $C_{14}H_{17}N_2O_2Cl$, 280.0979 found, 280.0986.

2-(4-chlorophenyl)-5-cyclohexyl-1,2,4-oxadiazole (5): The reaction procedure was based on previous work by Stabile et al.[45] 4-Chloro-2-(cyclohexylcarbonyl) hydrazide benzoic acid (246 mg, 0.870 mmol, 1.0 equiv.) was dissolved in 20 mL dried DMF.. To the reaction flask, p-toluenesulfonyl chloride (497 mg, 2.61 mmol, 3.0 equiv.), and triethylamine (128 μL, 1.74 mmol, 2.0 equiv.) were added and the reaction was left to stir at room temperature overnight. The following morning, excess TsCl was quenched with a 14 % NH_3 solution, and stirred for 30 minutes. The resulting crude reaction mixture was separated by preparative TLC using hexane : EtOAc as eluent, to obtain MLS000545091 (6.9 mg, 3.3 %). ^{1}H NMR (400 MHz, DMSO-d_6) δ 7.96 (d, 2H, J = 9 Hz) 7.62 (d, 2H, J = 9) 2 .95-3.05 (m, 1H) 2.00 – 2.05 (m, 2H) 1.68 – 1.77 (m, 2H) 1.16 – 1.66 (m, 7H) ^{13}C NMR (400 MHz, DMSO-d_6) δ 170.2, 163.3, 136.9,130.0, 128.7, 122.9, 34.6, 30.0, 25.6, 25.1 HRMS (*m/z*): [M + H]$^+$ calcd for 262.0873 $C_{14}H_{15}N_2OCl$, found 262.08676.

2.6 References

1. Dixon, S. J.; Lemberg, K.; Lamprecht, M.; Skouta, R.; Zaitsev, E.; Gleason, C.; Patel, D.; Bauer, A.; Cantley, A.; Yang, W.S.; Morrison III, B.; Stockwell, B. Ferroptosis: An Iron-Dependent Form of Non-Apoptotic Cell Death. *Cell* **149**, 1060–1072 (2012).
2. Sabatini, K., Mattila, J.-P., Megli, F. M. & Kinnunen, P. K. J. Characterization of Two Oxidatively Modified Phospholipids in Mixed Monolayers with DPPC. *Biophys. J.* **90**, 4488–4499 (2006).

3. Dobretsov, G. E., Borschevskaya, T. A., Petrov, V. A. & Vladimirov, Yu. A. The increase of phospholipid bilayer rigidity after lipid peroxidation. *FEBS Lett.* **84**, 125–128 (1977).

4. Boulanger Chantal M., Amabile Nicolas, & Tedgui Alain. Circulating Microparticles. *Hypertension* **48**, 180–186 (2006).

5. Porter, N. A., Caldwell, S. E. & Mills, K. A. Mechanisms of free radical oxidation of unsaturated lipids. *Lipids* **30**, 277–290 (1995).

6. Porter, F. D.; Scherrer, D.; Lanier, M.; Langmade, J.; Molugu, V.; Gale, S.; Olzeski, D.; Sidhu, R.; Dietzen, D.; Fu, R.; Wassif, C.; Yanjanin, N.; Marso, S.; House, J.; Vite, C.; Schaffer, J.; Ory, D. Cholesterol Oxidation Products Are Sensitive and Specific Blood-Based Biomarkers for Niemann-Pick C1 Disease. *Sci. Transl. Med.* **2**, 56ra81-56ra81 (2010).

7. Montine, T. J.; Montine, K.; McMahan, W.; Markesbery, W.; Quinn, J.; Morrow, J. F2-Isoprostanes in Alzheimer and Other Neurodegenerative Diseases. *Antioxid. Redox Signal.* **7**, 269–275 (2004).

8. Lee, C.-Y. J., Seet, R. C. S., Huang, S. H., Long, L. H. & Halliwell, B. Different Patterns of Oxidized Lipid Products in Plasma and Urine of Dengue Fever, Stroke, and Parkinson's Disease Patients: Cautions in the Use of Biomarkers of Oxidative Stress. *Antioxid. Redox Signal.* **11**, 407–420 (2008).

9. Fukai, M.; Hayashi, T.; Yokota, R.; Shimamura, T.; Suzuki, T.; Taniguchi, M.; Matsushita, M.; Furukawa, H.; Todo, S.Lipid peroxidation during ischemia depends on ischemia time in warm ischemia and reperfusion of rat liver. *Free Radic. Biol. Med.* **38**, 1372–1381 (2005).

10. Wu, R. P; Hayashi, T.; Cottam, H.; Jin, G.; Yao, S.; Wu, C.; Rosenbach, M.; Corr, M.; Schwab, R.; Carson, D. Nrf2 responses and the therapeutic selectivity of electrophilic compounds in chronic lymphocytic leukemia. *Proc. Natl. Acad. Sci.* **107**, 7479–7484 (2010).

11. Roveri, A., Maiorino, M., Nisii, C. & Ursini, F. Purification and characterization of phospholipid hydroperoxide glutathione peroxidase from rat testis mitochondrial membranes. *Biochim. Biophys. Acta BBA - Protein Struct. Mol. Enzymol.* **1208**, 211–221 (1994).

12. Thomas, J. P., Geiger, P. G., Maiorino, M., Ursini, F. & Girotti, A. W. Enzymatic reduction of phospholipid and cholesterol hydroperoxides in artificial bilayers and lipoproteins. *Biochim. Biophys. Acta BBA - Lipids Lipid Metab.* **1045**, 252–260 (1990).

13. Ingold, I.; Berndt, C.; Schmitt, S.; Doll, S.; Poschmann, G.; Buday, K.; Roveri, A.; Peng, X.; Freitas, F.P.; Seibt, T.; Mehr, L.; Aichler, M.; Walch, A.; Lamp, D.; Jastroch, M.; Miyamoto, S.; Wurst, W.; Ursini, F.; Arnér, E.; Fradejas-Villar, N.; Schweizer, U.; Zischka, H.; Friedmann Angeli, J.P.; Conrad, M. Selenium Utilization by GPX4 Is Required to Prevent Hydroperoxide-Induced Ferroptosis. *Cell* **172**, 409-422 (2018).

14. Soula, M.; Weber, R.; Zilka, O.; Alwaseem, H.; La, K.; Yen, F.; Molina, H.; Garcia-Bermudez, J.; Pratt, D.; Birsoy, K. Metabolic determinants of cancer cell sensitivity to canonical ferroptosis inducers. *Nat. Chem. Biol.* **16** 1351 - 1360 (2020).

15. Doll, S.; Freitas, F.; Shah, R.; Aldrovandi, M.; Costa da Silva, M.; Ingold, I.; Grocin, A.; Xavier da Silva,

T.N.; Panzilius, E.; Scheel, C.; Mourão, A.; Buday, K.; Sato, M.; Wanninger, J.; Vignane, T.; Mohana, V.; Rehberg, M.; Flatley, A.; Schepers, A.; Kurz, A.; White, D.; Sauer, M.; Sattler, M.; Tate, E.; Schmitz, W.; Schulze, A.; O'Donnell, V.; Proneth, B.; Popowicz, G.; Pratt, D.; Friedmann Angeli, J.P.; Conrad, M. FSP1 is a glutathione-independent ferroptosis suppressor. *Nature* **575**, 693–698 (2019).

16. Yang, W. S.; Stockwell, B. R. Synthetic Lethal Screening Identifies Compounds Activating Iron-Dependent, Nonapoptotic Cell Death in Oncogenic-RAS-Harboring Cancer Cells. *Chem. Biol.* **15**, 234–245 (2008).

17. Yang, W. S.; SriRamartnam, R.; Welsch, M.; Shimada, K.; Skouta, R.; Viswanathan, V.; Cheah, J.; Clemons, P.; Shamji, A.; Clish, C.; Brown, L.; Girotti, A.; Cornish, V.; Schreiber, S.; Stockwell, B. Regulation of Ferroptotic Cancer Cell Death by GPX4. *Cell* **156**, 317–331 (2014).

18. Dolma, S., Lessnick, S. L., Hahn, W. C. & Stockwell, B. R. Identification of genotype-selective antitumor agents using synthetic lethal chemical screening in engineered human tumor cells. *Cancer Cell* **3**, 285–296 (2003).

19. Tan, S., Wood, M. & Maher, P. Oxidative Stress Induces a Form of Programmed Cell Death with Characteristics of Both Apoptosis and Necrosis in Neuronal Cells. *J. Neurochem.* **71**, 95–105 (1998).

20. Murphy, T. H., Miyamoto, M., Sastre, A., Schnaar, R. L. & Coyle, J. T. Glutamate toxicity in a neuronal cell line involves inhibition of cystine transport leading to oxidative stress. *Neuron* **2**, 1547–1558 (1989).

21. Yin, H., Xu, L. & Porter, N. A. Free Radical Lipid Peroxidation: Mechanisms and Analysis. *Chem. Rev.* **111**, 5944–5972 (2011).

22. Howard, J. A. & Ingold, K. U. The Inhibited Autoxidation of styrene: Part I. The deuterium isotope effect for inhibition by 2,6-di-tert-butyl-4-methylphenol. *Can. J. Chem.* **40**, 1851–1864 (1962).

23. Litwinienko, G. & Ingold, K. U. Solvent Effects on the Rates and Mechanisms of Reaction of Phenols with Free Radicals. *Acc. Chem. Res.* **40**, 222–230 (2007).

24. Haeggström, J. Z. & Funk, C. D. Lipoxygenase and Leukotriene Pathways: Biochemistry, Biology, and Roles in Disease. *Chem. Rev.* **111**, 5866–5898 (2011).

25. Li, Y., Maher, P. & Schubert, D. A Role for 12-lipoxygenase in Nerve Cell Death Caused by Glutathione Depletion. *Neuron* **19**, 453–463 (1997).

26. Tan, S., Schubert, D. & Maher, P. Oxytosis: A novel form of programmed cell death. *Curr. Top. Med. Chem.* **1**, 497–506 (2001).

27. Seiler, A.; Schneider, M.; Förster, H.; Roth, S.; Wirth, E.; Culmsee, C.; Plesnila, N.; Kremmer, E.; Rådmark, O.; Wurst, W.; Bornkamm, G.; Schweizer, U.; Conrad, M. Glutathione Peroxidase 4 Senses and Translates Oxidative Stress into 12/15-Lipoxygenase Dependent- and AIF-Mediated Cell Death. *Cell Metab.* **8**, 237–248 (2008).

28. Friedmann Angeli, J. P.; Schneider, M.; Proneth, B.; Tyurina, Y.; Tyurina, V.; Hammond, V.; Herbach, N.; Aichler, M.; Walch, A.; Eggenhofer, E.; Basavarajappa, D.; Rådmark, O.; Kobayashi, S.; Seibt, T.; Beck, H.; Neff, F.; Esposito, I.; Wanke, R.; Förster, H.; Yefremova, O.; Heinrichmeyer, M.; Bornkamm, G.;

Geissler, E.; Thomas, S.; Stockwell, B.; O'Donnell, V.; Kagan, V.; Schick, J.; Conrad, M. Inactivation of the ferroptosis regulator Gpx4 triggers acute renal failure in mice. *Nat. Cell Biol.* **16**, 1180–1191 (2014).

29. Skouta, R.; Dixon, S.; Wang, J.; Dunn, D.; Orman, M.; Shimada, K.; Rosenberg, P.; Lo, D.; Weinberg, J.; Linkemann, A.; Stockwell, B. Ferrostatins Inhibit Oxidative Lipid Damage and Cell Death in Diverse Disease Models. *J. Am. Chem. Soc.* **136**, 4551–4556 (2014).

30. Zilka, O.; Shah, R.; Friedmann Angeli, J.P.; Griesser, M.; Conrad, M.; Pratt, D. On the Mechanism of Cytoprotection by Ferrostatin-1 and Liproxstatin-1 and the Role of Lipid Peroxidation in Ferroptotic Cell Death. *ACS Cent. Sci.* **3**, 232–243 (2017).

31. Shah, R., Shchepinov, M. S. & Pratt, D. A. Resolving the Role of Lipoxygenases in the Initiation and Execution of Ferroptosis. *ACS Cent. Sci.* **4**, 387–396 (2018).

32. Yang, W. S.; Kim, K.; Gaschler, M.; Patel, M.; Shchepinov, M.; Stockwell, B. Peroxidation of polyunsaturated fatty acids by lipoxygenases drives ferroptosis. *Proc. Natl. Acad. Sci. U. S. A.* **113**, E4966–E4975 (2016).

33. Wenzel, S. E.; Tyurina, Y.; Zhao, J.; St Croix, C.; Dar, H.; Mao, G.; Tyurin, V.; Anthonymuthu, T.; Kapralov, A.; Amoscato, A.; Mikulska-Ruminska, K.; Shrivastava, I.; Kenny, E.; Yang, Q.; Rosenbaum, J.; Sparvero, L.; Emlet, D.; Wen, X.; Minami, Y.; Qu, F.; Watkins, S.; Holman, T.; Vandenmark, A.; Kelum, J.; Bahar, I.; Bayir, H.; Kagan, V. PEBP1 Wardens Ferroptosis by Enabling Lipoxygenase Generation of Lipid Death Signals. *Cell* **171**, 628-641.e26 (2017).

34. Anthonymuthu, T. S.; Tyurina, Y.; Sun, W.Y.; Mikulska-Ruminska, K.; Shrivastava, I.; Tyurin, V.; Cinemre, F.; Dar, H.; Vandemark, A.; Holman, T.; Sadovsky, Y.; Stockwell, B.; He, R.R.; Bahar, I.; Bayir, H.; Kagan, V. Resolving the paradox of ferroptotic cell death: ferrostatin-1 binds to 15LOX/PEBP1 complex, suppresses generation of peroxidized ETE-PE, and protects against ferroptosis. *Redox Biol.* 101744 (2020).

35. Deschamps, J. D., Kenyon, V. A. & Holman, T. R. Baicalein is a potent in vitro inhibitor against both reticulocyte 15-human and platelet 12-human lipoxygenases. *Bioorg. Med. Chem.* **14**, 4295–4301 (2006).

36. Suzuki, H.; Ueda, T.; Juránek, I.; Yamanmoto, S.; Katoh, T.; Node, M.; Suzuki, T. Hinokitiol, a Selective Inhibitor of the Platelet-Type Isozyme of Arachidonate 12-Lipoxygenase. *Biochem. Biophys. Res. Commun.* **275**, 885–889 (2000).

37. Luci, D. K.; Jameson II, B.; Yasgar, A.; Diaz, G.; Joshi, N.; Kantz, A.; Markham, K.; Perry, S.; Kuhn, N.; Yeung, J.; Kerns, E.; Schultz, L.; Holinstat, M.; Nadler, J.; Taylor-Fishwick, D.; Jadhav, A.; Simeonov, A.; Holman, T.; Maloney, D. Synthesis and Structure–Activity Relationship Studies of 4-((2-Hydroxy-3-methoxybenzyl)amino)benzenesulfonamide Derivatives as Potent and Selective Inhibitors of 12-Lipoxygenase. *J. Med. Chem.* **57**, 495–506 (2014).

38. Bocan, T. M. A.; Rosebury, W.; Mueller, S.B.; Kuchera, S.; Welch, K.; Daugherty, A.; Cornicelli, J. A specific 15-lipoxygenase inhibitor limits the progression and monocyte–macrophage enrichment of hypercholesterolemia-induced atherosclerosis in the rabbit. *Atherosclerosis* **136**, 203–216 (1998).

39. Rai, G.; Kenyon, V.; Jadhav, A.; Schultz, L.; Armstrong, M.; Jameson II, J.B.; Hoobler, E.; Leister, W.; Simeonov, A.; Holman, T.; Maloney, D. Discovery of Potent and Selective Inhibitors of Human Reticulocyte 15-Lipoxygenase-1. *J. Med. Chem.* **53**, 7392–7404 (2010).

40. Rai, G.; Joshi, N.; Jung, J.E.; Liu, Y.; Schultz, L.; Yasgar, A.; Perry, S.; Diaz, G.; Zhang, Q.; Kenyon, V.; Jadhav, A.; Simeonov, A.; Lo, E.H.; Van Leyen, K.; Maloney, D.; Holman, T. Potent and Selective Inhibitors of Human Reticulocyte 12/15-Lipoxygenase as Anti-Stroke Therapies. *J. Med. Chem.* **57**, 4035–4048 (2014).

41. Whitman, S., Gezginci, M., Timmermann, B. N. & Holman, T. R. Structure−Activity Relationship Studies of Nordihydroguaiaretic Acid Inhibitors toward Soybean, 12-Human, and 15-Human Lipoxygenase. *J. Med. Chem.* **45**, 2659–2661 (2002).

42. Carter, G. W.; Young, P.; Albert, D.; Bouska, J.; Dyer, R.; Bell, R.; Summers, J.; Brooks, D.W. 5-lipoxygenase inhibitory activity of zileuton. *J. Pharmacol. Exp. Ther.* **256**, 929–937 (1991).

43. Armstrong, M. M. Lipoxygenase Investigations Lead to the Discovery of Potent Inhibitors and their Mechanisim of Action. (UC Santa Cruz, 2016).

44. Hung, M-C.; Liao, J.L.; Chen, S.A.; Chen, S.H.; Su, A.C. Fine Tuning the Purity of Blue Emission from Polydioctylfluorene by End-Capping with Electron-Deficient Moieties. *J. Am. Chem. Soc.* **127**, 14576–14577 (2005).

45. Stabile, P.; Lamonica, A.; Ribecai, A.; Castoldi, D.; Guercio, G.; Curcuruto, O. Mild and convenient one-pot synthesis of 1,3,4-oxadiazoles. *Tetrahedron. Let.* **51**, 4801–4805 (2010).

46. Simantov, R. Glutamate Neurotoxicity in Culture Depends on the Presence of Glutamine: Implications for the Role of Glial Cells in Normal and Pathological Brain Development. *J. Neurochem.* **52**, 1694–1699 (1989).

47. Yang, W. S.; Kim, K.; Gaschler, M.; Patel, M.; Shchepinov, M.; Stockwell, B. Peroxidation of polyunsaturated fatty acids by lipoxygenases drives ferroptosis. *Proc. Natl. Acad. Sci.* **113**, E4966–E4975 (2016).

48. Haidasz, E.A.; Van Kessel, A.T.M.; Pratt, D. A Continuos Visible light Spectrophotometric Approach to Accurately Determining The Reactivity of Radical-Trapping Antioxidants. *J. Org. Chem.* **81**, 737-744 (2015).

49. Litwinienko, G. & Ingold, K. U. Solvent Effects on the Rates and Mechanisms of Reaction of Phenols with Free Radicals. *Acc. Chem. Res.* **40**, 222–230 (2007).

50. Ingold, K. U. & Pratt, D. A. Advances in Radical-Trapping Antioxidant Chemistry in the 21st Century: A Kinetics and Mechanisms Perspective. *Chem. Rev.* **114**, 9022–9046 (2014).

51. Ingold, K. U. Inhibition of the Autoxidation of Organic Substances in the Liquid Phase. *Chem. Rev.* **61**, 563–589 (1961).

52. Floriano-Sánchez, E.; Villanueva, C.; Medina-Campos, O.N.; Rocha, D.; Sánchez-González, D.J.; Cárdenas-Rodríguez, Chaverrí, J.P. Nordihydroguaiaretic acid is a potent in vitro scavenger of

peroxynitrite, singlet oxygen, hydroxyl radical, superoxide anion and hypochlorous acid and prevents in vivo ozone-induced tyrosine nitration in lungs. *Free Radic. Res.* **40**, 523–533 (2006).

53. Končić, M. Z., Barbarić, M., Perković, I. & Zorc, B. Antiradical, Chelating and Antioxidant Activities of Hydroxamic Acids and Hydroxyureas. *Molecules* **16**, 6232–6242 (2011).

54. Shah, R., Farmer, L. A., Zilka, O., Van Kessel, A. T. M. & Pratt, D. A. Beyond DPPH: Use of Fluorescence-Enabled Inhibited Autoxidation to Predict Oxidative Cell Death Rescue. *Cell Chem. Biol.* **26**, 1594-1607 (2019).

55. Tan, S., Wood, M. & Maher, P. Oxidative Stress Induces a Form of Programmed Cell Death with Characteristics of Both Apoptosis and Necrosis in Neuronal Cells. *J. Neurochem.* **71**, 95–105 (1998).

56. Grillo, A. S.; SantaMaria, A.; Kafina, M.; Cioffi, A.; Huston, N.; Han, M.; Seo, Y.A.; Yien, Y.; Nardone, C.; Menon, A.; Fan, J.; Svoboda, D.; Anderson, J.; Hong, J.; Nicolau, B.; Subedi, K.; Gewirth, A.; Wessling-Resnick, M.; Kim, J.; Paw, B.; Burke, M. Restored iron transport by a small molecule promotes absorption and hemoglobinization in animals. *Science* **356**, 608–616 (2017).

57. Bjelakovic, G., Nikolova, D., Gluud, L. L., Simonetti, R. G. & Gluud, C. Mortality in Randomized Trials of Antioxidant Supplements for Primary and Secondary Prevention: Systematic Review and Meta-analysis. *JAMA* **297**, 842 (2007).

58. Yagoda, N.; Van Rechenberg, M.; Zaganjor, E.; Bauer, A.; Yang, W.S.; Fridman, D.; Wolpaw, A.; Smukste, I.; Peltier, J.; Boniface, J.; Smith, R.; Lessnick, S.; Sahasrabudhe, S.; Stockwell, B. RAS–RAF–MEK-dependent oxidative cell death involving voltage-dependent anion channels. *Nature* **447**, 865–869 (2007).

59. Li, B.; Harjani, J.; Cormier, N.; Madarati, H.; Atkinson, J.; Cosa, G.; Pratt, D. Besting Vitamin E: Sidechain Substitution is Key to the Reactivity of Naphthyridinol Antioxidants in Lipid Bilayers. *J. Am. Chem. Soc.* **135**, 1394–1405 (2013).

2.7 Appendix

Uncropped Western Blots

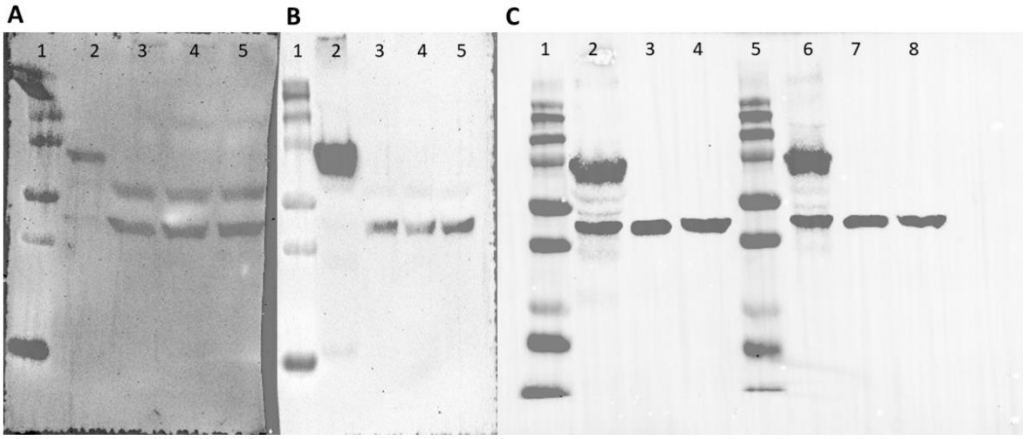

Figure 2.28 (**A**) (1) protein ladder (2) 15-LOX-2 HEK293 cell lysate (3) –(5) Increasing counts of HT-1080 cell lysate (1 million – 3 million) (**B**) (1) protein ladder (2) 15-LOX-1 HEK293 cell lysate (3)-(5) increasing counts of HT-1080 cell lysate (1 million – 3 million) (**C**) (1) protein ladder (2) p12-LOX HEK293 cell lysate (3) 15-LOX-1 HEK293 cell lysate (4) 15-LOX-2 HEK293 cell lysate (5) protein ladder (6) p12-LOX HEK293 cell lysate (7) 15-LOX-1 HEK293 cell lysate (8) 15-LOX-2 HEK293 cell lysate.

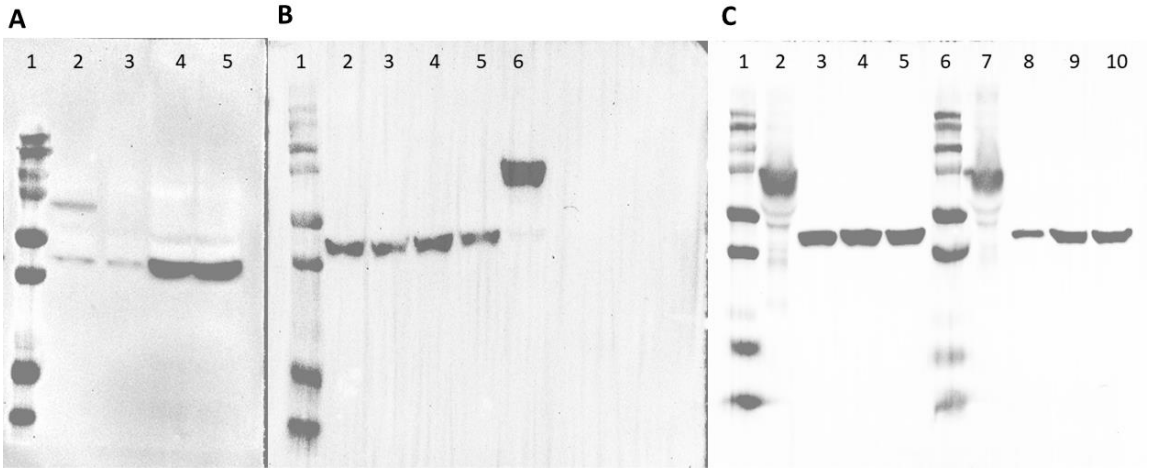

Figure 2.29 (**A**) (1) protein ladder (2) 15-LOX-2 HEK293 cell lysate (3) –(5) Increasing counts of HT-22 cell lysate (1-million – 3 million cells). (**B**) (1) protein ladder (2)-(5) Increasing counts of HT-22 cell lysate (1million – 3million cells) (6) 15-LOX-1 HEK293 cell lysate (**C**) (1) protein ladder (2) p12-LOX HEK293 cell lysate (3)-(5) Increasing counts of HT-22 cell lysate (1million – 3million) (6) protein ladder (7) p12-LOX EK293 cell lysate (8)-(10) Increasing counts of HT-1080 cell lysate (1million – 3million).

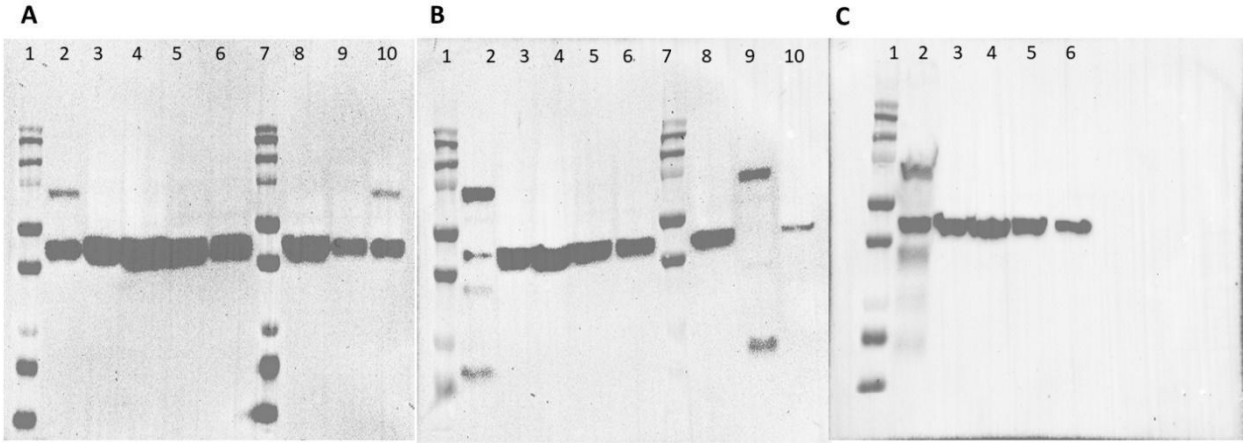

Figure 2.30 (**A**) (1) protein ladder (2) 15-LOX-2 HEK293 cell lysate (3) HT-22 cell lysate(4) HT-22 cells stressed with 5 mM glutamate 4 hours (5) HT-1080 cell lysate (6) HT-1080 cells stressed with 2 μM RSL3 (7) protein ladder (8) p12-LOX HEK293 cell lysate (9) 15-LOX-1 HEK293 cell lysate (10) 15-LOX-2 HEK293 cell lysate (**B**) (1) protein ladder (2) 15-LOX-1 HEK293 cell lysate 3) HT-22 cell lysate (4) HT-22 cells stressed with 5 mM glutamate 4 hours (5) HT-1080 cell lysate (6) HT-1080 cells stressed with 2 μM RSL3 (7) protein

ladder (8) p12-LOX HEK293 cell lysate (9) 15-LOX-1 HEK293 cell lysate (9) 15-LOX-2 HEK293 cell lysate (**C**) (1) protein ladder (2) p12-LOX HEK293 cell lysate 3) HT-22 cell lysate (4) HT-22 cells stressed with 5 mM glutamate 4 hours (5) HT-1080 cell lysate(6) HT-1080 cells stressed with 2 μM RSL3.

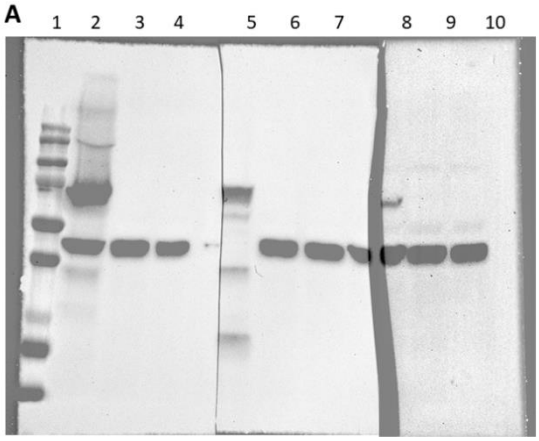

Figure 2.31 (**A**) (1) protein ladder (2) p12-LOX HEK293 cell lysate (3) HT-1080 cell lysate (4) HT-1080 cells stressed with 10 μM erastin 4 hours (5) 15-LOX-1 HEK293 cell lysate (6) HT-1080 cell lysate (7) HT-1080 cell lysate stressed with 10 μM erastin 4 hours (8) 15-LOX-2 HEK293 cell lysate (9) HT-1080 cell lysate (10) HT-1080 cell lysate stressed with 10 μM erastin 4 hours.

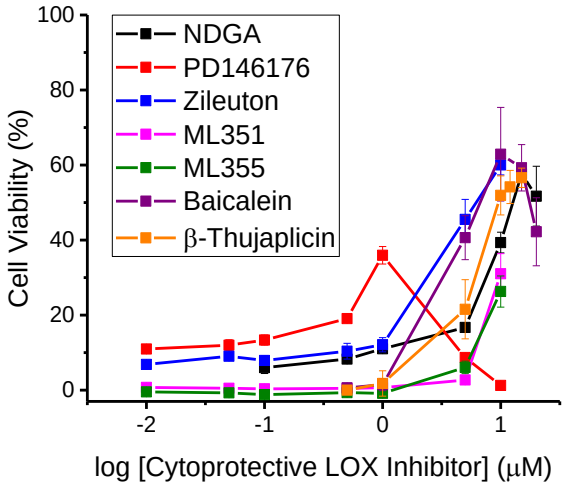

Figure 2.32 Non-truncated cell rescue plot. HT-1080 cells (3000 cells / 100 μL) were treated with 10 μM erastin and varying concentrations of LOX inhibitors for 24 hours. Cell viability was assessed using Aquabluer assay, wherein, fluorescence intensity (540 ex/ 590 em) of treated cells was compared to a live cell control.

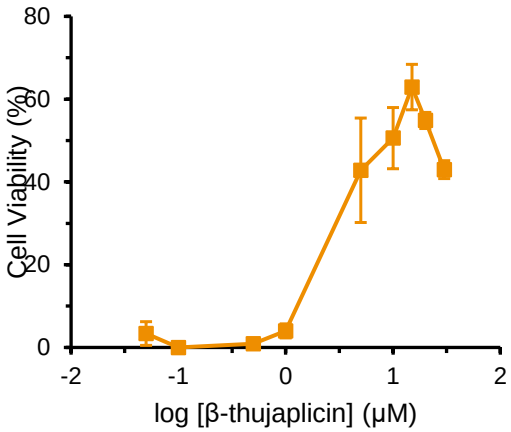

Figure 2.33 Non-truncated cell rescue plot. 15-LOX-2 overexpressing HEK 293 (3000 cells / 100 μL) were treated with 5.5 μM RSL3 and varying concentrations of β-thujaplicin for 4 hours. Cell viability was assessed using Aquabluer assay, wherein, fluorescence intensity (540 ex/ 590 em) of treated cells was compared to a live cell control.

Table 2.1 Reaction stoichiometry (*n*) for LOX inhibitors in cumene autoxidations (37˚C) as calculated using equation (2) from **Figure 2.20**.

Compound	**Stoichiometry (*n*)**
ML351	0.99 +/- 0.01

Characterization of synthesized LOX inhibitors

^{1}H NMR (400 MHz, DMSO d_6)

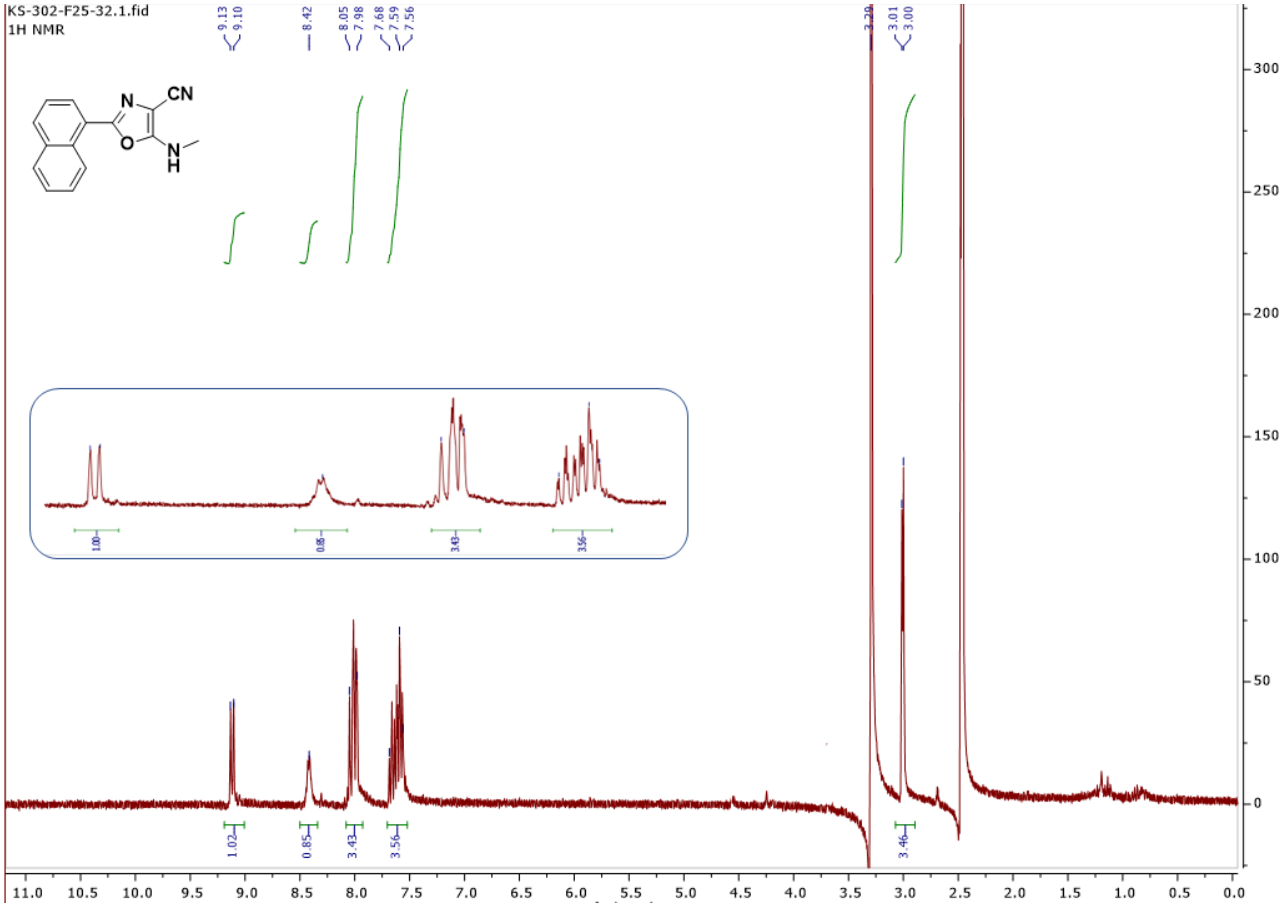

Figure 3.34 ^{1}H NMR of ML351 with expansion on 7.5 – 9.5 ppm region.

^{1}H NMR (400 MHz, $CDCl_3$)

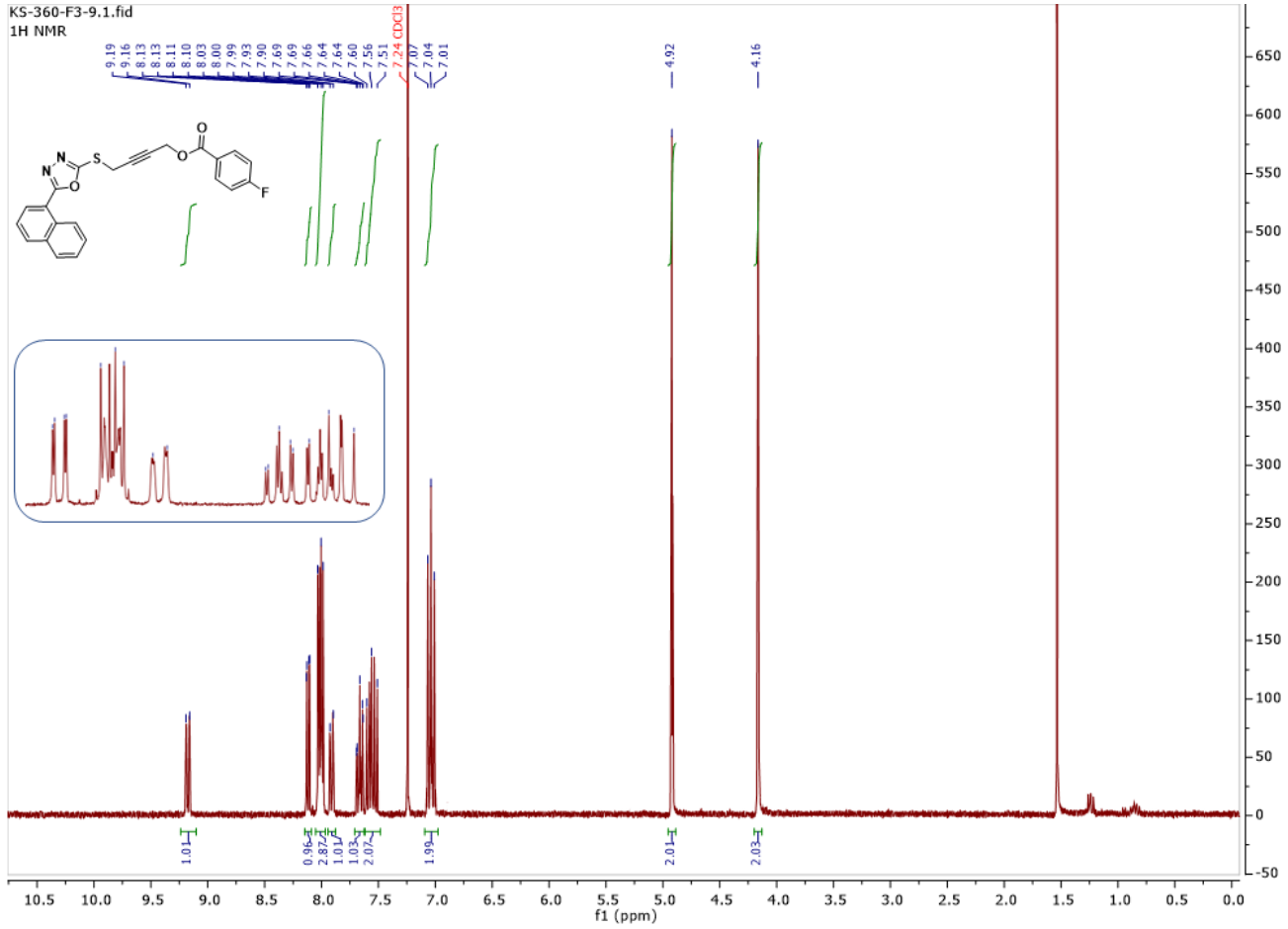

Figure 3.35 ^{1}H NMR of ML094 with expansion on 7.5 – 8.5 ppm region.

^{1}H NMR (400 MHz, $CDCl_3$)

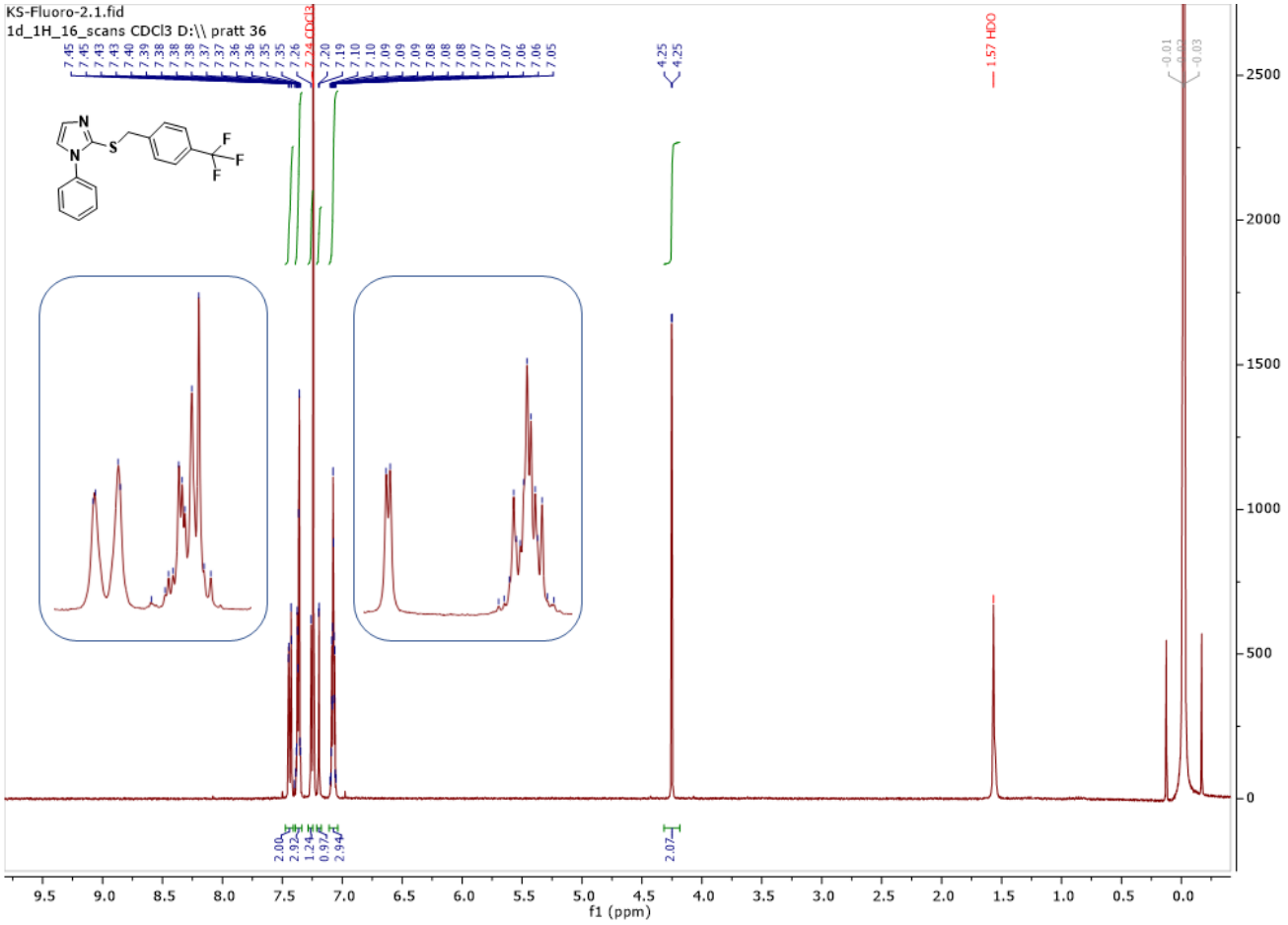

Figure 3.36 ^{1}H NMR of MLS000327069 with expansion on 7.0 – 7.2 and 7.3-7.5 ppm region.

^{13}C NMR (400 MHz, $CDCl_3$)

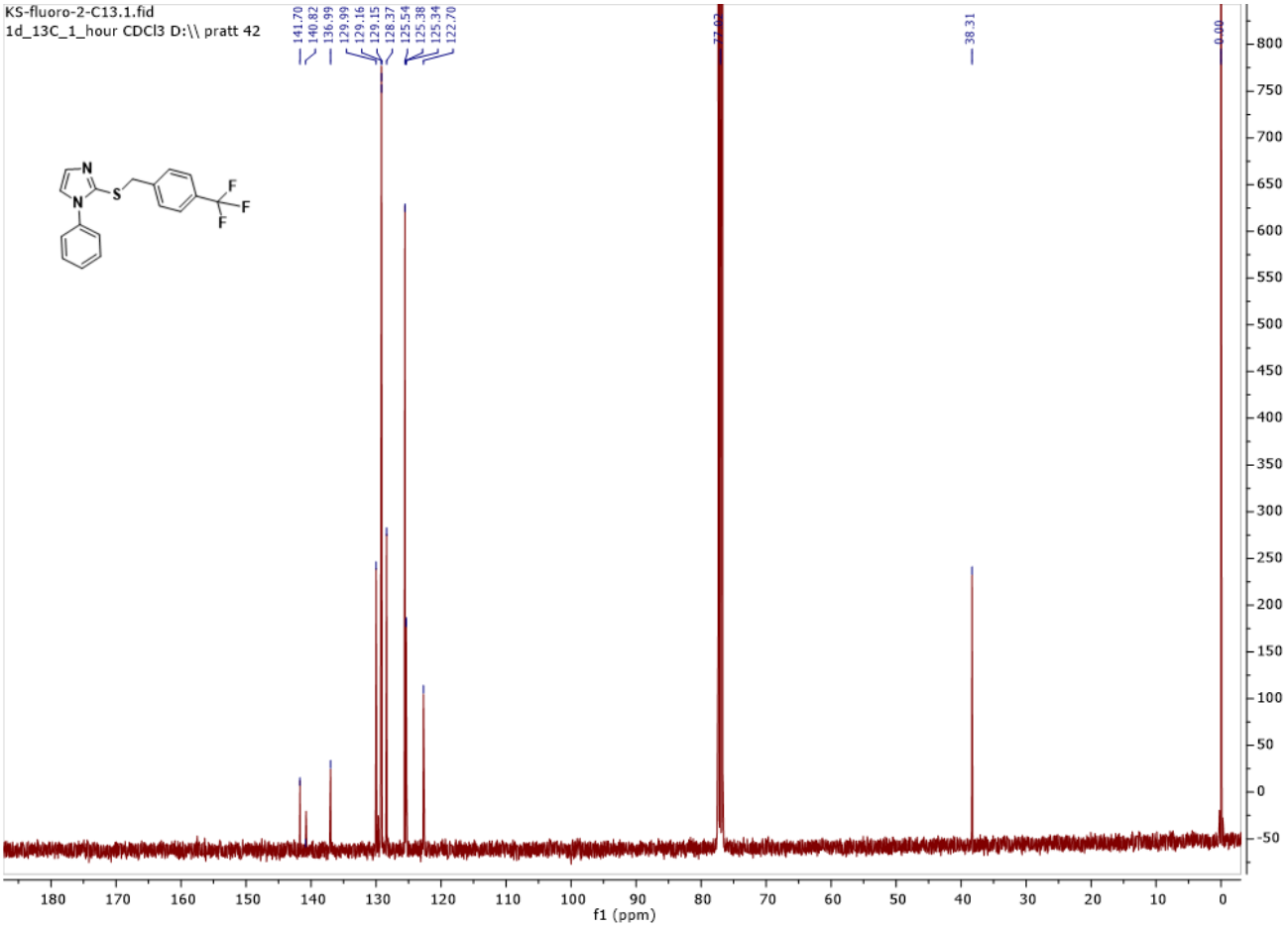

Figure 3.37 ^{13}C NMR of MLS000327069.

^{1}H NMR (400 MHz, $CDCl_3$)

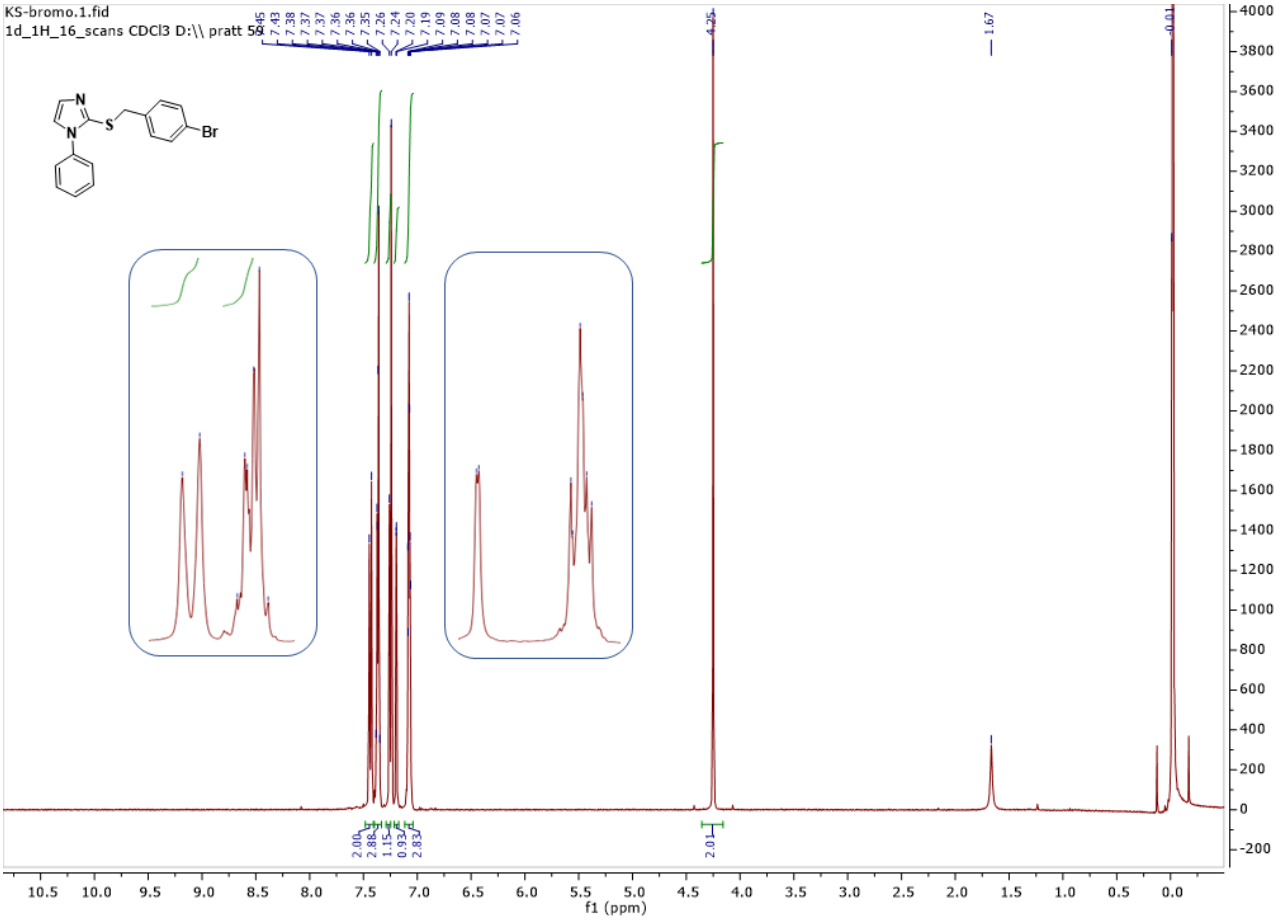

Figure 3.38 ^{1}H NMR of MLS000327186 with expansion on 7.0 – 7.2 and 7.3-7.5 ppm region.

^{13}C NMR (400 MHz, $CDCl_3$)

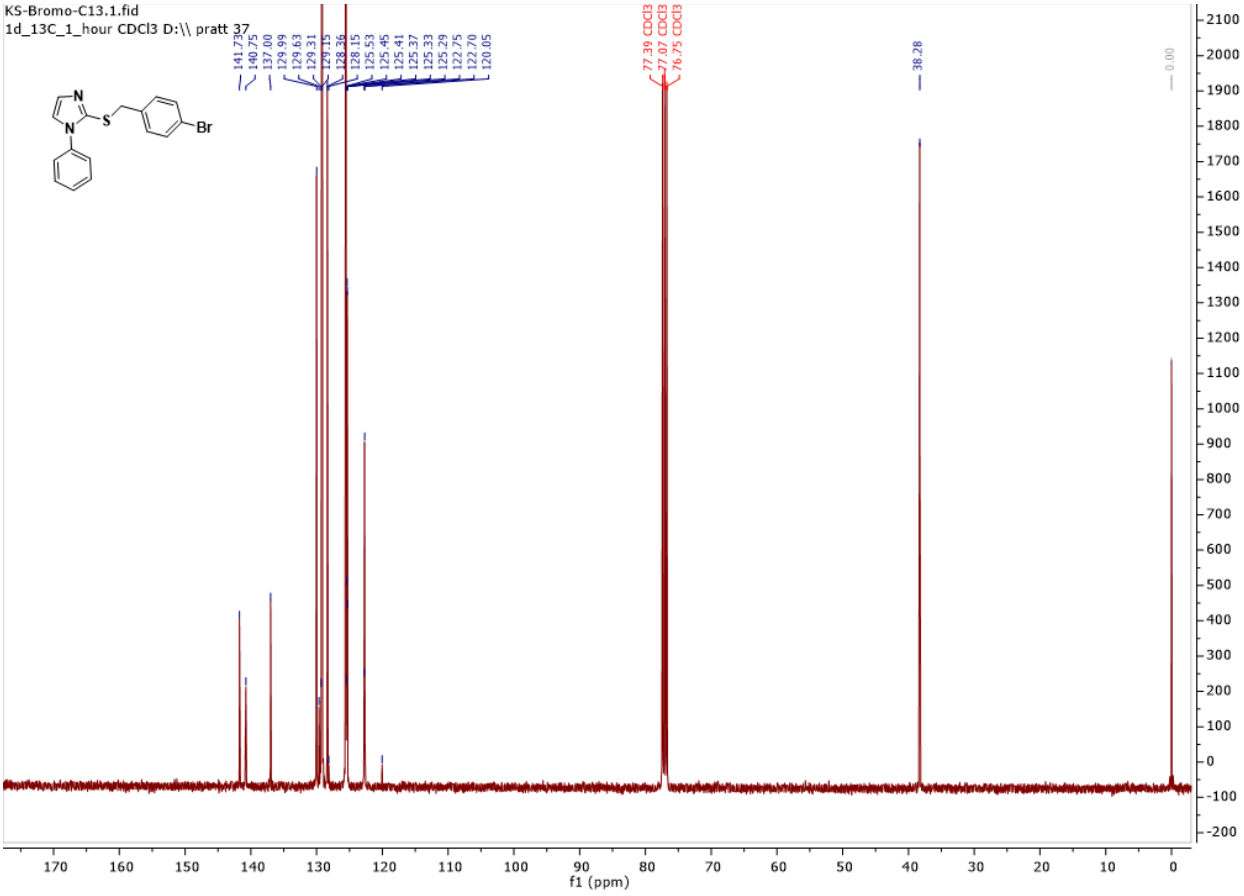

Figure 3.39 ^{13}C NMR of MLS000327186.

^{1}H NMR (400 MHz, $CDCl_3$)

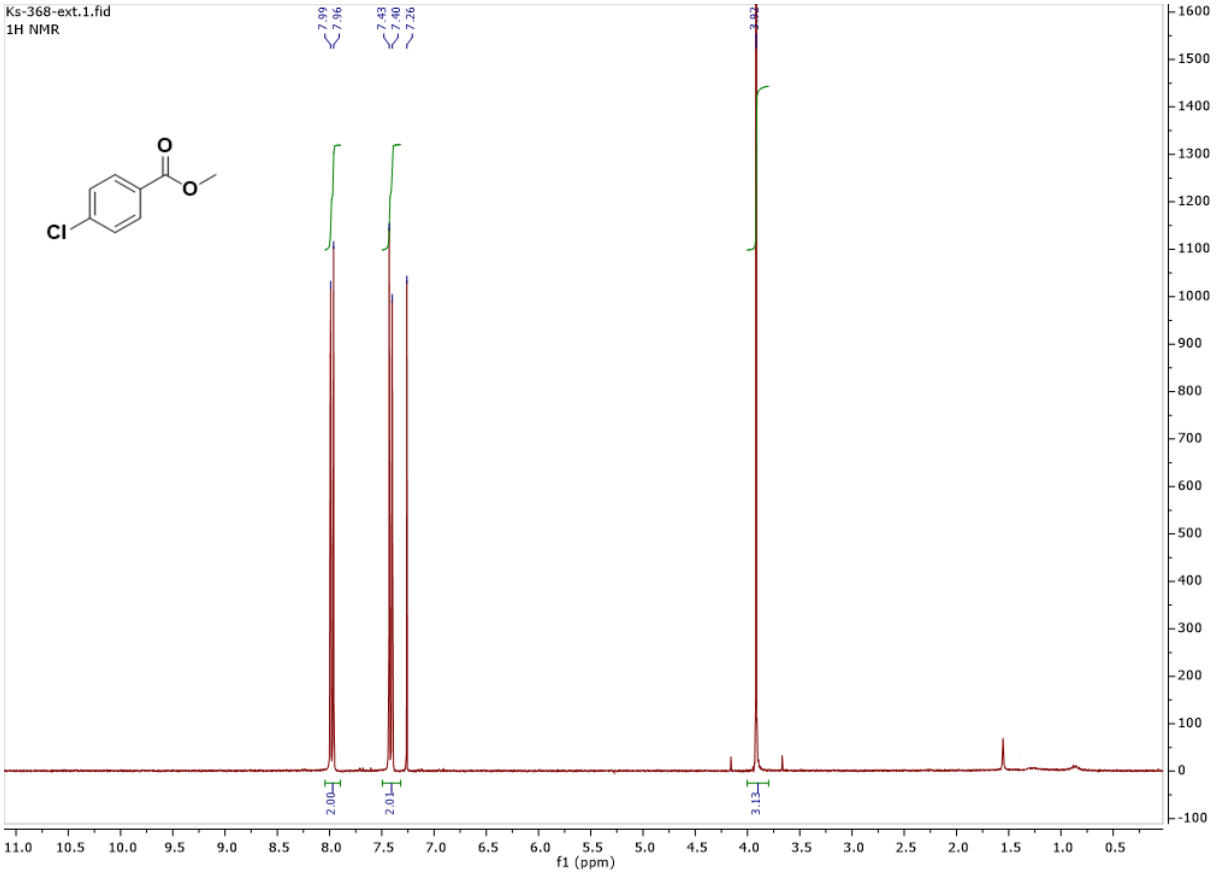

Figure 3.40 ^{1}H NMR of methyl 4-chlorobenzoate.

^{1}H NMR (400 MHz, $CDCl_3$)

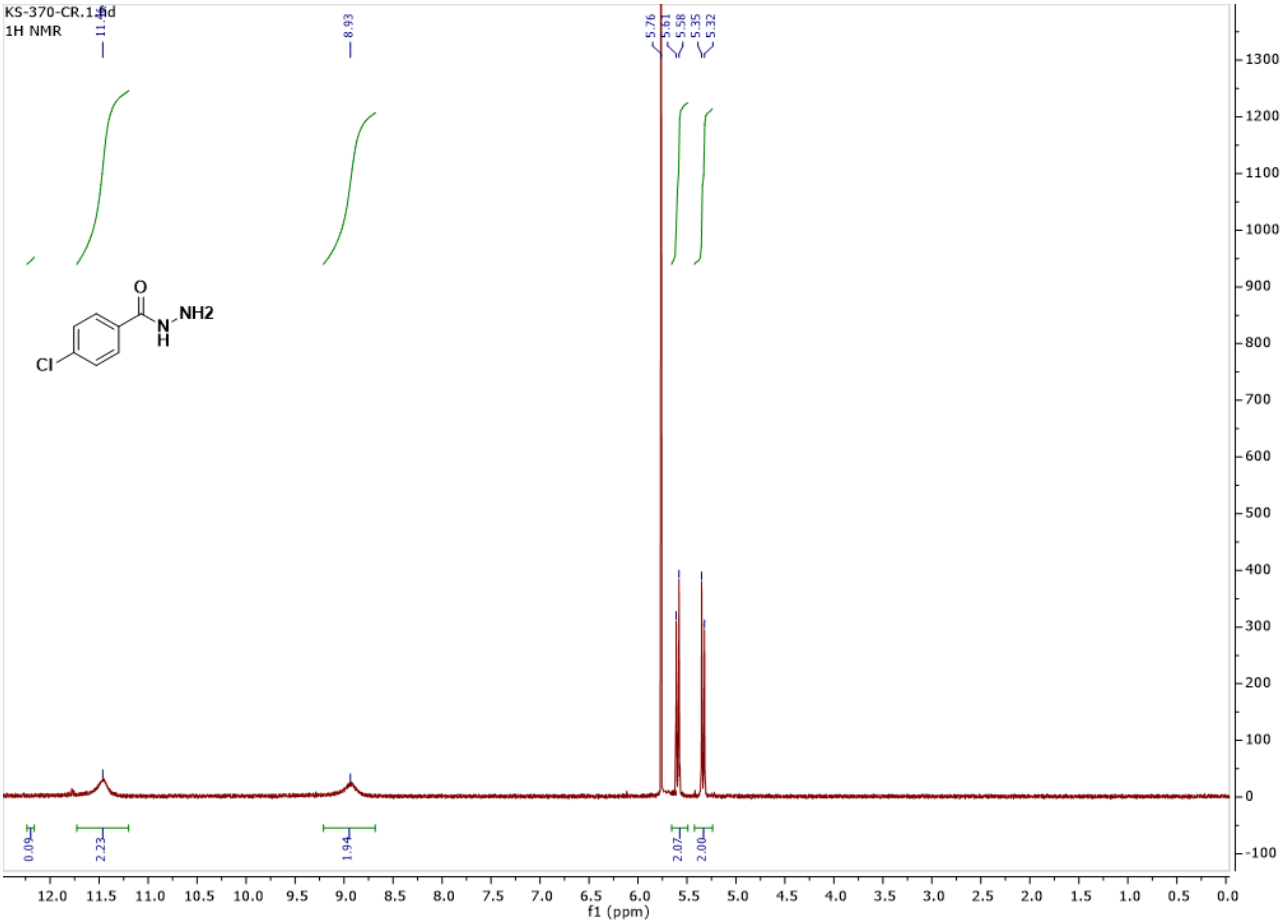

Figure 3.41 ^{1}H NMR of 4-chloro-hydrazide benzoic acid (2)

^{13}C NMR (400 MHz, DMSO d_6)

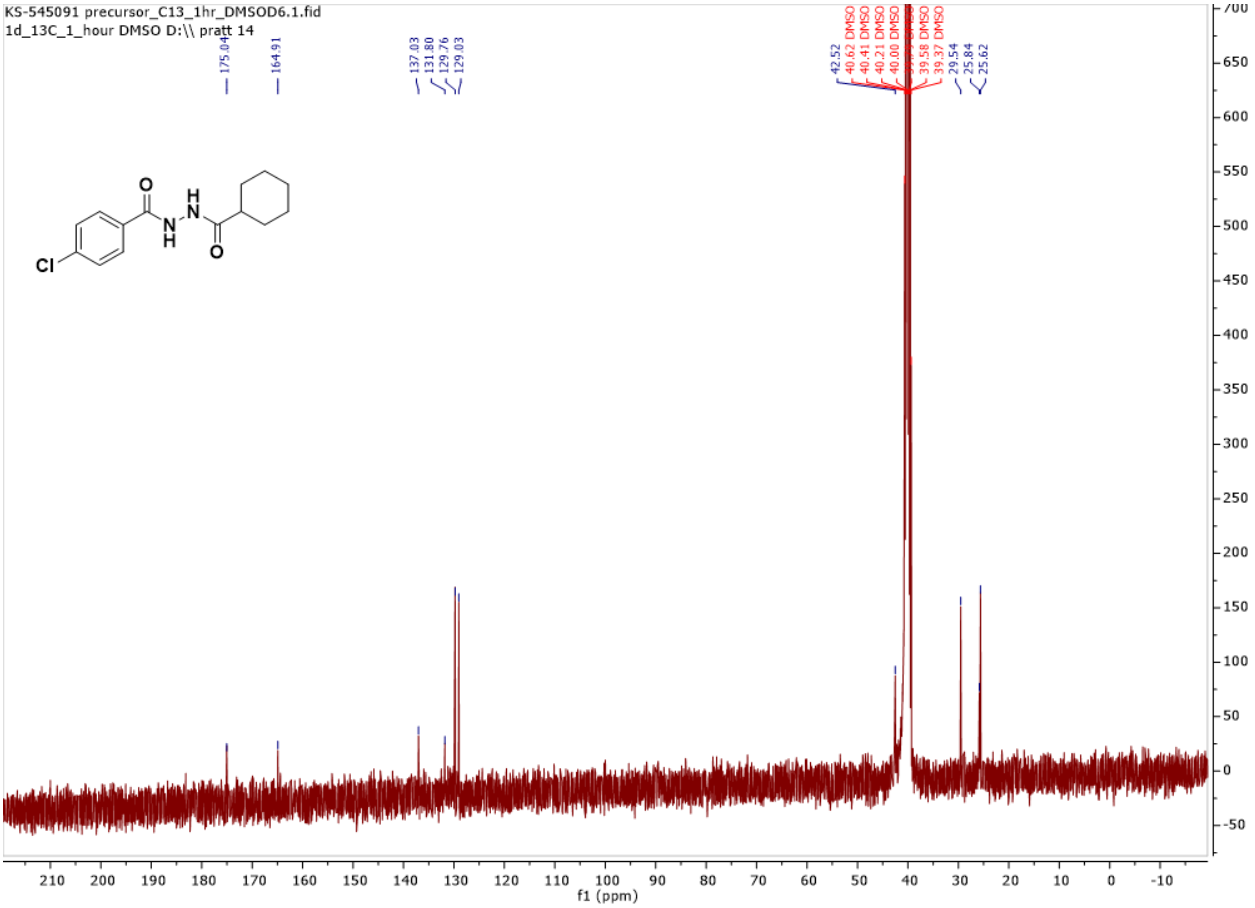

Figure 3.42 ^{13}C NMR of 4-chloro-2-(cyclohexylcarbonyl) hydrazide benzoic acid (4).

^{1}H NMR (400 MHz, DMSO d_6)

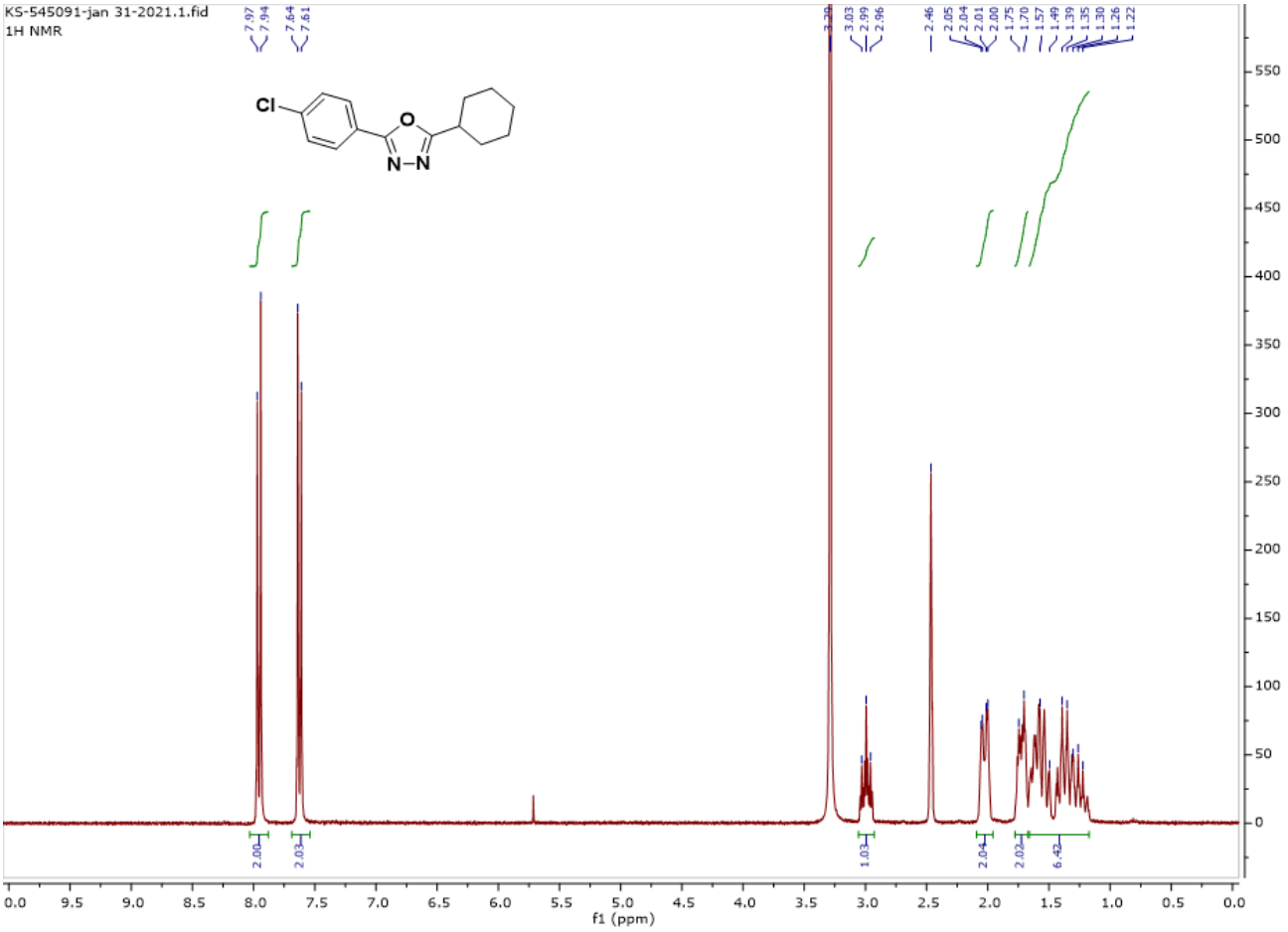

Figure 3.43 ^{1}H NMR of 545091 (5).

^{13}C NMR (400 MHz, DMSO d_6)

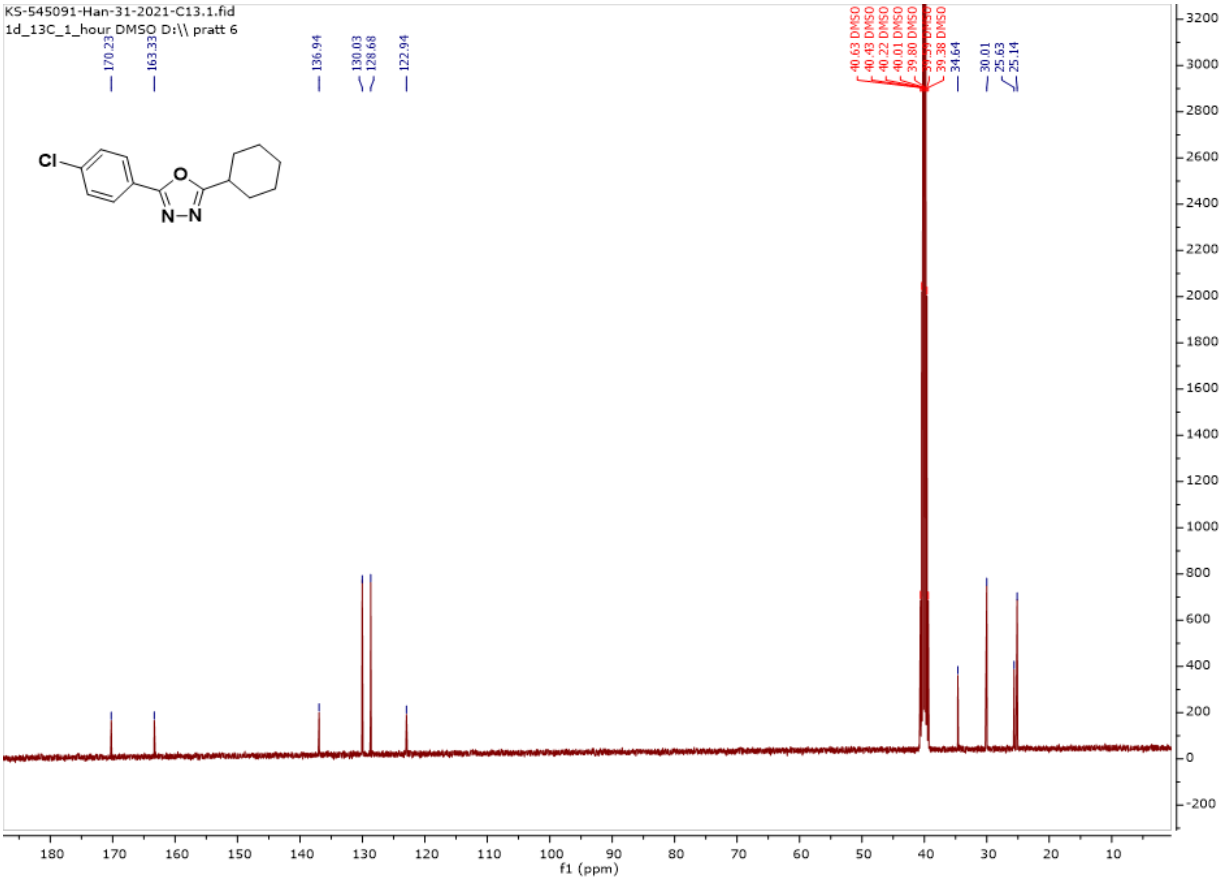

Figure 3.44 ^{13}C NMR of 545091 (5).